

Real-space  
renormalization group approach  
to the  
integer quantum Hall effect



TECHNISCHE UNIVERSITÄT  
CHEMNITZ

von der Fakultät für Naturwissenschaften der  
Technischen Universität Chemnitz genehmigte Dissertation  
zur Erlangung des akademischen Grades

doctor rerum naturalium

(Dr. rer. nat.)

vorgelegt von: Dipl.-Phys. Philipp Cain  
geboren am: 19.09.1973 in Karl-Marx-Stadt  
eingereicht am: 5. März 2004

Gutachter: Prof. Dr. K. H. Hoffmann, TU Chemnitz  
Dr. habil. R. A. Römer, Univ. of Warwick  
Prof. Dr. M. Schreiber, TU Chemnitz

Tag der Verteidigung: 14. Juli 2004

Archiv: <http://archiv.tu-chemnitz.de/pub/2004/0099>



## Bibliographische Beschreibung

Philipp Cain: *Real-space renormalization group approach to the integer quantum Hall effect*

Technische Universität Chemnitz, Fakultät für Naturwissenschaften

Dissertation, 2004 (in englischer Sprache)

106 Seiten, 52 Abbildungen, 1 Tabelle

## Referat

In dieser Dissertation werden Eigenschaften des ganzzahligen Quanten-Hall-Effekts (QHE) numerisch untersucht. Im Mittelpunkt steht der Übergang zwischen den charakteristischen Plateaus des Hall-Leitwertes, die sich bei ganzzahligen Vielfachen von  $e^2/h$  ausbilden. Im Gegensatz zum fraktionalen QHE kann dieser Phasenübergang beim ganzzahligen QHE ohne Teilchen-Teilchen Wechselwirkung allein mit der Annahme eines Lokalisierung-Delokalisierung-Übergangs der Wellenfunktion in der Mitte jedes Landau-Bandes erklärt werden. In dieser Arbeit wird das Chalker-Coddington(CC)-Netzwerk als Modell eines einzelnen QHE Übergangs verwendet. Um hohe Systemgrößen zu erreichen, wird zusätzlich ein Ortsraum-Renormierungsgruppenansatz (RG) auf das Netzwerk angewendet. Diese Vorgehensweise erlaubt außerdem eine einfache, aber statistisch sehr gute Beschreibung der starken charakteristischen Fluktuationen am Übergang im Rahmen von Verteilungsfunktionen. Die RG Methode kann ein CC Netzwerk allerdings nur in Näherung darstellen, da innerhalb der RG Iterationen nur ein Bruchstück des gesamten Netzwerks, die RG Einheit, berücksichtigt wird. Die Konstruktion der RG Einheit besitzt deshalb besonderen Einfluß auf die Genauigkeit der Ergebnisse. Aus diesem Grund werden zunächst die RG Resultate mit Ergebnissen anderer Methoden verglichen. Dabei werden die kritische Verteilungsfunktion  $P_c(G)$  des Leitwertes  $G$  am QHE Übergang und deren Momente ermittelt. Aus dem Verhalten von  $P(G)$  in der Nähe des Übergangs läßt sich der Wert des kritischen Exponenten  $\nu$  der Lokalisierungslänge ableiten. Diese Ergebnisse stimmen sehr gut mit exakten numerischen Simulationen überein. Die RG Methode wird daraufhin zur Berechnung der Energieniveaustatistik (ENS) erweitert. Die kritische ENS  $P_c(s)$  der normierten Abstände  $s$  von benachbarten Energieniveaus und  $\nu$  werden bestimmt. Anschließend wird der Einfluß von makroskopischen Inhomogenitäten in Form von langreichweitiger korrelierter Unordnung auf die kritischen Eigenschaften des QHE Übergangs untersucht. Die Ergebnisse zeigen eine Vergrößerung von  $\nu$ . Zuletzt wird die RG zur Berechnung des Hall Widerstandes  $R_H$  eingesetzt. Die kritische Verteilung  $P_c(R_H)$  läßt auf sehr starke Fluktuationen von  $R_H$  am Übergang schließen. Abseits des Übergangs in Richtung Isolator wird, nach Wahl einer geeigneten Mittelung  $\langle R_H \rangle$ , kein quantisiertes Verhalten, sondern Divergenz von  $\langle R_H \rangle$ , gefunden. Zusammenfassend demonstrieren alle Ergebnisse die Robustheit universeller Eigenschaften am QHE Übergang.

## Schlagwörter

Fluktuationen, Lokalisierung, Netzwerkmodell, numerische Verfahren, Quanten-Hall-Effekt, Renormierungsgruppenansatz, Universalität, ungeordnete Systeme



# Contents

List of Figures	7
List of Tables	9
List of Abbreviations	10
<b>1 Introduction</b>	<b>11</b>
<b>2 The quantum Hall effect</b>	<b>15</b>
2.1 Introduction . . . . .	15
2.2 The quantized Hall effect . . . . .	16
2.3 Theory of the integer quantum Hall effect . . . . .	18
2.3.1 Landau quantization . . . . .	18
2.3.2 The Chalker-Coddington network model . . . . .	21
2.3.3 Universality . . . . .	24
<b>3 RG approach to the CC model</b>	<b>25</b>
3.1 Introduction . . . . .	25
3.2 Quantum RG approach . . . . .	28
3.3 Critical exponent . . . . .	31
3.4 Numerical results . . . . .	32
3.5 Comparison with other works . . . . .	34
3.6 Test of a different RG unit . . . . .	37
3.7 Conclusion . . . . .	40
<b>4 RG approach to the LSD</b>	<b>41</b>
4.1 Introduction . . . . .	41
4.2 Description of the RG approach to the LSD . . . . .	43
4.3 Numerical results . . . . .	47
4.3.1 The LSD at the QH transition . . . . .	47
4.3.2 Small- $s$ and large- $s$ behavior . . . . .	48
4.4 Scaling results for the LSD . . . . .	51
4.4.1 Finite-size scaling at the QH transition . . . . .	51
4.4.2 Scaling for $\alpha_P$ and $\alpha_I$ . . . . .	51
4.4.3 Test of different initial distributions . . . . .	53
4.5 Conclusion . . . . .	58

<b>5</b>	<b>Macroscopic inhomogeneities</b>	<b>61</b>
5.1	Introduction . . . . .	61
5.2	Macroscopic inhomogeneities in classical percolation . . . . .	63
5.3	Macroscopic inhomogeneities in the RG approach . . . . .	65
5.4	Numerical results . . . . .	66
5.5	Intrinsic short-range disorder in quantum percolation . . . . .	70
5.6	Conclusion . . . . .	71
<b>6</b>	<b>RG approach to the Hall resistivity</b>	<b>73</b>
6.1	Introduction . . . . .	73
6.2	RG equation for $R_H$ . . . . .	74
6.3	Numerical results . . . . .	77
6.3.1	Behavior at the QH transition . . . . .	77
6.3.2	Behavior away from the QH transition . . . . .	81
6.4	Conclusion . . . . .	84
<b>7</b>	<b>Summary</b>	<b>86</b>
<b>8</b>	<b>Outlook</b>	<b>89</b>
	<b>Bibliography</b>	<b>91</b>
	<b>Publications</b>	<b>103</b>
	<b>Erklärung gemäß Promotionsordnung §6 (2) 4, 5</b>	<b>104</b>
	<b>Lebenslauf</b>	<b>105</b>
	<b>Acknowledgments</b>	<b>106</b>

# List of Figures

2.1	Illustration of the Hall experiment. . . . .	15
2.2	Result of the Hall measurement from [KDP80]. . . . .	17
2.3	The more recent Hall measurement [WES <sup>+</sup> 87] shows various plateaus. . . . .	18
2.4	Illustration of the integer QH effect explained due to a sequence of LD transitions. . . . .	20
2.5	Illustration of the separation of the electron motion. . . . .	21
2.6	From the equipotentials of Fig. 2.5 SPs of the potential can be identified. . . . .	22
2.7	Construction of the CC network. . . . .	23
3.1	2D bond percolation networks on a $30 \times 30$ square lattice. . . . .	26
3.2	Illustration of the RG approach to the 2D bond percolation. . . . .	27
3.3	All possible configurations for a connecting 2D bond RG unit. . . . .	27
3.4	Two illustrations of the same RG unit used for Eq. (3.8). . . . .	29
3.5	$P(G)$ and $Q(z)$ at a QH plateau-to-plateau transition. . . . .	33
3.6	Critical exponent $\nu$ obtained by the QH-RG approach as function of effective linear system size $L = 2^n$ for RG step $n$ . . . . .	34
3.7	Moments $\langle(G - \langle G \rangle)^m\rangle$ of the FP distribution $P_c(G)$ . . . . .	35
3.8	$P_c(G)$ found by Avishai <i>et al.</i> [ABB99]. . . . .	36
3.9	Experimental results for $P_c(G)$ from [CK96]. . . . .	37
3.10	RG unit constructed from 4SP. . . . .	38
3.11	Comparison of the critical distribution of the conductance $P_c(G)$ at the QH transition obtained using the 5SP and 4SP RG unit. . . . .	39
3.12	The critical exponent $\nu$ as function of the effective system size $N = 2^n$ for 4SP and 5SP unit. . . . .	39
4.1	Illustration how to construct the LSD. . . . .	43
4.2	The RG unit used to construct the matrix (4.5). . . . .	44
4.3	Energy dependence of the quasideigenenergies $\omega$ for two sample configurations. . . . .	46
4.4	FP distributions $P_c(s)$ obtained from the spectrum of $\omega_l(E = 0)$ and from the RG approach using the real eigenenergies $E_k$ . . . . .	48
4.5	FP distributions $P_c(s)$ for a linear and an arcsin energy dependence of the phases $\Phi_j$ . . . . .	49
4.6	$P_c(s)$ for small $s$ in agreement with the predicted $s^2$ behavior. . . . .	50
4.7	The large $s$ tail of $P_c(s)$ compared with fits according to the predictions of [SSS <sup>+</sup> 93]. . . . .	50
4.8	RG of the LSD used for the computation of $\nu$ . . . . .	52

4.9	Behavior of $\alpha_P$ at the QH transition as results of the RG of the LSD.	54
4.10	Behavior of $\alpha_I$ at the QH transition and resulting FSS curves. . . . .	55
4.11	Behavior of $\alpha_S$ at the QH transition as results of the RG of the LSD.	57
4.12	Comparison of the LSD $P_c(s)$ and $P_{\text{Gau\ss}}(s)$ . . . . .	58
4.13	Behavior of $\alpha_P$ and $\alpha_I$ computed for initial distributions $P_{\text{Gau\ss}}$ . . . . .	59
5.1	Experimentally observed temperature dependence of the width $\Delta B$ of the $\rho_{xx}$ peak from [WTPP88]. . . . .	62
5.2	Saturation of the peak width $\Delta B$ for microwave frequency $f \rightarrow 0$ from [BMB98]. . . . .	63
5.3	Illustration of the influence of quenched disorder by means of classical bond percolation. . . . .	65
5.4	Critical exponent $\nu$ obtained by the QH-RG approach as a function of RG scale $2^n$ for $\beta = 1$ and different correlation exponents $\alpha$ . . . . .	68
5.5	Critical exponent $\nu$ obtained by the QH-RG for $\beta = 2$ . . . . .	68
5.6	Critical exponent $\nu$ obtained by the QH-RG for $\beta = 3$ . . . . .	69
5.7	Critical exponent $\nu$ obtained by the QH-RG for $\beta = 4$ . . . . .	69
5.8	Dependence of the critical exponent $\nu$ on correlation exponent $\alpha$ for different $\beta = 1, 2, 3$ , and 4 as obtained after eight QH-RG iterations. . . . .	70
6.1	Different behavior of the Hall resistivity $\rho_{xy}$ at the QH plateau to insulator transition. . . . .	74
6.2	Determination of the Hall resistance $R_H$ of the RG unit. . . . .	75
6.3	Critical distribution $P_c(R_H)$ at the QH transition for V-flip and H-flip method obtained with the 5SP RG unit. . . . .	77
6.4	Critical distribution $P_c(R_H)$ calculated with the 4SP RG unit. . . . .	78
6.5	Change of $P(R_H)$ in course of the QH RG iterations when starting with an initial shifts $z_0 = \pm 0.1$ using the 5SP RG unit. . . . .	79
6.6	Change of $P(R_H)$ in course of the QH RG iterations using the 4SP RG unit. . . . .	79
6.7	The typical value $R_{H,\text{typ}}$ as function of the RG iteration $n$ close to the QH transition. . . . .	80
6.8	Behavior of $P(R_H)$ calculated by the V-flip and the H-flip method for $t \rightarrow 0$ as a result of a single RG iteration using the 5SP unit. . . . .	82
6.9	Behavior of $P(R_H)$ for $t \rightarrow 1$ . . . . .	82
6.10	Comparison of the tails of $P(R_H)$ for $t \rightarrow 1$ , $t \rightarrow 0$ , and $P_c(R_H)$ calculated by the H-flip method for the 5SP unit. . . . .	83
6.11	$R_{H,\text{typ}}$ for $t \rightarrow 0$ and $t \rightarrow 1$ as a result of a single RG iteration using the 4SP and the 5SP unit. . . . .	83
6.12	$R_{H,\text{typ}}$ as function of $R_{L,\text{typ}}$ for the 4SP and the 5SP RG unit. . . . .	84



# List of Tables

4.1	Fit results for $\nu$ obtained from $\alpha_I$ and $\alpha_P$ for different system sizes $N$ , intervals around the transition, and orders $\mathcal{O}_\nu$ and $\mathcal{O}_z$ of the fitting procedure. . . . .	56
-----	--------------------------------------------------------------------------------------------------------------------------------------------------------------------------------------------------------------------	----

# Abbreviations

<b>2D</b>	Two-dimensional
<b>CC</b>	Chalker-Coddington
<b>FP</b>	Fixed point
<b>GUE</b>	Gaussian unitary ensemble
<b>LD</b>	Localization-delocalization
<b>LSD</b>	Level spacing distribution
<b>MOSFET</b>	Metal-oxide-semiconductor field-effect transistor
<b>QH</b>	Quantum Hall
<b>RG</b>	Renormalization group
<b>RMT</b>	Random matrix theory
<b>SP</b>	Saddle point
<b>4SP, 5SP</b>	Four saddle points, five saddle points

# Chapter 1

## Introduction

Measuring the resistance of a two-dimensional (2D) electron gas at very low temperature reveals a striking macroscopic phenomenon when subjected to a strong perpendicular magnetic field. Investigating such a system in form of a silicon metal-oxide-semiconductor field-effect transistor (MOSFET) von Klitzing *et al.* [KDP80] discovered in 1980 that the Hall resistance  $R_H$  shows very precise plateaus at  $(1/N)h/e^2$  where  $N$  is an integer number. In the same region the vanishing longitudinal resistance  $R_L$  indicates a dissipationless flow of current. Two years later in 1982, quantization was also found at fractional values  $N$  [TSG82], which led to the distinction between the fractional and the integer quantum Hall (QH) effect. Despite the similarities regarding the experimental observations the theoretical description of both effects differs considerably. The integer QH effect can be explained very well within a non-interacting electron picture, while interactions play an important role in the fractional QH effect. In this work the integer QH effect is studied. For more details about the fractional QH effect see [CP95, Yos02].

Because a fundamental microscopic description is still missing several other theories were proposed to explain the integer QH transition [AA81, CP95, JVFH94, Lau81, Pra81, Pru84, TKNN82, Yos02]. One successful approach provides the localization-delocalization (LD) scenario [AA81] where the QH effect follows from a series of LD transitions. One assumes that the density of states is formed of separated Landau bands. Each band consists of localized states in the tails and extended states in the middle of the band. The change of the Hall resistance from one to another plateau is then explained by the Fermi energy passing the extended states in the center of the Landau band. In the range between the bands and for the localized states the Hall resistance remains at the constant plateau value very precisely.

The focus of this work is the study of the QH transition rather than the plateau region. It is established that the QH transition is a second-order phase transition [Huc95] where a power-law divergence of characteristic length scales is observed. The divergence, e.g. of the localization length  $\lambda$  of the wave functions,  $\lambda \propto \epsilon^{-\nu}$ , where  $\epsilon$  corresponds to the distance from the transition, can be quantified by the value of the exponent  $\nu$ . The importance of the exponent stems from the fact that its value is independent from sample size and even material. It is influenced only by the dimensionality and by the universality class the system belongs to. A universality class covers a wide variety of systems which all share a common symmetry, like time-

---

reversal symmetry and rotational symmetry. Therefore universality has a great impact on the construction of theoretical models. In order to predict universal quantities measured in experiments one can investigate even very simple models with the only constraint that they belong to the same universality class as the experiments.

In this work the above idea is applied to the study of the QH transition. The QH sample is approximated by the Chalker-Coddington (CC) network model [CC88]. The CC model describes a single Landau band and thus contains only one QH transition. The electrons are treated semiclassically as non-interacting particles moving in a smoothly varying 2D disorder potential under a strong perpendicular magnetic field. The percolation of the electron through the sample then consists of two main components, the motion along equipotentials interrupted by the scattering events at saddle points (SPs) of the potential, which are mapped on links and nodes of a 2D network.

The CC model provides a fully quantum coherent description of the QH effect. This is similar to quantum coherent transport measurements such as in mesoscopic devices at low temperature, where the results clearly show the large influence of quantum interference and the measured quantities fluctuate strongly [JK88]. Therefore it is useful to look at full distribution functions, like  $P(G)$  of the conductance  $G$  of the sample, instead of calculating a single average quantity.

Furthermore, since the universal quantities of the QH transition are bulk properties of the sample numerical calculations have to be performed in principle for infinitely large CC networks. In reality the size of the network is restricted by the computational capacity. In order to obtain reliable results computations are performed for as large as possible but finite CC networks.

The alternative method to large-scale simulations used in this work is the real-space renormalization group (RG) approach [AJS97,GR97]. Here a very large system size is achieved by an iterative procedure. A characteristic part of the CC network - the RG unit - consisting of several SPs is mapped onto a single super-SP residing in a new CC-super network. With each of these iteration steps the size increases by a fixed factor defined by the size of the RG unit. The system grows according to a power law while each step requires the same numerical effort. This advantage is counterbalanced to a drawback of the method which is also the starting point of most criticism. The construction of the RG unit is only an approximation of the full network. Thus a specific choice of an RG unit has fundamental influence on the reliability of the results. Unfortunately, there is no a priori proof of the accuracy of the RG. One part of this work is therefore devoted to the demonstration of the accuracy and strength of the chosen RG approach in comparison to exact calculations such as large-scale simulations for example in [BS97, CC88, Huc92, KM97a, LWK93, Met98]. For this reason the critical distributions  $P_c(G)$  and  $P_c(s)$  of the conductance and the energy level spacings, respectively, as well as the critical exponent  $\nu$  of the localization length at the QH transition are considered. Based on this justification the RG approach is then employed in a further study of the QH effect.

One subject is motivated by contradicting experimental results questioning the universality. Contrary to the broad majority of experiments [HZH01, HZHP01,

HWE<sup>+</sup>93, KHKP91a, KHKP91b, KHKP92, KMDK00, SVO<sup>+</sup>00, WLTP92, WTP85, WTPP88] the measurements in [SHL<sup>+</sup>98] and [BMB98] did not observe the expected universal power-law behavior characterized by a critical exponent. The reason of this disagreement might be due to screening of the real critical behavior by some other effect. In this work one possible effect - the influence of macroscopic inhomogeneities on the QH transition - is considered. On the experimental side, an estimate about number and kind of inhomogeneities in a sample is difficult. On the theoretical side it is known from a classical model that long-range correlated disorder, describing macroscopic inhomogeneities, leads to an increase of the critical exponent  $\nu$  at the transition [WH83]. Using the RG approach to the CC model allows one to investigate this problem now in the quantum regime.

Another problem concerns the existence of the quantized Hall insulator. While it is established that plateau-plateau and insulator-plateau transitions exhibit the same critical behavior [GWSS93, HSS<sup>+</sup>98, HNF<sup>+</sup>94, LPV<sup>+</sup>02, MHL<sup>+</sup>00, PST<sup>+</sup>97, STS<sup>+</sup>95, STS<sup>+</sup>97a, STS<sup>+</sup>96, STS<sup>+</sup>97b, SVO<sup>+</sup>00] the value of the Hall resistance  $R_H$  in this insulating phase is still rather controversial. Various experiments have found that  $R_H$  remains very close to its quantized value  $h/e^2$  even deep in the insulating regime [HSS<sup>+</sup>98, LPV<sup>+</sup>02, PSC<sup>+</sup>03, STS<sup>+</sup>97a, STS<sup>+</sup>96]. This scenario has been dubbed the *quantized Hall insulator*. On the other hand, theoretical predictions based on quantum coherent models show that a diverging  $R_H$  should be expected [PA99, ZS01]. Extending the RG approach to the calculation of the distribution function  $P(R_H)$  one can study the transformation of  $P(R_H)$  in the transition region toward the insulating and the plateau side, respectively.

The results of this study are presented as follows. Chapter 2 explains the QH effect in more detail. After a brief review of the experimental facts the QH effect is derived from a semiclassical theory. On this basis the CC model is then introduced and further remarks about the importance of universality are given. The main tool of this work, the RG approach to the CC model, is content of Chapter 3. It starts with an illustration of the RG approach to classical percolation. The approach is then applied to the CC model. Using the obtained RG equation one can compute the critical conductance distribution  $P_c(G)$  at the QH transition and also the value of the exponent  $\nu$  of the localization length. The results are compared to other works and the dependence on the constructed RG unit is examined. In Chapter 4 the RG approach is extended to the study of the energy level spacing distribution (LSD). The critical LSD is computed and compared to the predictions of universality. The change of the LSD around the transition can be characterized by a single quantity derived from the shape of the LSD. For a suitably chosen quantity a finite-size scaling analysis then reveals the value of the exponent  $\nu$  again, now by an alternative method. The chapter ends with a discussion of the influence of the initial distribution used in the RG iteration. Chapter 5 considers how macroscopic inhomogeneities affect the critical properties of the QH transition. As a motivation the contradicting experimental results are reviewed. The extended Harris-criterion describing the influence of a power-law correlated disorder potential on the value of  $\nu$  for classical percolation is introduced. The long-range correlation is then incorporated into the RG approach. The obtained results are discussed in comparison to the classical

---

prediction. The determination of  $R_H$  in Chapter 6 requires to derive further RG equations. The result allows one to study not only the distribution  $P_c(R_H)$  at the QH transition but also the shape of  $P(R_H)$  toward the insulating or the plateau regime. Because of the strong fluctuations of  $R_H$  a suitable averaging procedure has to be chosen. Chapter 7 summarizes the results of this work. And Chapter 8 gives a brief outlook on pursued studies and unanswered questions.

# Chapter 2

## The quantum Hall effect

### 2.1 Introduction

The first foundation of this field was laid by the discovery of the Hall effect by Edwin H. Hall in 1879 [Hal79]. It is well known as a purely classical effect based on the interplay of electric and magnetic field in a spatially extended conductor. For example, consider a 2D homogeneous isotropic conducting sample as shown in Fig. 2.1 which is penetrated by an electric field  $\mathbf{E}$  parallel to the probe. Without a magnetic field ( $\mathbf{B} = 0$ ) the sample acts as a normal resistor where  $\mathbf{E} = \rho \mathbf{j}$  depends linearly on the resistivity  $\rho$  and the current density  $\mathbf{j}$ . This situation changes when a magnetic field ( $\mathbf{B} \neq 0$ ) is applied perpendicular to the sample. Due to the Lorentz force  $\mathbf{F}_L = q(\mathbf{v} \times \mathbf{B})$  charge carriers with velocity  $\mathbf{v}$  and charge  $q$  are deflected laterally which creates an additional electric field  $\mathbf{E}_H$  perpendicular to  $\mathbf{E}$ . The resulting force  $\mathbf{F}_H$  leads to a compensation of  $\mathbf{F}_L$ . When  $\mathbf{F}_H = \mathbf{F}_L$  the  $\mathbf{E}_H$  corresponds to the so-called *Hall voltage*  $U_H = L_y |\mathbf{v}| |\mathbf{B}|$  where  $L_y$  is the width of the sample. In order to relate  $U_H$  to  $\mathbf{j}$  one employs  $\mathbf{j} = qn_q \mathbf{v}$  where  $n_q$  is the carrier density [AM76]. It follows

$$U_H = \frac{1}{qn_q} L_y |\mathbf{j}| |\mathbf{B}| = A_H L_y |\mathbf{j}| |\mathbf{B}|. \quad (2.1)$$

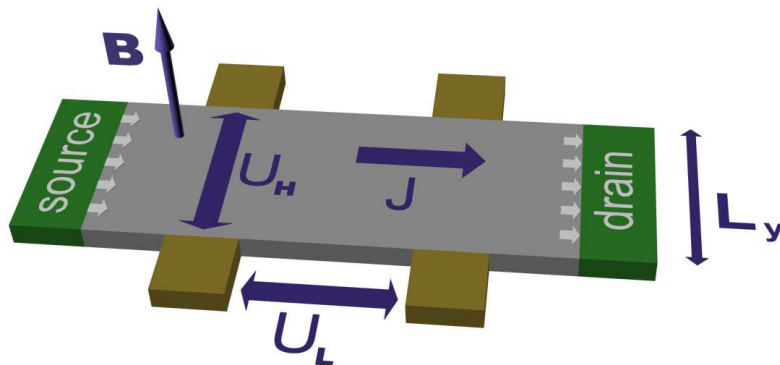


Figure 2.1: Illustration of the Hall experiment. The magnetic field  $\mathbf{B}$  leads to a potential difference perpendicular to the direction of the current  $\mathbf{J}$ .

The Hall coefficient  $A_H = 1/(qn_q)$  takes the role of a proportionality constant which depends on the material properties  $n_q$  and  $q$ , where for electrons as the usual charge carriers  $q = -e$ . The value of  $A_H$  follows from the band structure of the sample material and is therefore not influenced by the particularities of the experimental setup [AM76]. Consequently, the experimental extraction of  $A_H$  is a suitable method to obtain information about the charge transport within a material. Besides the information about carrier density  $n_q$ , the sign of  $A_H$  allows one to distinguish between the normal Hall effect ( $A_H < 0$ ) with electrons and the anomalous Hall effect ( $A_H > 0$ ) with holes as charge carriers.

From the above explanation it is obvious that the resistivity of the 2D Hall sample cannot be described by a simple scalar but rather by a tensor. Therefore

$$\mathbf{E} = \begin{pmatrix} \rho_{xx} & \rho_{xy} \\ -\rho_{xy} & \rho_{xx} \end{pmatrix} \mathbf{j}, \quad (2.2)$$

where  $\rho_{xx}$  is called longitudinal and  $\rho_{xy}$  Hall resistivity. Often one prefers the conductivity instead of the resistivity tensor. The conductivity tensor is defined as the inverse of the resistivity tensor which yields

$$\sigma_{xx} = \sigma_{yy} = \frac{\rho_{xx}}{\rho_{xx}^2 + \rho_{xy}^2} \quad \text{and} \quad \sigma_{xy} = -\sigma_{yx} = -\frac{\rho_{xy}}{\rho_{xx}^2 + \rho_{xy}^2}. \quad (2.3)$$

Analogous to the resistivity,  $\sigma_{xx}$  is called longitudinal and  $\sigma_{xy}$  Hall conductivity. As particularity for 2D samples one should note that  $\rho_{xy}$  and  $\sigma_{xy}$  coincide with the Hall resistance  $R_H$  and Hall conductance  $G_H$ , respectively. This fact is useful especially in experiments because the less accurate measurement of the sample geometry is not required and therefore has no influence on the accuracy of the result.

## 2.2 The quantized Hall effect

How does the result of the Hall measurement change when it is performed not in a classical but in a quantum regime? In order to answer this question experimentally one has to comply with the conditions of (i) a very low temperature  $T < 4\text{K}$ , (ii) a high magnetic field of order  $B = 10\text{T}$  and (iii) a very well defined 2D electron system. For the latter different experimental realizations are possible. One way is to place electrons on a free liquid helium surface, which allows densities up to  $10^{12}\text{m}^{-2}$ . The electrons move along the surface only and do not enter the helium volume which would require an additional energy. The Fermi energy  $E_F$  for this system is at most  $2\text{mK}$  thus the electrons can be considered as non-degenerate classical particles for experimental  $T > 10\text{mK}$ . Much more importance than to the Helium surface can be attributed to 2D semiconductor systems, mainly because of the high charge densities of  $10^{15} - 10^{17}\text{m}^{-2}$  attainable. Together with the low effective mass of the electrons this results in an  $E_F$  of an order of  $100\text{K}$ . Therefore the electron system is degenerate for experimental  $T$ . 2D semiconductor systems have been realized by MOSFET and semiconductor heterostructures, where the 2D electron gas forms either at the interface between oxide and semiconductor or at heterojunctions between adjacent



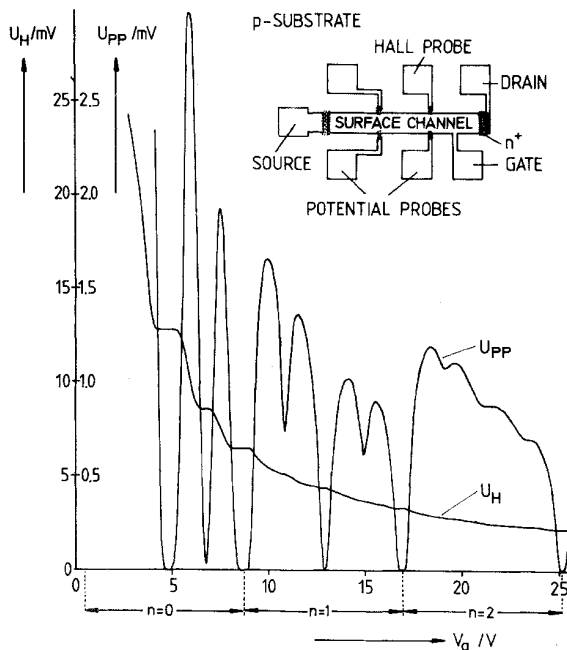


Figure 2.2: Result of the Hall measurement from [KDP80]. Both the characteristic plateaus of the Hall voltage  $U_H$  and the decrease of the longitudinal voltage drop  $U_{PP}$  at the plateaus are demonstrated by varying the gate voltage  $V_g$ .

semiconductor layers, respectively. When using MOSFETs the electron density of the 2D system and thereby  $E_F$  can be varied by adjusting the gate voltage at a fixed magnetic field which requires experimentally less effort. In the context of the Hall measurement this method gives equivalent results to the variation of the magnetic field where  $E_F$  is constant because  $U_H$  depends only on the ratio  $B/n_q$  as follows from Eq. (2.1). A deeper understanding is provided by the theoretical considerations in the next Section. On the other hand, the heterostructures allow one to construct higher-quality 2D electron systems because the electrons are spatially separated from impurities caused by dopant atoms and therefore have an increased mobility. A higher mobility leads to an increased conductivity and improves the sensitivity of the Hall measurement.

The first accurate measurement of the resistivity tensor was performed in 1980 by von Klitzing, Dorda, and Pepper [KDP80]. In their experiment they were using a Si-MOSFET at  $T = 1.5\text{K}$  and  $B = 18\text{T}$ . When changing the gate voltage they observed, as shown in Fig. 2.2, characteristic plateaus in the Hall resistivity at quantized values  $\rho_{xy} = (1/N)h/e^2$  for integer values  $N \geq 1$  while at the same time  $\rho_{xx}$  drops almost to zero. The particular relevance of this *integer* QH effect, especially for metrology, lies in the remarkable accuracy of the plateau value, from which a standard resistor can be defined. Because of the importance of this discovery the Nobel prize was awarded to von Klitzing in 1985. The resistance standard  $R_K = h/e^2$  is called the von Klitzing constant with the official value  $R_{K-90} = 25812.807\Omega$  recommended by the International Metrology Committee. In addition the authors of [KDP80] could also propose a new method for the determination of the fine-

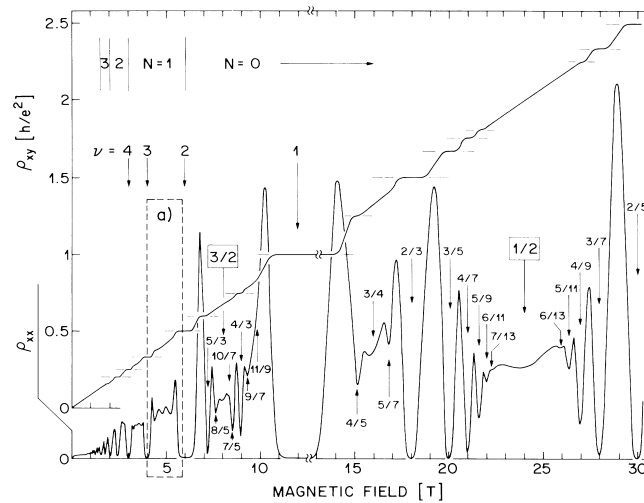


Figure 2.3: The more recent Hall measurement from [WES<sup>+</sup>87] shows various plateaus of the Hall resistivity  $\rho_{xy}$  also at fractional values.

structure constant  $\alpha_{\text{fsc}} = e^2/(hc)$  because the speed of light  $c$  is also known very precisely and since 1983 is even set to a fixed value by the SI-unit definition.

In order to test whether plateaus occur only at integer values also GaAs heterostructures with higher mobilities were studied. In their experiment Tsui, Störmer, and Gossard [TSG82] could show for their sample an additional plateau at a fractional value  $\rho_{xy} = 1/\frac{1}{3}(h/e^2)$ . In later experiments at lower temperature and using cleaner samples further fractional plateaus were observed. Figure 2.3 shows results from [WES<sup>+</sup>87].

To summarize the current experimental situation, it is established that  $\rho_{xy}$  in the plateau region stays constant with an accuracy of at least  $10^{-9}$  [JJI97] independent of sample size, sample material, and plateau number. In the same region  $\rho_{xx} = 0$  is found with an accuracy of at least  $10^{-8}$ .

## 2.3 Theory of the integer quantum Hall effect

### 2.3.1 Landau quantization

After the experimental discovery of the integer QH effect there have been numerous different theoretical attempts to explain the effect. And still, more than 23 years later, there is no fundamental theory available which describes the macroscopic phenomenon of the integer QH effect starting from a microscopic picture. Instead the theories rely on initial assumptions.

Apparently the integer QH effect is connected to the Landau quantization that provides a quantum mechanical description of the electron motion in a magnetic field. An instructive way to explain the integer QH effect is the following semi-phenomenological approach. First, consider the electrons within the 2D Hall sample as free particles moving in a magnetic field which corresponds to the following

Hamiltonian

$$\hat{H} = \frac{1}{2m^*} (\hat{\mathbf{p}} + e\mathbf{A})^2, \quad (2.4)$$

where  $\hat{\mathbf{p}}$  is the momentum operator,  $m^*$  the effective mass of the electrons and  $\mathbf{A}$  the vector potential with  $\text{rot}\mathbf{A} = \mathbf{B}$ . Due to the magnetic field the electrons move along cyclotron orbits. Therefore it is suitable to split their coordinates into two parts

$$\hat{x} = \hat{X} + \hat{\zeta} \quad \text{and} \quad \hat{y} = \hat{Y} + \hat{\eta}. \quad (2.5)$$

Here  $(\hat{X}, \hat{Y})$  describes the center of the cyclotron motion and  $(\hat{\zeta}, \hat{\eta})$  is the relative coordinate of the motion around this center. Now, using the Hamiltonian (2.4), the equations of motion

$$\dot{\hat{\zeta}} = -\omega_c \hat{\eta} \quad \text{and} \quad \dot{\hat{\eta}} = \omega_c \hat{\zeta} \quad (2.6)$$

can be derived from which follows that  $(\hat{\zeta}, \hat{\eta})$  rotates with cyclotron frequency  $\omega_c = eB/m$ . Using Eq. (2.6) the Hamiltonian (2.4) can now be rewritten in the form of a harmonic oscillator in terms of  $(\hat{\zeta}, \hat{\eta})$

$$H = \frac{\hbar\omega_c}{2l_B^2} (\hat{\zeta}^2 + \hat{\eta}^2). \quad (2.7)$$

By this, the Landau quantization of a free electron moving in a magnetic field is related to the problem of the harmonic oscillator. Consequently, in 2D one observes also discrete eigenenergies which are now called Landau levels

$$E_N = \left(N - \frac{1}{2}\right) \hbar\omega_c, \quad (2.8)$$

where the Landau level index  $N$  corresponds to the experimentally observed plateaus at integer values  $N \geq 1$ . The Landau levels are equidistant with  $\Delta E = \hbar\omega_c$ . Besides this analogy there are also differences to the oscillator. First, one should note that values of  $\hat{\zeta}$  and  $\hat{\eta}$  have an uncertainty resulting from the commutation relation

$$[\hat{\zeta}, \hat{\eta}] = -il_B^2 \quad (2.9)$$

in which the cyclotron radius  $l_B = (\hbar/eB)^{1/2}$  of the ground state defines the *magnetic length* scale. Second, in contrast to the harmonic oscillator the Landau levels are degenerate. Because the cyclotron motion of the electrons described by  $(\hat{\zeta}, \hat{\eta})$  is bound spatially to the radius  $l_B$  there exist various  $(\hat{X}, \hat{Y})$  at the same energy since their cyclotron orbits are not overlapping. This degeneracy depends therefore on  $l_B$  and the size  $L_x \times L_y$  of the sample

$$N_L = \frac{L_x L_y}{2\pi l_B^2}. \quad (2.10)$$

The degeneracy then allows one to derive the so-called filling factor

$$f = 2\pi l_B^2 n_e = 2\pi \frac{\hbar}{eB} n_e. \quad (2.11)$$

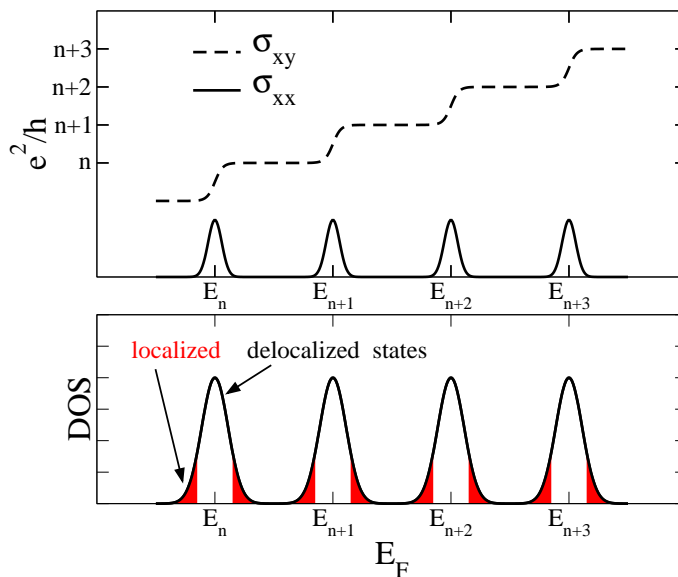


Figure 2.4: Illustration of the integer QH effect explained due to a sequence of LD transitions. For finite systems the width of the extended states at the band centers of the disorder-broadened Landau levels is finite.

The filling factor is usually denoted by the variable  $\nu$  in literature. Because of a conflict with the critical exponent, which has historically the same symbol, here  $f$  is used instead.

By the definition (2.11), the single dimensionless quantity  $f$  can describe both experimental situations, the change of electron density  $n_e$ , e.g. by adjusting the gate voltage, and the variation of the magnetic field. On the other hand  $f$  can be expressed in a microscopic view as the ratio between the number of electrons and the number of flux quanta  $h/e$  in the sample. So the value of  $f$  shows the filling of Landau levels, e.g. an integer value  $f = 2$  means that exactly the lowest two Landau levels are occupied.

The Landau quantization of the energy spectrum can explain the position of integer QH transitions. But it does not provide an insight why between the transitions plateaus in  $\rho_{xy}$  and  $\sigma_{xy}$  are observed nor why in the same regime  $\rho_{xx}$  and  $\sigma_{xx}$  drop to nearly zero. Therefore disorder has been incorporated into the model. As a result of disorder in the sample, the Landau levels broaden to bands as illustrated in Fig. 2.4. It is known from other models handling disorder, e.g. the Anderson model of localization [And58], that not all states in the band are extended. Due to disorder the states in the tails of the bands are localized (see Fig. 2.4). Thus they do not contribute to charge transport. Following from this assumption the QH effect can now be understood as a series of LD transitions. The peak in  $\sigma_{xx}$  occurs exactly at the position of integer  $f$  where the  $E_F$  passes the extended states existing in the center of the Landau band. In the region between the Landau band centers states are localized and therefore  $\sigma_{xx} = 0$ . For  $\sigma_{xy}$  the same argument holds. The difference with respect to  $\sigma_{xx}$  is the non-dissipative character of the Hall current, where the extended states of all filled Landau levels contribute. Therefore  $\sigma_{xy}$  is

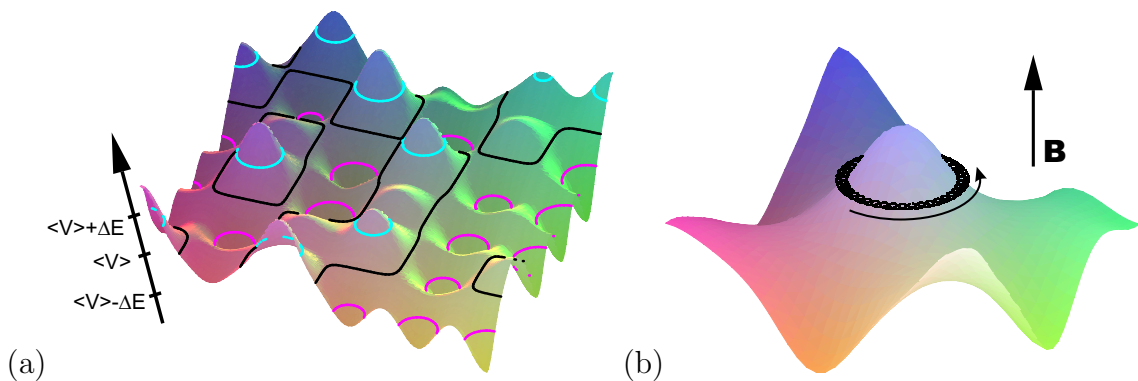


Figure 2.5: Illustration of (a) the weakly varying random potential  $V$  with equipotential lines at  $\langle V \rangle$  and  $\langle V \rangle \pm \Delta E$  which allows one (b) in a strong magnetic field  $\mathbf{B}$  to separate the electron motion (black orbit) into cyclotron motion and motion of the guiding center along equipotentials.

constant while  $E_F$  is in the range of localized states and increases by  $e^2/h$  to the next plateau exactly when passing a Landau band center.

Besides this semi-phenomenological models simply assuming an LD transition, more sophisticated theories [CP95, JVFH94, Yos02] exist considering, e.g. gauge invariance [Lau81], topological quantization [TKNN82], scattering [Pra81] and field theoretical approaches [Pru84].

### 2.3.2 The Chalker-Coddington network model

In this work a semi-classical approach is used to model the integer QH transition. It is based on an extension of the high-field model [Ior82] suggested by Chalker and Coddington [CC88], the so-called CC network model which is one of the main "tools" for the quantitative study of the QH transition [JMZ99, KHA95, KHA97, KM95, KM97a, KZ01, LC94, LCK94, LWK93, Met98, RF95, WLW94].

In order to include the LD scenario the classical high-field model relies on two basic prerequisites. First, the 2D sample is penetrated by a very strong perpendicular magnetic field and second the electrons are non-interacting and move in a smoothly varying 2D potential energy landscape  $V(\mathbf{r})$  illustrated in Fig. 2.5. As a result the magnetic field  $B$  forces an electron onto a cyclotron motion with radius  $l_B$  much smaller than the potential fluctuations. Thus the electron motion can be separated into cyclotron motion and a motion of the guiding center along equipotentials of the energy landscape [Ior82]. The cyclotron motion leads to the required quantization into discrete Landau levels whereas its influence on the electron motion in the potential can be neglected. Besides the fundamental assumption about the difference of length scales the model therefore contains no further dependence on  $B$ . The quantum effects of the electron transport through the sample are only determined by the height of the SPs in the potential energy landscape. This picture is related to a classical bond percolation problem on a square lattice [SA95] when mapping SPs onto bonds. A bond is connecting only when the potential of the corresponding SP equals the potential energy  $\varepsilon$  of the electron. From percolation theory [SA95]

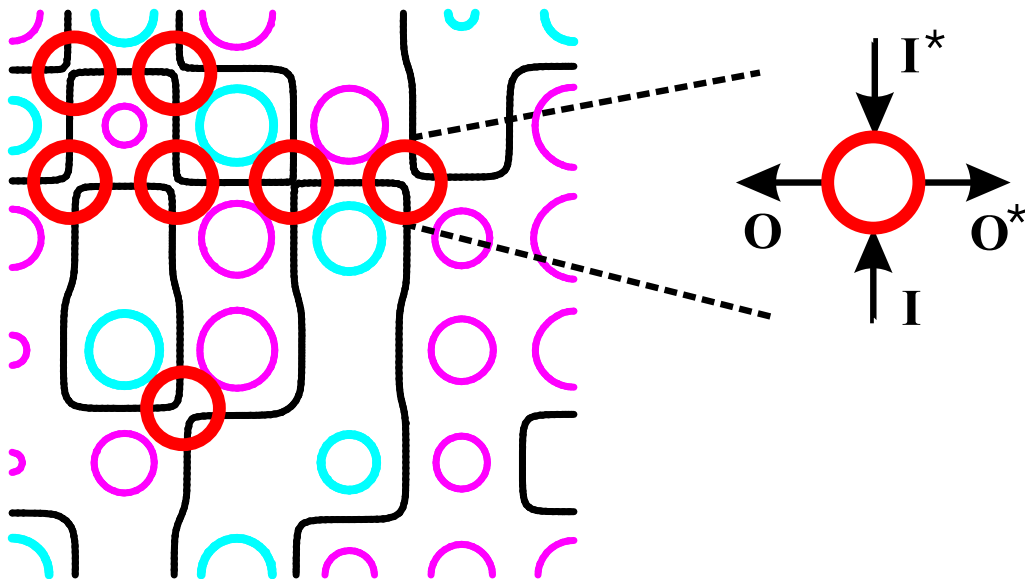


Figure 2.6: From the equipotentials of Fig. 2.5a at  $E = \langle V \rangle$ ,  $\langle V \rangle \pm \Delta E$  SPs of the potential can be identified. A single SP acts as a scatterer connecting two incoming with two outgoing channels.

follows that an infinite system is conducting only at a single  $\varepsilon = \langle V \rangle$ . Consequently, the high-field model describes only a single QH transition. It provides a qualitative understanding of the existence of an LD transition and thus the quantized plateaus in the conductivity  $\sigma_{xy}$  observed in the integer QH effect [JV FH94]. However, because of its purely classical assumptions the model is unable to exactly reproduce the critical properties of the transition found in experiments, i.e., the divergence of the correlation length at the transition with an exponent of  $\nu \approx 2.3$  [KH KP91a]. Instead, it predicts  $\nu = 4/3$ , the value appropriate for classical percolation.

The CC network model improved the high-field model by introducing quantum corrections [CC88], namely tunneling and interference. Tunneling occurs, in a semi-classical view, when electron orbits come so close to each other that the cyclotron orbits overlap. From Fig. 2.6 one can conclude that this happens at the SPs, which now act as quantum scatterers described by a unitary scattering matrix  $S$

$$\begin{pmatrix} O \\ O^* \end{pmatrix} = S \begin{pmatrix} I \\ I^* \end{pmatrix} = \begin{pmatrix} t & r \\ -r & t \end{pmatrix} \begin{pmatrix} I \\ I^* \end{pmatrix} \quad (2.12)$$

which connects two incoming with two outgoing channels. Assuming a symmetric potential at the SP the scattering rates are given by a pair of a complex transmission and a reflection coefficient  $t$  and  $r$ , respectively. From the required unitarity of  $S$  it follows that  $|t|^2 + |r|^2 = 1$ . Obviously,  $t$  and  $r$  depend on the potential energy of the SP. It was shown [GR97] that  $t$  and  $r$  can be parametrized by

$$t = \left( \frac{1}{e^z + 1} \right)^{\frac{1}{2}} \quad \text{and} \quad r = \left( \frac{1}{e^{-z} + 1} \right)^{\frac{1}{2}} \quad (2.13)$$

where  $z$  corresponds to a dimensionless energy difference between SP potential and electron energy  $\varepsilon$ . Without restricting the generality  $\langle V \rangle = 0$  is assumed in the

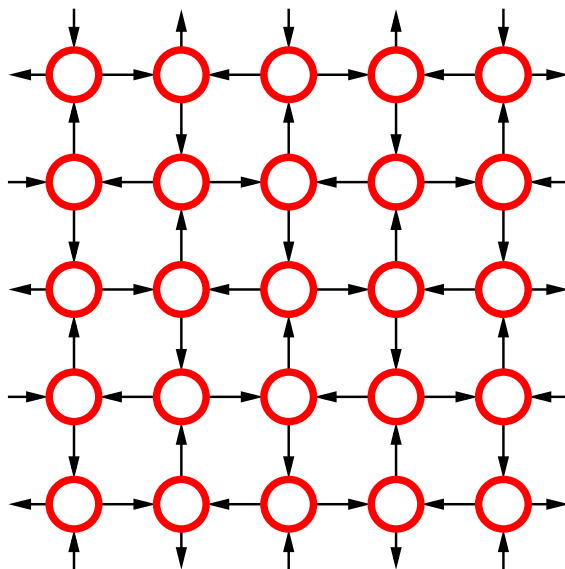


Figure 2.7: Construction of the CC network by mapping of SPs to nodes and equipotentials to links of a regular 2D square lattice.

following. In case of  $\varepsilon = 0$  the value of  $z$  then coincides with the dimensionless SP height. Similar to bond percolation now a network of SPs can be constructed. The SPs are mapped onto nodes and the equipotentials correspond to links as shown in Fig. 2.7.

While moving along an equipotential an electron accumulates a random phase  $\Phi$  which reflects the randomness of the potential. The corresponding phase factor  $e^{i\Phi}$  can be included in the matrix  $S$ . In this work  $S$  and  $\Phi$  are kept separately. As in the high-field model this quantum percolation describes only a single QH transition with exactly one extended state in the middle of the Landau band at  $\varepsilon = 0$ . The critical properties at the transition, especially the value of the exponent  $\nu \approx 2.4 \pm 0.2$  [LWK93], agree with experiments [KHKP91a, SVO<sup>+</sup>00] as well as with results of other theoretical approaches [HK90, HB92]. For numerical investigations of the CC model, one constructs a regular 2D lattice out of the SPs. Then the 2D plane is cut into 1D slices with the associated scattering matrices transformed into a transfer matrix. The conductivity may be calculated by transversing perpendicular to the slices along the sample by transfer matrix multiplications [LWK93] according to the Landauer-Büttiker approach [BILP85]. The spatial extension of the 2D plane is limited by the computational effort although an additional disorder averaging over many samples is not necessary for quasi-1D samples [LWK93].

The CC model is a strong-magnetic-field (chiral) limit of a general network model, first introduced by Shapiro [Sha82] and later utilized for the study of LD transitions within different universality classes [CRK<sup>+</sup>02, FJM98, FJM99, Jan98, KHAC99, MJH98]. In addition to the QH transition, the CC model applies to a much broader class of critical phenomena since the correspondence between the CC model and thermodynamic, field-theory and Dirac-fermions models [GRS97, HC96, Kim96, KM97b, Lee94, LFSG94, MT99, Zir94, Zir97] was demonstrated.

### 2.3.3 Universality

Although there exists a variety of different theoretical descriptions a fundamental microscopic understanding of the integer QH effect is still missing. In contrast, approaches like the CC model are based on a simplified picture of the real world. The reason that one can nevertheless describe and also predict experimental results is based on the hypothesis of *universality*. Phase transitions, like the QH transition, are characterized by critical behavior, e.g., the divergence of length scales, which can be quantified by a set of critical parameters. Universality assumes that these parameters are not specific for a single experiment, material or theoretical model. This idea was first demonstrated by Wigner [Wig51, Wig55] when studying the statistics of nuclear spectra. Instead of using the real energy levels, the correlations in the spectra could be reproduced by considering the eigenvalues of a large set of  $2 \times 2$  matrices with elements chosen randomly according to a Gaussian distribution. The success of the approach led to the development of random matrix theory (RMT) [Meh91]. Following from universality one expects the same universal quantities, like critical exponents, in a variety of different systems which agree only in dimensionality and the fundamental underlying symmetry. Depending on this fundamental symmetry which manifests itself in the symmetry of the Hamiltonian one can distinguish between several *universality classes*. The classes with relevance to this work are the basic Gaussian ensembles where the Hamiltonian is (i) orthogonal (GOE) with time-reversal invariance and rotational symmetry, (ii) unitary (GUE) with broken time-reversal symmetry but rotational symmetry, and (iii) symplectic (GSE) with time-reversal invariance and broken rotational symmetry. Because the contribution of the magnetic field breaks the time reversal symmetry, the description of the QH transition using the CC model can be classified into GUE.



# Chapter 3

## RG approach to the CC model

### 3.1 Introduction

RG techniques provided a powerful tool for the study of phase transitions [BDFN92, Wil83]. One can distinguish between real-space [Car96] and field-theoretical [Sal99] RGs. Common to both variants is the elimination of irrelevant (either short-range or short-period) degrees of freedom. Afterward the original phase volume is restored by a scale transformation. The system has now the same structure as the original one but the values of its parameters, e.g. coupling constants, are *renormalized*. During iteration of the above steps the parameters approach fixed points (FP), where analysis of this convergence allows one to derive critical properties of the transition. The technical details of RG approaches vary widely.

In this work a real-space RG approach is used. For better understanding, it is illustrated by its application to the classical case of bond percolation on a 2D square lattice [Ber78, RKS77, SA92], which is an instructive example showing advantages and as well as drawbacks of this technique. For the chosen 2D percolation network, the connectivity of the network is based on links between next-neighbor nodes only. These bonds between neighboring nodes are placed with a certain probability  $p$  which is the same all over the network. In Fig. 3.1 four sample percolation networks, each for a different value of  $p$ , are shown. Starting with an empty network ( $p = 0$ ) of size  $L \times L$ , single separated bonds appear for larger  $p$ . When increasing  $p$  further, nodes connected by bonds start to form clusters (see Fig. 3.1a). These clusters then grow in size until the first cluster extends over the whole sample, connecting one side with the opposite side of the network as shown in Fig. 3.1c. At this point the percolation threshold  $p_c(L)$  is reached and the cluster is percolating. The value obtained for  $p_c(L)$  depends on the actual random realization of the network. Only in the limit  $L \rightarrow \infty$  a unique value  $p_c$  is found which is a characteristic sample-independent quantity for the specific network. A high precision numerical calculation of  $p_c$  requires large computational effort. As it is demonstrated in the following the RG approach permits to approximate  $p_c$  rather easily.

The real-space RG approach is based on the assumption that a certain part of the network, the so-called RG unit, can represent the essential physics of the entire network. In the case of bond percolation the RG unit therefore consists of a small number of bonds. This unit is replaced within the RG transformation by a single

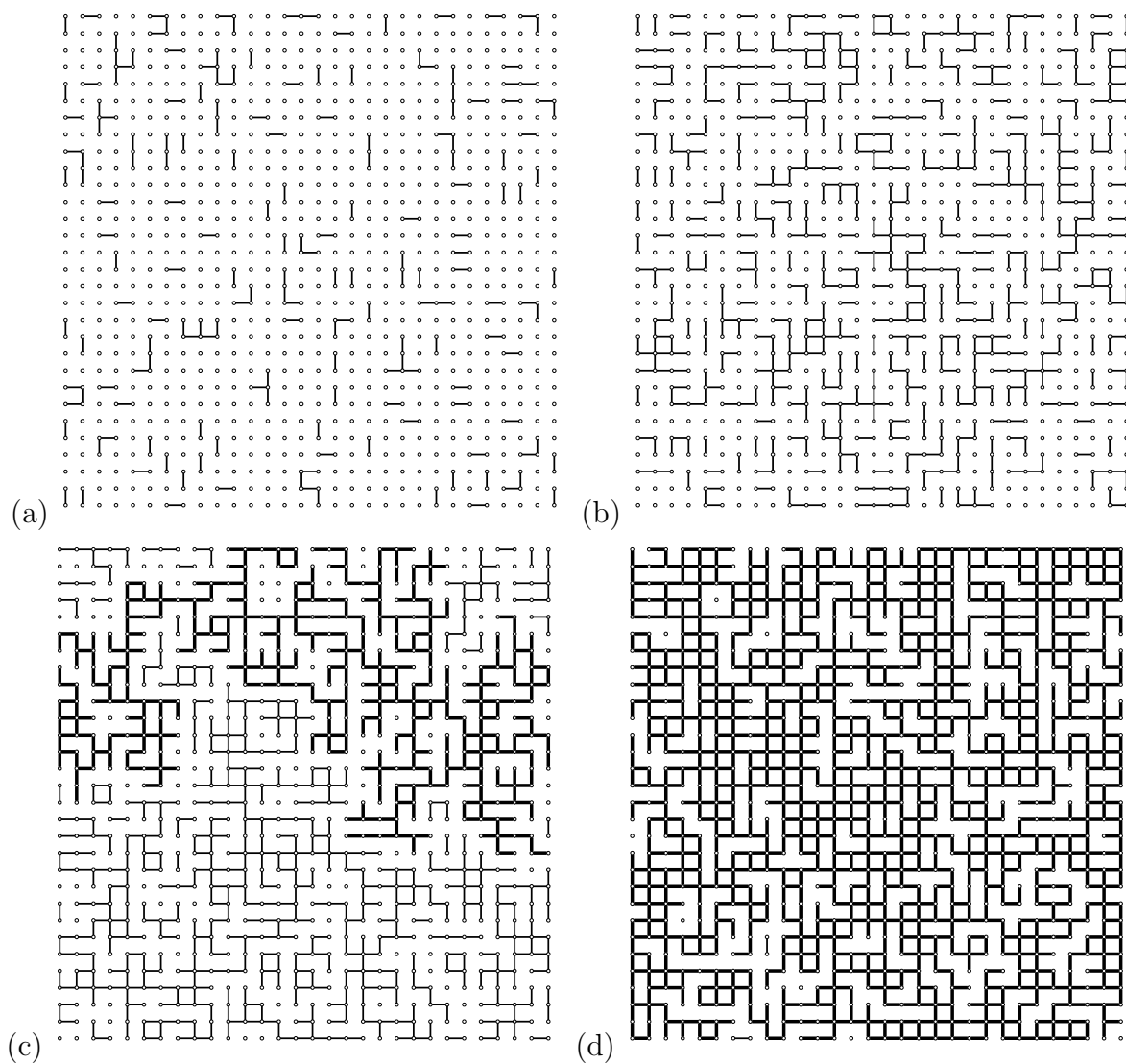


Figure 3.1: 2D bond percolation networks on a  $30 \times 30$  square lattice (dots) for different bond probabilities  $p = 0.1$  (a),  $0.3$  (b),  $0.5$  (c), and  $0.7$  (d). The bonds are indicated by lines. Thick bonds belong to the percolating cluster connecting opposite borders of the sample. The percolation threshold is at  $p = 0.5$ .



Figure 3.2: Illustration of the RG approach to the 2D bond percolation. A five-bond RG unit (left) is mapped onto a single super bond (right).

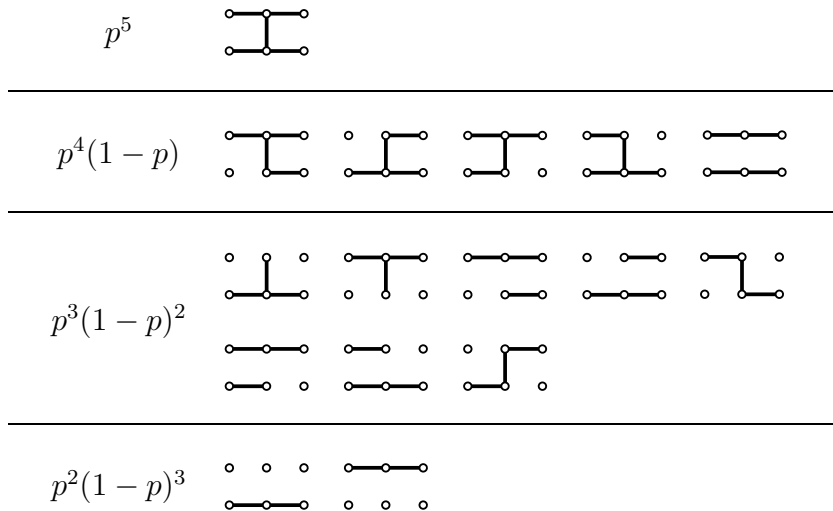


Figure 3.3: All possible configurations for a connecting 2D bond RG unit grouped according to their probability.

super bond with its probability  $p'$  determined by the  $p$ 's of the constituting bonds. From the super bonds one can construct again a percolation network which is then renormalized in the same way as the original network. Successive repetition of the RG transformation yields the information about very large samples, since, after each RG step, the effective sample size grows by a certain factor determined by the geometry of the original RG unit. For this example an RG unit proposed in [RKS77] is used. A super bond consists of 5 bonds forming an H-like shape as shown in Fig. 3.2. The probability  $p'$  of a super bond can now be calculated by the sum over all configurations which connect the left to the right end of the RG unit as illustrated in Fig. 3.3. The probability of a single configuration is the product over the five bond probabilities where a closed bond contributes  $p$  while an open bond is associated with  $1 - p$ . Therefore one obtains

$$p' = p^5 + 5p^4(1 - p) + 8p^3(1 - p)^2 + 2p^2(1 - p)^3. \quad (3.1)$$

In order to determine  $p_c$  the FP condition  $p' = p_c = p$  at the percolation threshold is utilized. Solving Eq. (3.1) one finds three FPs. Two coincide with the trivial solutions  $p_c = 0$  and 1. The third nontrivial result is  $p_c = 1/2$  [Gri89]. For the estimation of the critical exponent  $\nu_{\text{bond}}$  of the correlation length at the percolation transition one can define a characteristic length

$$\xi = a(p_c - p)^{-\nu_{\text{bond}}}, \quad (3.2)$$

where  $a$  is the lattice constant in the original network. In the super network the same behavior should be observed, but here the lattice constant is  $2a$  since the size of the RG unit has to be taken into account. Using  $\xi = \xi'$  and  $p_c = 1/2$  one obtains from Eq. (3.2)

$$\nu_{\text{bond}} = \frac{\ln 2}{\ln(dp'/dp)} \Big|_{p=1/2} \approx 1.428 \quad (3.3)$$

This result is derived purely analytical. Therefore the deviation from the exact value  $\nu_{\text{bond}} = 4/3$  [SA92] of only 7% is the consequence of the chosen RG unit and its ability to describe the network.

The above example demonstrates that the RG approach is very appropriate for the study of large systems since with each RG transformation the system size scales with a certain factor depending on the size of the RG unit. On the other hand it is obvious, that the RG approach cannot provide exact results because a single RG unit is a rather crude approximation of the real network, e.g, the full connectivity of the network cannot be preserved. It is therefore necessary to check the accuracy of the method for each application.

In the next Section the RG approach to the CC model is introduced. The derivation of the critical exponent is explained in Section 3.3. It follows the presentation of the numerical results in Section 3.4 and an extensive comparison with previous works in Section 3.5. In Section 3.6 the influence of the RG unit is studied. Concluding remarks are given in Section 3.7.

## 3.2 Quantum RG approach

The real-space RG approach [AJS97, GR97] can be applied to the CC network analogously to the case of 2D bond percolation described in the previous Section. An RG unit is constructed containing several SPs from a CC network. For these SPs the RG transformation has to relate their  $S$  matrices with the  $S$  matrix of the super-SP. The RG unit used here is extracted from a CC network on a regular 2D square lattice. The super-SP consists of five original SPs connected according to Fig. 3.4. In Fig. 3.4 the very same RG unit is illustrated in two different ways. In Fig. 3.4a circles correspond to SPs and lines to links in the network. Using this intuitive picture one can identify the loss of connectivity in comparison with the original CC network, namely, the four edge nodes within a  $3 \times 3$  SP pattern are fully neglected and their outer bonds are left out. Thus the super-SP has the same number of incoming and outgoing channels as an original SP. Fig. 3.4b is used to emphasize the relation with the 2D bond percolation RG. Here SPs are drawn as lines and links as arcs. In analogy to bond percolation the SPs of the RG unit form an H-like shape. Therefore, also for this RG to the CC network, the size of the RG unit in terms of lattice spacings equals 2.

Between the SPs of the RG unit an electron travels along equipotential lines, and accumulates a certain Aharonov-Bohm phase as in the original network. Different phases are uncorrelated, which reflects the randomness of the original potential landscape. As mentioned in Section 2.3 each SP is described by an  $S$  matrix which

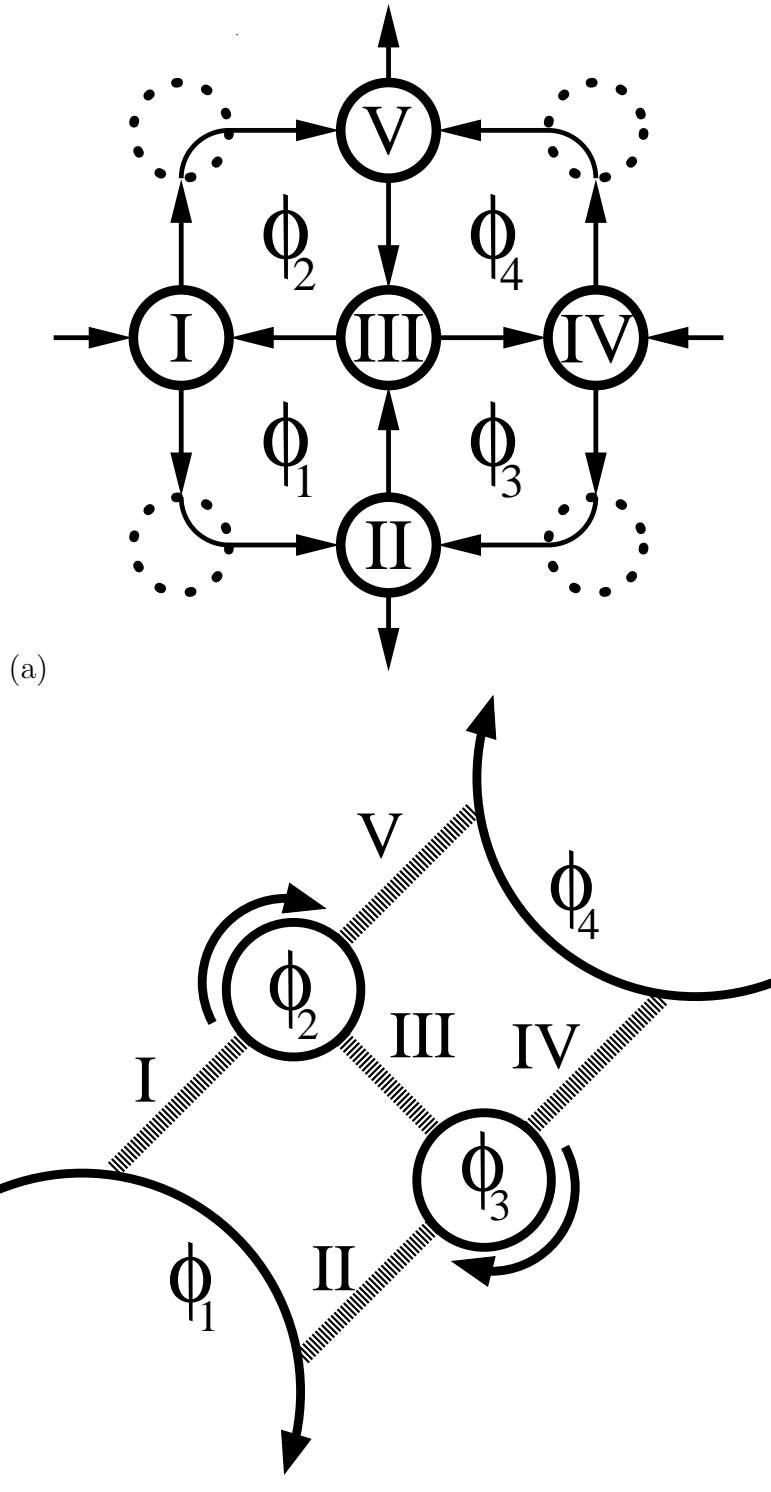


Figure 3.4: Two illustrations of the same RG unit used for Eq. (3.8) combining five SPs. The upper figure shows nodes as circles and links as lines. The dotted circles indicate nodes of the CC network that are neglected in the construction of the RG unit. In the lower picture the nodes correspond to thick dashed lines — in analogy with classical 2D bond percolation RG presented in Fig. 3.2 [Ber78, RKS77].  $\Phi_1, \dots, \Phi_4$  are the phases acquired by an electron drifting along the contours indicated by the arrows.

contributes two equations relating the wave-function amplitudes of incoming  $I_i, I_i^*$  and outgoing  $O_i, O_i^*$  channels. All amplitudes  $I_i, I_i^*$  besides the external  $I_1$  and  $I_4^*$  can then be expressed by  $O_i, O_i^*$  using the phases, e.g.  $I_5 = e^{i\Phi_{15}}O_1$ , where  $\Phi_{15}$  is the phase shift along the link between SPs  $I$  and  $V$ . The resulting ten modified scattering equations form a linear system which has to be solved in order to obtain the transmission properties of the corresponding super-SP:

$$A\mathbf{x} = \mathbf{b} \quad (3.4)$$

with

$$A = \begin{pmatrix} 1 & 0 & 0 & 0 & 0 \\ 0 & 1 & 0 & 0 & 0 \\ 0 & -t_2 e^{i\Phi_{12}} & 1 & 0 & 0 \\ 0 & -r_2 e^{i\Phi_{12}} & 0 & 1 & 0 \\ 0 & 0 & -r_3 e^{i\Phi_{23}} & 0 & 1 \\ 0 & 0 & t_3 e^{i\Phi_{23}} & 0 & 0 \\ 0 & 0 & 0 & 0 & t_4 e^{i\Phi_{34}} \\ 0 & 0 & 0 & 0 & -r_4 e^{i\Phi_{34}} \\ -t_5 e^{i\Phi_{15}} & 0 & 0 & 0 & 0 \\ -r_5 e^{i\Phi_{15}} & 0 & 0 & 0 & 0 \end{pmatrix} \Rightarrow \quad (3.5)$$

$$\Rightarrow \begin{pmatrix} -r_1 e^{i\Phi_{31}} & 0 & 0 & 0 & 0 \\ t_1 e^{i\Phi_{31}} & 0 & 0 & 0 & 0 \\ 0 & 0 & -r_2 e^{i\Phi_{42}} & 0 & 0 \\ 0 & 0 & t_2 e^{i\Phi_{42}} & 0 & 0 \\ 0 & 0 & 0 & 0 & -t_3 e^{i\Phi_{53}} \\ 1 & 0 & 0 & 0 & -r_3 e^{i\Phi_{53}} \\ 0 & 1 & 0 & 0 & 0 \\ 0 & 0 & 1 & 0 & 0 \\ 0 & -r_5 e^{i\Phi_{45}} & 0 & 1 & 0 \\ 0 & t_5 e^{i\Phi_{45}} & 0 & 0 & 1 \end{pmatrix},$$

$$\mathbf{x} = (O_1, O_1^*, O_2, O_2^*, O_3, O_3^*, O_4, O_4^*, O_5, O_5^*)^T \quad (3.6)$$

and

$$\mathbf{b} = (t_1 I_1, r_1 I_1, 0, 0, 0, 0, r_4 I_4^*, t_4 I_4^*, 0, 0)^T. \quad (3.7)$$

Note that the amplitudes on the external links coincide with the amplitudes of the super-SP as  $I_1 = I', I_4^* = I'^*$ ,  $O_5 = O'$  and  $O_2^* = O'^*$ . Setting the incoming links of the super-SP according to  $I' = 1, I'^* = 0$  one can deduce the transmission coefficient  $t'$  of the super-SP, since  $O' = t'I' = t'1 = t'$ . For the transmission coefficient of the super-SP this method yields the following expression [GR97]:

$$t' = \left| \frac{t_1 t_5 (r_2 r_3 r_4 e^{i\Phi_3} - 1) + t_2 t_4 e^{i(\Phi_1 + \Phi_4)} (r_1 r_3 r_5 e^{-i\Phi_2} - 1) + t_3 (t_2 t_5 e^{i\Phi_1} + t_1 t_4 e^{i\Phi_4})}{(r_3 - r_2 r_4 e^{i\Phi_3})(r_3 - r_1 r_5 e^{i\Phi_2}) + (t_3 - t_4 t_5 e^{i\Phi_4})(t_3 - t_1 t_2 e^{i\Phi_1})} \right|. \quad (3.8)$$

Here  $\Phi_j$  corresponds to the sum over the three phases forming a closed loop within the RG unit (see Fig. 3.4). Equation (3.8) is the RG transformation, which allows one to generate (after averaging over  $\Phi_j$ ) the distribution  $P(t')$  of the transmission coefficients of super-SPs using the distribution  $P(t)$  of the transmission coefficients of the original SPs. Since the transmission coefficients of the original SPs depend on the electron energy  $\varepsilon$ , the fact that delocalization occurs at  $\varepsilon = 0$  implies that a certain distribution,  $P_c(t)$  — with  $P_c(t^2)$  being symmetric with respect to  $t^2 = \frac{1}{2}$  — is the FP distribution of the RG transformation Eq. (3.8). The distribution  $P_c(G)$  of the dimensionless conductance  $G$  can be obtained from the relation  $G = t^2$ , so that

$$P_c(G) \equiv \frac{1}{2t} P_c(t) \quad . \quad (3.9)$$

### 3.3 Critical exponent

Since the dimensionless SP height  $z_i$  and the transmission coefficient  $t_i$  at  $\varepsilon = 0$  are related by Eq. (2.13), transformation (3.8) also determines the height of a super-SP by the heights of the five constituting SPs. Correspondingly, the distribution  $P(G)$  determines the distribution  $Q(z)$  of the SP heights via  $Q(z) = P(G)|dG/dz| = \frac{1}{4} \cosh^{-2}(z/2) P[(e^z + 1)^{-1}]$ . In fact,  $Q(z)$  is not a characteristic of the actual SPs, but rather, as demonstrated below, represents a convenient parametrization of the conductance distribution.

The language of the SP heights provides a natural way to extract the critical exponent  $\nu$ . Suppose that the RG procedure starts with an initial distribution,  $Q_0(z) = Q_c(z - z_0)$ , that is shifted from the critical distribution,  $Q_c(z)$ , by a small  $z_0 \propto \varepsilon$ . The meaning of  $z_0$  is an additional electron energy measured from the center of the Landau band. The fact that the QH transition is infinitely sharp at  $z_0 = 0$  implies that for any  $z_0 \neq 0$ , the RG procedure drives the initial distribution  $Q(z - z_0)$  away from the FP. Since  $z_0 \ll 1$ , the first RG step would yield  $Q_c(z - \tau z_0)$  with some number  $\tau$  independent of  $z_0$ . At the  $n$ th step the center of the distribution will be shifted by  $z_{\max, n} = \tau^n z_0$ , while the sample size will be magnified by  $2^n$ . After a certain number of steps, say  $n_L$ , the shift will grow to

$$z_{\max, n_L} = \tau^{n_L} z_0 \sim 1, \quad (3.10)$$

where a typical SP is no longer transmittable. Then the localization length  $\xi$  can be identified with the system size  $2^{n_L} a$  where  $a$  is the lattice constant of the original RG unit. Using this relation one can rewrite  $\tau^{n_L}$  in Eq. (3.10) as a power of  $(\xi/a)$

$$(\xi/a)^{(\ln \tau / \ln 2)} z_0 \sim 1. \quad (3.11)$$

from which follows that  $\xi$  diverges as

$$\xi \sim a z_0^{-(\ln 2 / \ln \tau)} = a z_0^{-\nu} \quad (3.12)$$

with  $\nu = \ln 2 / \ln \tau$ . When the RG procedure is carried out numerically, one should check that  $z_0$  is small enough so that  $z_{\max, n} \propto z_0$  for large enough  $n$ . Consequently,

the working formula for the critical exponent can be presented as

$$\nu = \frac{\ln 2^n}{\ln \left( \frac{z_{\max,n}}{z_0} \right)} \quad (3.13)$$

which should be independent of  $n$  for large  $n$ .

### 3.4 Numerical results

In order to find the FP conductance distribution  $P_c(G)$ , the RG is started from a certain initial distribution of transmission coefficients,  $P_0(t)$  (see below). The distribution is discretized in at least 1000 bins, such that the bin width is typically 0.001 for the interval  $t \in [0, 1]$ . From  $P_0(t)$ , the  $t_i$ ,  $i = 1, \dots, 5$ , are obtained and substituted into the RG transformation (3.8). The phases  $\Phi_j$ ,  $j = 1, \dots, 4$  are chosen randomly from the interval  $\Phi_j \in [0, 2\pi)$ . In this way at least  $10^7$  super-transmission coefficients  $t'$  are calculated. In order to decrease statistical fluctuations the obtained histogram  $P_1(t')$  is then smoothed using a Savitzky-Golay filter [PFTV92] over 13 consecutive bins approximated by a 6th order polynomial. At the next step the procedure is repeated using  $P_1$  as an initial distribution. The convergence of the iteration process is assumed when the mean-square deviation  $\int dt [P_n(t) - P_{n-1}(t)]^2$  of the distribution  $P_n$  and its predecessor  $P_{n-1}$  deviate by less than  $10^{-4}$ .

The actual initial distributions,  $P_0(t)$ , were chosen in such a way that corresponding conductance distributions,  $P_0(G)$ , were either uniform or parabolic, or identical to the FP distribution found semianalytically [GR97]. All these distributions are symmetric with respect to  $G = 0.5$ . One can observe that, regardless of the choice of the initial distribution, after 5–10 steps the RG procedure converges to the *same* FP distribution which remains unchanged for another 4–6 RG steps. Small deviations from the symmetry with respect to  $G = 0.5$  finally accumulate due to numerical instabilities in the RG procedure, so that typically after 15–20 iterations the distribution becomes unstable and flows toward one of the classical FPs  $P(G) = \delta(G)$  or  $P(G) = \delta(G - 1)$ . Therefore the symmetry of the  $P_0(G)$  with respect to  $G = 0.5$  is an important requirement in order to converge to the quantum FP at all. Note that the FP distribution can be stabilized by forcing  $P_n(G)$  to be symmetric with respect to  $G = 0.5$  in the course of the RG procedure.

Figure 3.5 illustrates the RG evolution of  $P(G)$  and  $Q(z)$ . In order to reduce statistical fluctuations the FP distribution is averaged over nine results obtained from three different  $P_0(G)$ 's. The FP distribution  $P_c(G)$  exhibits a flat minimum around  $G = 0.5$ , and sharp peaks close to  $G = 0$  and  $G = 1$ . It is symmetric with respect to  $G \approx 0.5$  with  $\langle G \rangle = 0.498 \pm 0.004$ , where the error is the standard error of the mean of the obtained FP distribution. Consequently, the FP distribution  $Q_c(z)$  is symmetric with respect to  $z = 0$ , which corresponds to the center of the Landau band. The shape of  $Q_c(z)$  is close to Gaussian.

Let us now turn to the critical exponent  $\nu$ . As a result of the general instability of the FP distribution, an initial shift of  $Q_c(z)$  by a value  $z_0$  results in the further drift of the maximum position,  $z_{\max,n}$ , away from  $z = 0$  after each RG step. As



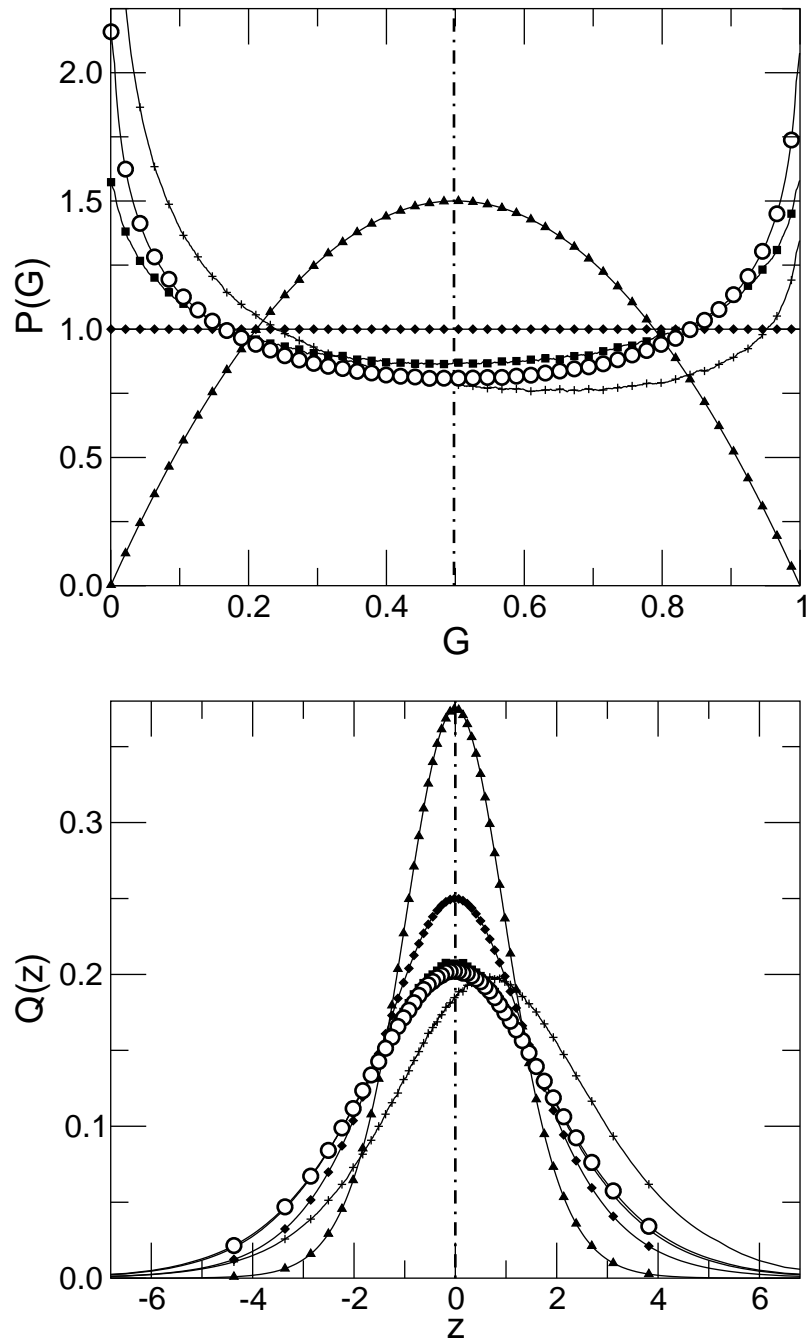


Figure 3.5: Top:  $P(G)$  (thin lines) as function of conductance  $G$  at a QH plateau-to-plateau transition. Symbols mark every 20th data point for different initial distributions ( $\blacksquare, \blacklozenge, \blacktriangle$ ), the FP distribution ( $\circ$ ) and a distribution for RG step  $n = 16$  ( $+$ ). The vertical dashed line indicates the average of the FP distribution. Bottom: Corresponding plots for the distribution  $Q(z)$  of SP heights.

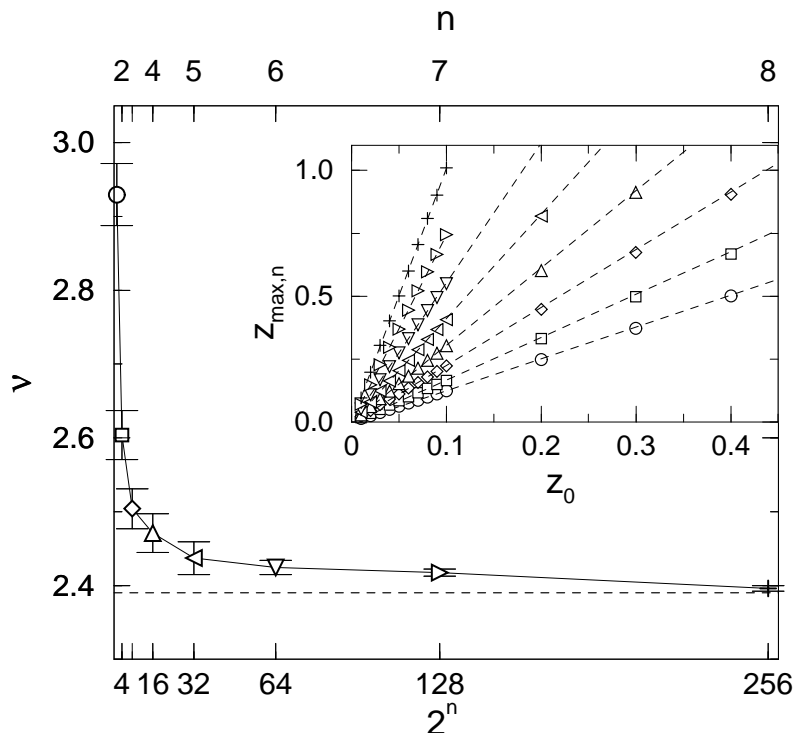


Figure 3.6: Critical exponent  $\nu$  obtained by the QH-RG approach as function of effective linear system size  $L = 2^n$  for RG step  $n$ . The error bars correspond to the error of linear fits to the data. The dashed line shows  $\nu = 2.39$ . Inset:  $\nu$  is determined by the dependence of the maximum  $z_{\max,n}$  of  $Q_n(z)$  on a small initial shift  $z_0$ . Symbols indicate the eight RG steps in accordance with the main plot. Dashed lines indicate the linear fits.

expected,  $z_{\max,n}$  depends linearly on  $z_0$ . This dependence is shown in Fig. 3.6 (inset) for different  $n$  from 1 to 8. The critical exponent is then calculated from the slope according to Eq. (3.13). Figure 3.6 illustrates how the critical exponent converges with  $n$  to the value  $2.39 \pm 0.01$ . The error corresponds to a confidence interval of 95% as obtained from the fit to a linear behavior.

Due to the high accuracy of the calculation of  $P_c(G)$ , one is able to reliably determine many central moments  $\langle (G - \langle G \rangle)^m \rangle$  of the FP distribution  $P_c(G)$ . These moments are plotted in Fig. 3.7. The results in the context of other works are discussed more thoroughly in the next Section.

## 3.5 Comparison with other works

By dividing the CC network into units, the RG approach completely disregards the interference of the wave-function amplitudes between different units at each RG step. For this reason it is not clear to what extent this approach captures the main features and reproduces the quantitative predictions at the QH transition. Therefore, a comparison of the RG results with the results of direct simulations of the CC model is crucial. These direct simulations are usually carried out by employing

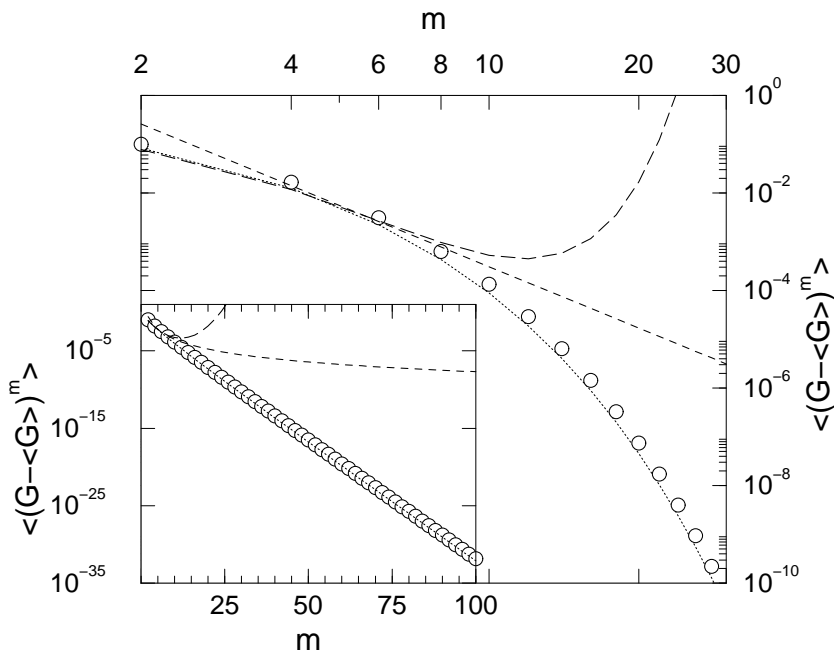


Figure 3.7: Moments  $\langle (G - \langle G \rangle)^m \rangle$  of the FP distribution  $P_c(G)$  ( $\circ$ ). Dashed lines are the results from [WJL96]. The dotted line corresponds to the moments of a constant distribution. Inset: Higher moments of  $P_c(G)$  following an exponential behavior.

either the quasi-1D version [MK81] or the 2D version [FL81] of the transfer-matrix method. The results when applying the version of [MK81] to the CC model are reported in [CC88] and [LWK93]. In [CF97, JW98, WJL96] the other version [FL81] was utilized. For the critical exponent the values  $\nu = 2.5 \pm 0.5$  [CC88] and later  $\nu = 2.4 \pm 0.2$  [LWK93] were obtained. Note that the result of the previous Section is in excellent agreement with these values, and is also consistent with the most precise  $\nu = 2.35 \pm 0.03$  [Huc92]. This already indicates the remarkable accuracy of the RG approach.

In [CF97, JW98, WJL96] the critical distribution  $P_c(G)$  of the conductance was studied.  $P_c(G)$  was found to be broad, which is in accordance with Fig. 3.5. However, a more detailed comparison is impossible, since the results of the simulations [CF97, JW98, WJL96] do not obey the electron-hole symmetry condition  $P_c(G) = P_c(1 - G)$ . On the other hand, within the RG approach, the latter condition is satisfied automatically. Nevertheless, one can compare the moments of  $P_c(G)$  to those calculated in [WJL96] and [CF97]. In [CF97] only the standard deviation  $(\langle G^2 \rangle - \langle G \rangle^2)^{1/2} \approx 0.3$  was computed. The RG result is 0.316. In [WJL96] moments up to  $m = 8.5$  were obtained and fitted by two analytical functions, which are shown in Fig. 3.7. They agree with the RG calculations up to the sixth moment. Here one should point out that the moments from [WJL96] can hardly be distinguished from the moments of a uniform distribution. This reflects the fact that  $P_c(G)$  is practically flat except for the peaks close to  $G = 0$  and  $G = 1$ .

In [WLS98] and [ABB99]  $P_c(G)$  was studied by methods which are not based on

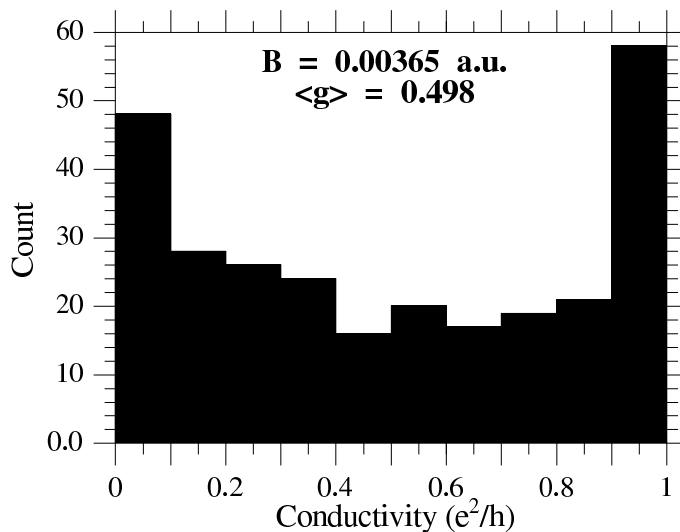


Figure 3.8:  $P_c(G)$  found by Avishai *et al.* [ABB99] showing similar behavior as the RG result in Fig. 3.5 but with less accurate statistics.

the CC model. Both works reported a broad distribution  $P_c(G)$ . In [WLS98]  $P_c(G)$  was found to be almost flat. The major difference between [WLS98] and Fig. 3.5 is the behavior of  $P_c(G)$  near the points  $G = 0$  and 1. That is,  $P(G)$  drops in [WLS98] to zero at the ends, while Fig. 3.5 exhibits maxima. In [ABB99], as shown in Fig. 3.8, the behavior of  $P_c(G)$  is qualitatively similar to Fig. 3.5, with maxima at  $G = 0$  and 1. However, the statistics in [ABB99] are rather poor, which again rules out the possibility of a more detailed comparison with the results presented here.

Finally, one should point out that the results of this work agree completely with [JMMW98, JMW98, WJ98] where a similar RG treatment of the CC model was carried out. The numerical data of this work have a higher resolution, and show significantly less statistical noise. This is because one could take advantage of faster computation by using the analytical solution (3.8) of the RG [GR97]. Also note that in [WJ98] and [JMMW98] the critical exponent  $\nu = 3.5 \pm 0.3$  was calculated using a procedure different from that described in Section 3.3. In order to compare the results  $\nu$  has to be rescaled by  $\ln 2 / \ln 3$  which yields  $\nu \approx 2.2$  [WJ98]. Thus the values of  $\nu$  determined by both methods are close. One should emphasize that a systematic improvement of the RG procedure, i.e., by inclusion of more than five SPs into the basic RG unit as reported in [JMMW98, JMW98, WJ98], leads to similar results. In contrast, using a smaller RG unit [ZS01] discussed in the next Section fails in describing the critical properties of the QH transition correctly. In order to study the critical distribution of the conductance experimentally the measurement has to be performed in a coherent transport regime. Due to the relatively large sample size in usual QH experiments the measured conductance is an average over the incoherent parts of the sample. Then one obtains a smooth behavior at the transition as demonstrated in Figs. 2.2 and 2.3 instead of fluctuations. For a coherent measurement mesoscopic QH samples were used [CBF99, CK96]. Figure 3.9 shows that an almost uniform conductance distribution was found [CK96]. Although this

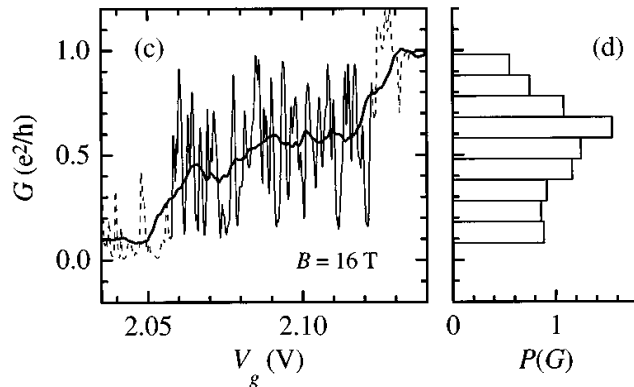


Figure 3.9: Experimental results for  $P_c(G)$  from [CK96]. The left plot shows the fluctuations of the two-terminal conductance at the first QH transition as function of the gate voltage  $V_g$ . Averaging over a 16mV interval yields the thick line. The right plot displays  $P_c(G)$  as a histogram of the conductance data from the left side.

result is consistent with theoretical predictions with respect to the dominating flat part of the distribution, further detailed analysis of the mesoscopic pattern [CBF99] has revealed the crucial role of the charging effects, which were neglected in all theoretical studies.

### 3.6 Test of a different RG unit

Apparently, the quality of the RG approach crucially depends on the choice of the RG unit. For the construction of a properly chosen RG unit two conflicting aspects have to be considered. (i) With the size of the RG unit also the accuracy of the RG approach increases since the RG unit can preserve more connectivity of the original network. (ii) As a consequence of larger RG units the computational effort for solving the scattering problem rises, especially in the case where an analytic solution, as Eq. (3.8), is not attained. Because of these reasons building an RG unit is an optimization problem depending mainly on the computational resources available. As mentioned in the previous Section larger RG units were already studied in [JMMW98, JMW98, WJ98]. In these works the authors could not benefit from an analytic solution and achieve only a similar and less accurate statistics in comparison with the results presented here. In this Section the opposite case is studied using a small RG unit proposed in [ZS01] in the context of the Hall resistivity.

The super-SP now consists only of 4SP as shown in Fig. 3.10. It resembles the 5SP unit (see Fig. 3.4) used previously leaving out the SP in the middle of the structure. Again the scattering problem can be formulated as a system of now 8 equations which is solved analytically:

$$t'_{4SP} = \left| \frac{t_1 t_4 (r_2 r_3 e^{i\Phi_3} - 1) + t_2 t_3 e^{i\Phi_2} (r_1 r_4 e^{-i\Phi_1} - 1)}{(1 - r_2 r_3 e^{i\Phi_3})(1 - r_1 r_4 e^{i\Phi_1}) + t_1 t_2 t_3 t_4 e^{i\Phi_2}} \right|. \quad (3.14)$$

The result can be verified using Eq. (3.8) after setting  $t_3 = 0$  and  $r_3 = 1$ , joining

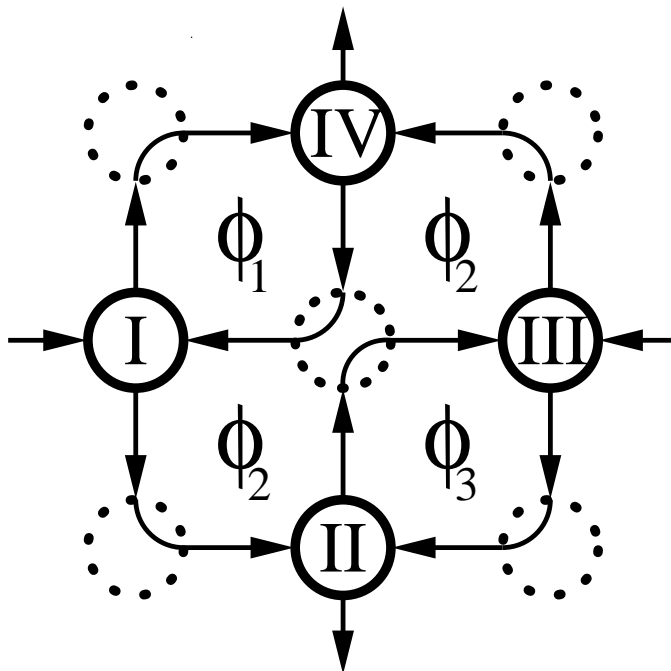


Figure 3.10: RG unit constructed from 4SP indicated by full circles. Some connectivity is neglected (dotted circles). The phases  $\Phi_j$  are accumulated by the electron motion (arrows) along contours of the energy potential.

the phases  $\Phi_1$  and  $\Phi_4$  and renumbering the indices.

The RG transformation (3.14) is then applied within the RG approach analogously to the 5SP unit. First the FP distribution  $P_c(G)$  is obtained. A comparison of  $P_c(G)$  for both RG units is shown in Fig. 3.11. The 4SP unit yields differing results. While  $P_c(G)$  is still rather flat it is clearly asymmetric, which already indicates that the 4SP unit cannot describe all of the underlying symmetry of the CC network.

The  $P_c(G)$  for the 4SP unit is then used in the calculation of the critical exponent  $\nu$  to construct the shifted initial distributions  $Q_0(z)$ . Note that the maximum of  $Q_c(z)$  is already shifted away from  $z = 0$  due to the asymmetry of  $P_c(G)$ . The behavior of  $\nu$  as function of  $n$  for the 4SP and 5SP RG units is demonstrated in Figure 3.12. Both curves approach convergence monotonously from larger values of  $\nu$ . During all iteration steps,  $\nu$  for the 4SP differs from the 5SP result by an almost constant positive shift. After 8 iterations, which equals an increase of system size by a factor of 256, one finds  $\nu_{5SP} = 2.39 \pm 0.01$  and  $\nu_{4SP} = 2.74 \pm 0.02$ . The error describes a confidence interval of 95% as obtained from the fit to a linear behavior. The result for  $\nu_{4SP}$  deviates clearly from the 5SP result and also from the values obtained by other methods [CC88, Huc92, LWK93]. In addition to these findings also the discussion in Section 3.4 indicates that the 4SP RG unit fails to describe the critical properties at the QH transition correctly. This fact underlines again the importance of the RG unit for a successful application of the RG approach.

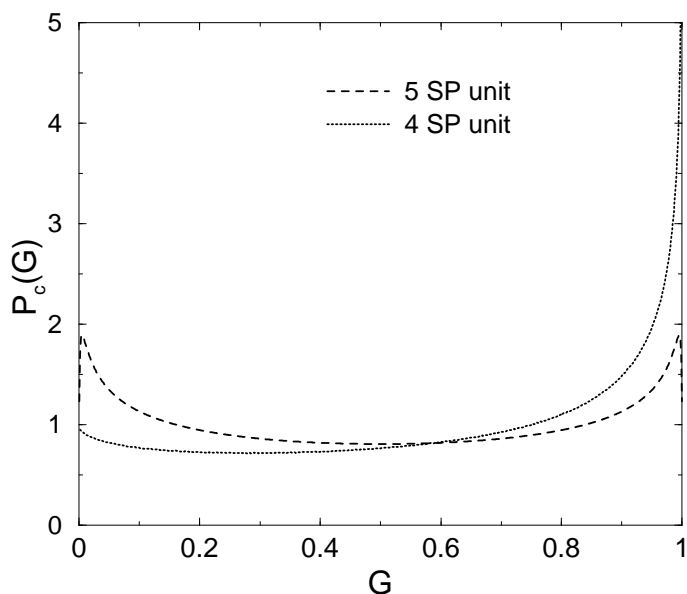


Figure 3.11: Comparison of the critical distribution of the conductance  $P_c(G)$  at the QH transition obtained using the 5SP (dashed line) and 4SP (dotted line) RG unit. The latter clearly deviates from the expected symmetry with respect to  $G = 0.5$ .

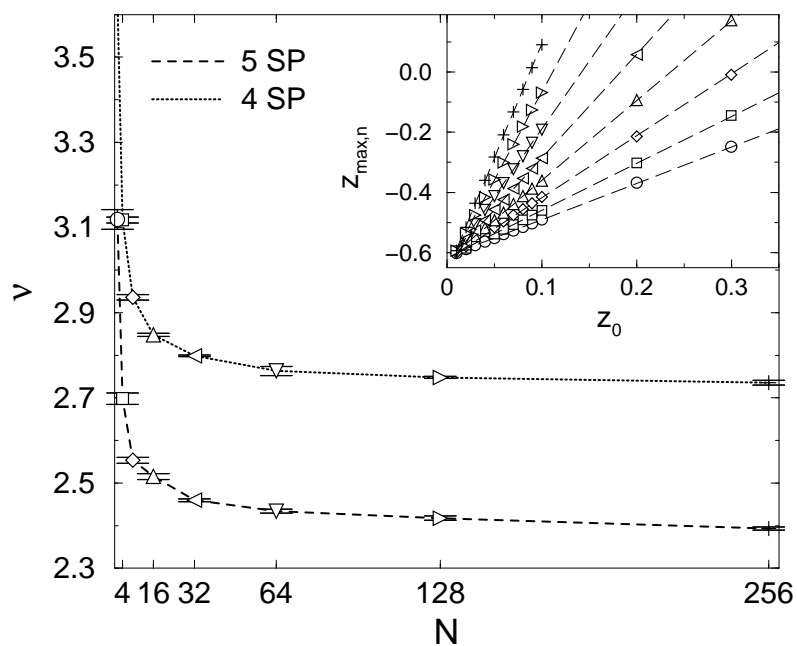


Figure 3.12: The critical exponent  $\nu$  as function of the effective system size  $N = 2^n$  for 4SP (dotted line) and 5SP unit (dashed line). Inset: Maximum  $z_{\max,n}$  of  $Q(z)$  vs. initial shift  $z_0$  for 8 RG iterations (symbols) using 4SP. Dashed lines indicate linear fits. The iterations start with  $z_{\max} < 0$  because of the asymmetry of  $P_c(G)$  for the 4SP unit.

## 3.7 Conclusion

The real-space RG approach allows only a crude approximation of the network, since links of the network are cut and the full connectivity of the network is not preserved. Therefore for the determination of  $P_c(G)$  and  $\nu$ , it is essential to construct the RG unit in such a way that it includes the symmetry of the network and the corresponding physical problem.

It was shown that a suitable chosen 5SP unit permits the study of the QH transition with high accuracy. The critical distribution  $P_c(G)$  of the conductance was obtained precisely and the critical exponent  $\nu = 2.39 \pm 0.01$  could be calculated.

Furthermore it was demonstrated that a simple 4SP RG unit only provides a rough picture of the critical properties of the QH transition while the slightly larger 5SP unit yields surprisingly accurate results. It also seems obvious that the accuracy of the RG approximation should be further enhanced when increasing the size of the RG unit [WJ98]. However from a numerical point of view one benefits from the analytic form of Eq. (3.8), which is not known for larger RG units.

One can conclude that the test of the RG approach against other simulations proves that this approach provides a very accurate quantitative description of the QH transition. It can now be used to study the phases of the RG unit as presented in the following Chapter.



# Chapter 4

## RG approach to the LSD

### 4.1 Introduction

The calculation of the energy LSD is an established method in the study of an LD transition. It relies on the exact knowledge about consecutive eigenenergies of a system. The LSD  $P(s)$  describes the probability to find neighboring energy levels at an energy distance  $s$ . At the LD transition the wave functions of the electrons change from being extended in the conducting to being localized in the insulating regime. This crossover is also observed in the correlation of the corresponding energy levels. Hence the shape of the LSD at the LD transition is a consequence of the localization behavior of the wave function. Wave functions of localized electrons are bound to a small volume in space. Therefore the wave functions are spatially uncorrelated which results in an uncorrelated energy spectrum. Thus the LSD agrees with the Poisson statistics characterized by an exponential decay. On the conducting side wave functions extend over a large part of the sample. The overlap of the wave functions creates a correlation in the energy spectrum, which leads to level repulsion for small  $s$ . As explained in Section 2.3.3 the shape of  $P(s)$  in the metallic regime is predicted by RMT [Meh91, Wig55] and depends on the universality class the system belongs to. In case of the CC model this is the GUE from which follows

$$P_{\text{GUE}}(s) = \frac{32}{\pi^2} s^2 e^{-\frac{4}{\pi} s^2}. \quad (4.1)$$

Exactly at the mobility edge separating localized and extended states a third system-size independent, so-called critical LSD  $P_c(s)$  is found.  $P_c(s)$  lies between  $P_{\text{GUE}}(s)$  and the Poisson distribution and inherits properties of both distributions. The discussion of the shape of  $P_c(s)$  concentrates on the behavior in the tails. For small  $s$  it is established [BSZK96, KOSO96, Met98] that  $P_c(s)$  resembles the level repulsion found for extended wave functions. The large- $s$  behavior of  $P_c(s)$  attracted more attention [BS97, BSK98, BSZK96, Eva94, Eva95, FAB95, HS94b, KOSO96, Met98, Met99, MV98, OO95, SZ95, VHSP95, ZK97] because of contradicting initial predictions [KLAA94, SSS<sup>+</sup>93]. First numerical studies [Eva94, FAB95, HS94b, VHSP95] found agreement with the analytic prediction [KLAA94]  $P_c(s) \propto \exp(-as^\gamma)$  for  $s \gg 1$  obtained by mapping the LSD to a Gibbs distribution of a classical one-dimensional gas. Here level repulsion is partially preserved also for spacings much

larger than the mean level spacing. Furthermore the exponent  $\gamma = 1 + (\nu d)^{-1}$  was expected to be related to the spatial dimension  $d$  and the critical exponent  $\nu$  of the localization length at the LD transition. However, later numerical simulations [BSK98, Eva95, KOSO96, Met98, Met99, MV98, OO95, SZ95, ZK97] questioned these relations and rather favored a simple exponential decay  $P_c(s) \propto \exp(-bs)$  suggested previously by Shklovskii *et al.* [SSS<sup>+</sup>93]. The absence of level repulsion for spacings much larger than the mean level spacing could be demonstrated by high accuracy simulations [BSK98, ZK97]. The numerical works capture all mentioned universality classes and are based mainly on tight-binding models, like the Anderson model of localization [And58].

Moreover, the behavior of the LSD close to the mobility edge allows one to determine the value of the correlation length exponent  $\nu$  [SSS<sup>+</sup>93], thus avoiding an actual analysis of the spatial extent of the wave functions. For this reason, the energy level statistics constitutes an alternative to the MacKinnon-Kramer [PS81a, PS81b, MK81, MK83] and to the transmission-matrix [FL81, Lan70] approaches to the numerical study of localization. A common problem of all approaches is that the exponential divergence of the correlation length holds only for the infinite system, which is not evaluable directly by these numerical methods. Therefore calculations performed for finite system sizes are to be extrapolated by a suitable finite-size scaling (FSS) approach. In order to extract  $\nu$  from the LSD the one-parameter-scaling hypothesis [AALR79] is employed. This theory describes the scaling of a quantity  $\alpha(N; \{z_i\})$  — depending on the system size  $N$  and (external) system parameters  $\{z_i\}$  — onto a single curve by using a scaling function  $f$

$$\alpha(N; \{z_i\}) = f\left(\frac{N}{\xi_\infty(\{z_i\})}\right). \quad (4.2)$$

Using the scaling assumption one can now extrapolate  $f$  to  $N \rightarrow \infty$  from the finite-size results of the computations. The knowledge about  $f$  and  $\xi_\infty$  then allows one to derive the value of  $\nu$ .

Considering a 2D sample, all the states are localized in the absence of a magnetic field. The presence of a magnetic field breaks the time-reversal symmetry and leads to an infinitely sharp LD transition in two dimensions, the QH transition. For the critical LSD the existence of a Poissonian tail has been demonstrated by a numerical study [BS97]. Furthermore, using FSS a value of  $\nu$  close to the results of large-size simulations  $\nu = 2.5 \pm 0.5$  [CC88],  $2.4 \pm 0.2$  [LWK93], and  $2.35 \pm 0.03$  [Huc92] was obtained [BS97].

In this study again the CC model is employed together with a real-space RG approach. First, in Section 4.2 the RG approach is extended to the LSD at the QH transition. In Section 4.3 the numerical results for the LSD are presented and the validity of this method is demonstrated. The FSS analysis of the obtained LSD at the QH transition is subject of Section 4.4. Here a comparison with the obtained value of  $\nu$  from other works is given, in particular with the result of the RG approach to the conductance distribution from Section 3.4. The latter is by no means trivial, since the original RG transformation [GR97] related the conductances, i.e., the *absolute values* of the transmission coefficients, while the *phases* of the trans-

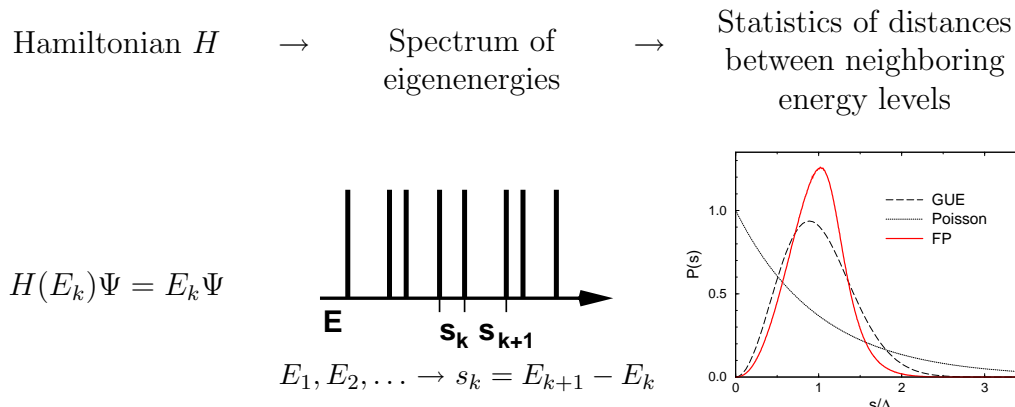


Figure 4.1: Illustration how to construct the LSD.

mission coefficients were assumed random and uncorrelated. In contrast, the level statistics at the transition corresponds to the FP in the distribution of these phases. Therefore, the success of the RG approach for conductances does not guarantee that it will be equally accurate *quantitatively* for the level statistics. Rather the universal features of the energy level statistics in a macroscopic fully coherent sample at the QH transition complement the universality in the conductance distribution.

## 4.2 Description of the RG approach to the LSD

The LSD is one of the prime level statistics besides the  $\Sigma_2$  and  $\Delta_3$  statistics [Meh91]. The evaluation of the LSD is schematically shown in Fig. 4.1. The necessary eigenenergies are usually obtained from the time-independent Schrödinger equation  $H\Psi = E_k\Psi$  by diagonalizing the Hamiltonian  $H$  [PFTV92]. After sorting the eigenenergies in ascending order the LSD is accumulated from spacings  $s_k = (E_{k+1} - E_k)/\Delta$ , where  $E_{k+1}$  and  $E_k$  are neighboring energy levels and  $\Delta$  corresponds to the mean level spacing. With the CC model based on wave propagation through the sample,  $H$  is not accessible directly. In this work therefore an alternative approach is used in order to reveal the eigenenergies. It has been shown by Fertig [Fer88], that the energy levels of a 2D CC network can be computed also from the energy dependence of the so-called network operator  $U(E)$ .  $U$  is constructed similar to the system of equations for obtaining the transmission coefficient  $t'$  of the RG unit as presented in Section 3.2. Every SP of the network contributes two scattering equations. Each of them describes the amplitude of one outgoing channel using the amplitudes of the two incoming channels weighted by the transmission and reflection coefficients  $t$  and  $r$  in which also the random phase  $\Phi$  of the links between SPs can be incorporated. When comparing to the calculation of the transmission coefficient  $t'$  an essential difference has to be taken into account. Energy levels are defined only in a closed system which requires to apply appropriate, usually periodic, boundary conditions. The energy dependence of  $U(E)$  enters through the energy dependence of the  $t_i(E)$  of the SPs, whereas the energy dependence of the phases  $\Phi_j(E)$  of the links is usually

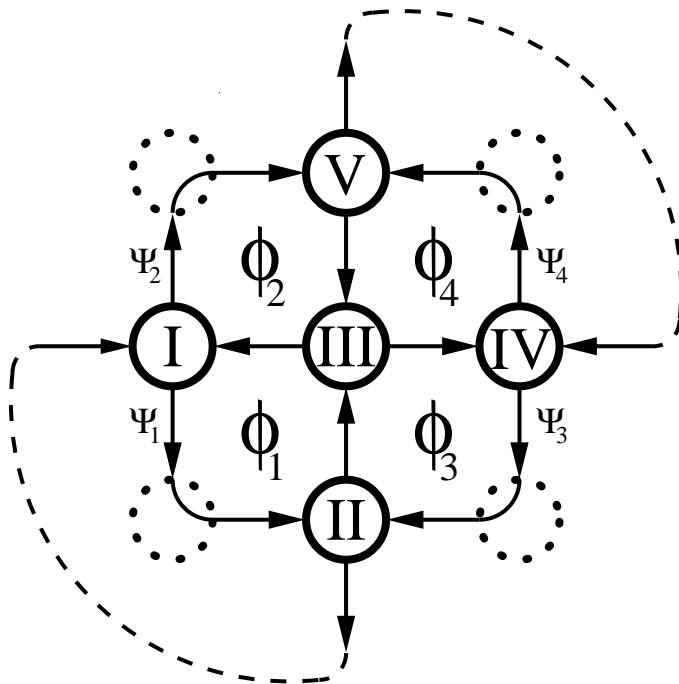


Figure 4.2: CC network on a square lattice consisting of nodes (circles) and links (arrows). The RG unit used to construct the matrix (4.5) combines five nodes (full circles) by neglecting some connectivity (dashed circles).  $\Phi_1, \dots, \Phi_4$  are the phases acquired by an electron along the loops as indicated by the arrows.  $\Psi_1, \dots, \Psi_4$  represent wave function amplitudes, and the thin dashed lines illustrate the boundary conditions used for the computation of level statistics.

neglected. Considering the vector  $\Psi$  of wave amplitudes on the links of the network,  $U$  acts similar as a time evolution operator. The eigenenergies can now be obtained from the stationary condition

$$U(E)\Psi = \Psi. \quad (4.3)$$

Nontrivial solutions exist only for discrete energies  $E_k$ , which coincide with the eigenenergies of the system [Fer88]. The eigenvectors  $\Psi_k$  correspond to the eigenstates on the links. The evaluation of the  $E_k$ 's according to Eq. (4.3) is numerically very expensive. For that reason a simplification was proposed [KM97a]. Instead of solving the real eigenvalue problem calculating a spectrum of quasienergies  $\omega$  is suggested following from

$$U(E)\Psi_l = e^{i\omega_l(E)}\Psi_l. \quad (4.4)$$

For fixed energy  $E$  the  $\omega_l$  are expected to obey the same statistics as the real eigenenergies [KM97a]. This approach makes it perfectly suited for large-size numerical simulations, e.g. studying  $50 \times 50$  SP networks.

In order to combine the above algorithm with the RG iteration, in which a rather small unit of SPs is considered, some adjustment is necessary. First, one has to “close” the RG unit at each RG step in order to discretize the energy levels. From the possible variants the closing is chosen as shown in Fig. 4.2 with dashed lines.

For a given closed RG unit with a fixed set of  $t_i$ -values at the nodes, the positions

of the energy levels are determined by the energy dependences,  $\Phi_j(E)$ , of the four phases along the loops. These phases change by  $\sim \pi$  within a very narrow energy interval, inversely proportional to the sample size. Within this interval the change of the transmission coefficients is negligibly small. The closed RG unit in Fig. 4.2 contains 10 links, and, thus, it is described by 10 amplitudes. Each link is characterized by an individual phase. On the other hand, it is obvious that the energy levels are determined only by the phases along the loops. One way to derive  $U$  is to combine the individual phases into phases  $\Phi_j$  connected to the four inner loops of the unit. The  $\Phi_j$  are associated with the corresponding ‘‘boundary’’ amplitudes  $\Psi_j$  (see Fig. 4.2). The original system of ten equations, which resembles Eq. (3.4) except for the boundary conditions, can then be transformed to four equations by expressing all amplitudes in terms of the  $\Psi_j$ . The resulting network operator takes the form

$$\begin{aligned}
 U = & \begin{pmatrix} (r_1 r_2 - t_1 t_2 t_3) e^{-i\Phi_1} & (t_1 r_2 + t_2 t_3 r_1) e^{-i\Phi_1} \\ -t_1 r_3 r_4 e^{-i\Phi_2} & r_1 r_3 r_4 e^{-i\Phi_2} \\ -t_1 t_4 r_3 e^{-i\Phi_4} & t_4 r_1 r_3 e^{-i\Phi_4} \\ -(t_2 r_1 + t_1 t_3 r_2) e^{-i\Phi_3} & -(t_1 t_2 - t_3 r_1 r_2) e^{-i\Phi_3} \end{pmatrix} \Rightarrow \\
 & \Rightarrow \begin{pmatrix} t_2 t_5 r_3 e^{-i\Phi_1} & t_2 r_3 r_5 e^{-i\Phi_1} \\ -(t_4 r_5 + t_3 t_5 r_4) e^{-i\Phi_2} & (t_4 t_5 - t_3 r_4 r_5) e^{-i\Phi_2} \\ (r_4 r_5 - t_3 t_4 t_5) e^{-i\Phi_4} & -(t_5 r_4 + t_3 t_4 r_5) e^{-i\Phi_4} \\ t_5 r_2 r_3 e^{-i\Phi_3} & r_2 r_3 r_5 e^{-i\Phi_3} \end{pmatrix}, \tag{4.5}
 \end{aligned}$$

which can be substituted in Eq. (4.4). Then the energy levels,  $E_k$ , of the closed RG unit including phases  $\Phi_j(E) = \Phi_j(E_k)$ , are the energies for which one of the four eigenvalues of the matrix  $U$  is equal to one, which corresponds to the condition  $\omega(E_k) = 0$ . Thus, the calculation of the energy levels reduces to a diagonalization of the  $4 \times 4$  matrix. It should be emphasized that the reduced size of  $U$  in comparison with the  $10 \times 10$  matrix resulting from the ‘‘straightforward’’ approach described in the beginning of this Section directly follows from considering the only relevant energy dependence in the four phases of the RG unit. Therefore a larger size of  $U$  would lead to redundant information for the energy levels.

The crucial step now is the choice of the energy dependence  $\Phi_j(E)$ . If each loop in Fig. 4.2 is viewed as a closed equipotential as it is the case for the first step of the RG procedure [CC88], then  $\Phi_j(E)$  is a true magnetic phase, which changes linearly with energy with a slope governed by the actual potential profile, which, in turn, determines the drift velocity. Thus

$$\Phi_j(E) = \Phi_{0,j} + 2\pi \frac{E}{s_j}, \tag{4.6}$$

where a random part,  $\Phi_{0,j}$ , is uniformly distributed within  $[0, 2\pi)$ , and  $2\pi/s_j$  is a random slope. Here the coefficient  $s_j$  acts as an initial level spacing connected to the loop  $j$  of the RG unit by defining a periodicity of the corresponding phase. Strictly speaking, the dependence (4.6) applies only for the first RG step. At each step,  $n > 1$ ,  $\Phi_j(E)$  is a complicated function of  $E$  which carries information about

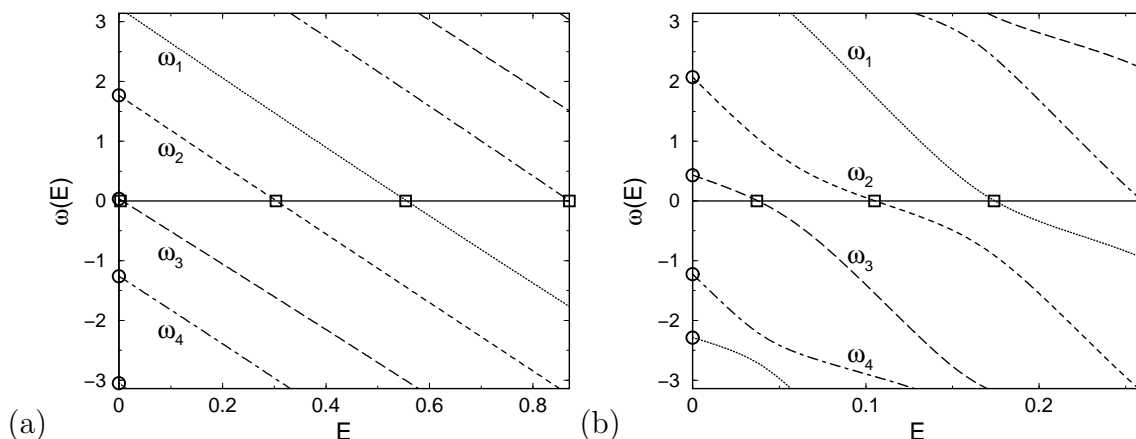


Figure 4.3: Energy dependence of the quasienergies  $\omega$  for two sample configurations. Instead of using the quasispectrum obtained from  $\omega_l(E = 0)$  ( $\circ$ ) the real eigenenergies are calculated according to  $\omega(E_k) = 0$  ( $\square$ ). Different line styles distinguish different  $\omega_l(E)$ . Note, that the observed behavior varies from sample to sample between remarkably linear (a) and strongly nonlinear (b).

all energy scales at previous steps. However, in the spirit of the RG approach, one can assume that  $\Phi_j(E)$  can still be linearized within a relevant energy interval. The conventional RG approach suggests that different scales in *real* space can be decoupled. Linearization of Eq. (4.6) implies a similar decoupling in *energy* space. In the case of phases, a “justification” of such a decoupling is that at each RG step, the relevant energy scale, that is the mean level spacing, reduces by a factor of four.

With  $\Phi_j(E)$  given by Eq. (4.6), the statistics of energy levels determined by the matrix equation (4.4) is obtained by averaging over the random initial phases  $\Phi_{0,j}$  and values  $t_i$  chosen randomly according to a distribution  $P(t)$ . For every realization the levels  $E_k$  are computed from the solutions  $\omega(E_k) = 0$  of Eq. (4.4) as illustrated in Fig. 4.3.

The energy interval is scanned in discrete energy steps  $\Delta E$  which define the accuracy of the obtained  $E_k$ . The used value  $\Delta E = \min\{s_j\}/250$  is adapted to each random realization of the  $\Phi_{0,j}$  and takes the periodicity in Eq. 4.6 and its influence on the behavior of  $\omega(E)$  into account. In particular, each realization yields three level spacings which are then used to construct a smooth LSD. Thus the situation is comparable with estimating the true RMT ensemble distribution functions from small, say,  $2 \times 2$  matrices only [Meh91, Wig51]. The outline of the RG procedure for the LSD is as follows. The slopes  $s_j$  in Eq. (4.6) determine the level spacings at the first step. They are randomly distributed with a distribution function  $P_0(s)$ . Subsequent averaging over many realizations yields the LSD,  $P_1(s)$ , at the second step. Then the key element of the RG procedure, as applied to the level statistics, is using  $P_1(s)$  as a *distribution of slopes* in Eq. (4.6). This leads to the next-step LSD and so on.

The approach of this work relies on the “real” eigenenergies of the RG unit. The simpler computation of the spectrum of quasienergies adopted in large-scale simulations within the CC model [KM97a, Met98] cannot be applied since the en-

ergy dependence of phases  $\Phi_j$  in the elements of the matrix is neglected and only the random contributions,  $\Phi_{0,j}$ , are kept. Nevertheless it is instructive to compare the two procedures: Fig. 4.3 shows the dependence of the four quasienergies  $\omega_k$  on the energy  $E$  calculated for two RG units, with  $t_i$  chosen from the critical distribution  $P_c(t)$ . The energy dependence of the phases  $\Phi_j$  was chosen from LSD of the GUE according to Eq. (4.6). One can see that the dependences  $\omega(E)$  range from remarkably linear and almost parallel (Fig. 4.3a) to strongly nonlinear (Fig. 4.3b).

## 4.3 Numerical results

### 4.3.1 The LSD at the QH transition

First, the shape of the LSD at the QH transition is considered. As the starting distribution  $P_0(s)$  of the RG iteration the LSD of GUE is chosen, since previous simulations [BS97, KM97a] indicate that the critical LSD is close to GUE. According to  $P_0(s)$ ,  $s_j$  is drawn randomly and  $\Phi_j$ ,  $j = 1, \dots, 4$  is set as in Eq. (4.6). For the transmission coefficients of the SP the FP distribution  $P_c(t)$ , obtained in Section 3.4, is used. As known from Section 3.4,  $P_n(t)$  drifts away from the FP within several further iterations due to unavoidable numerical inaccuracies. In order to stabilize the calculation, the FP distribution  $P_c(t)$  is therefore used in every RG step instead of  $P_n(t)$ . This trick does not alter the results and also speeds up the convergence of the RG for  $P_c(s)$  considerably. By finding solutions  $\omega(E_k) = 0$  of Eq. (4.4) the new LSD  $P_1(s')$  is constructed from the “unfolded” energy level spacings  $s'_k = (E_{k+1} - E_k)/\Delta$ , where  $k = 1, 2, 3$ , and the mean spacing  $\Delta = (E_4 - E_1)/3$ . Due to the “unfolding” [Haa92] with  $\Delta$ , the average spacing is set to one for each sample and in each RG-iteration step spacing data of  $2 \times 10^6$  super-SPs are taken into account. The resulting LSD is discretized in bins with largest width 0.01. In the following iteration step the procedure is repeated using the  $P_1(s)$  as initial distribution. Convergence of the iteration process is assumed when the mean-square deviation of  $P_n(s)$  deviates by less than  $10^{-4}$  from its predecessor  $P_{n-1}(s)$ . The above approach now enables one to determine the critical LSD  $P_c(s)$ . The RG iteration converges rather quickly after only 2 – 3 RG steps. The resulting  $P_c(s)$  is shown in Fig. 4.4 together with the LSD for the unitary random matrix ensemble from Eq. (4.1).

Although  $P_c(s)$  exhibits the expected features, namely, level repulsion for small  $s$  and a long tail at large  $s$ , the overall shape of  $P_c(s)$  differs noticeably from GUE. In the previous large-size lattice simulations [BS97, KM97a] the obtained critical LSD was much closer to GUE than  $P_c(s)$  in Fig. 4.4. This fact, however, does not necessarily imply a lower accuracy of the RG approach. Indeed, as it was demonstrated recently, the critical LSD – although being system-size independent – nevertheless depends on the geometry of the samples [PS98] and on the specific choice of boundary conditions [BMP98, SP98]. Sensitivity to the boundary conditions does not affect the asymptotics of the critical distribution, but rather manifests itself in the shape of the “body” of the LSD. One should note that the boundary conditions which have been imposed to calculate the energy levels (dashed lines in Fig. 4.2) are

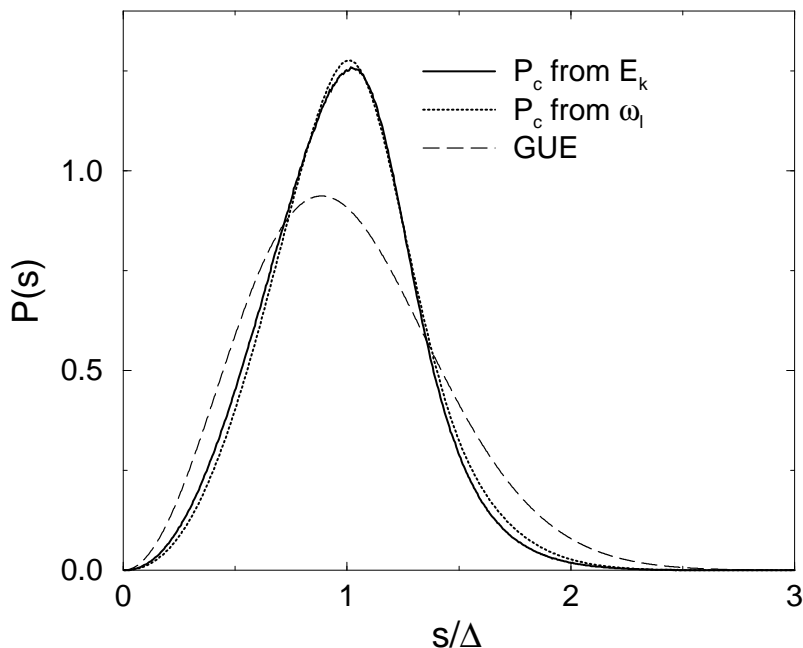


Figure 4.4: FP distributions  $P_c(s)$  obtained from the spectrum of  $\omega_l(E=0)$  and from the RG approach using the real eigenenergies  $E_k$  in comparison to the LSD for GUE. As in all other graphs  $P(s)$  is shown in units of the mean level spacing  $\Delta$ .

*non-periodic* in contrast to usual large-size lattice simulations [KM97a].

As mentioned in the last Section there is another possibility to assess the critical LSD, namely by the distribution of *quasienergies*. In Fig. 4.4 the result of this procedure is shown. It appears that the resulting distribution is almost *identical* to  $P_c(s)$ . This observation is highly non-trivial, since, as follows from Fig. 4.3, there is no simple relation between the energies and quasienergies. Moreover, if instead of the linear  $E$ -dependence of  $\Phi_j$ , another functional form is chosen, say,

$$\Phi_j(E) = \Phi_{0,j} + 2 \arcsin \left( \frac{E}{s_j} - 2p \right), \quad (4.7)$$

where the integer  $p$  insures that  $\left| \frac{E}{s_j} - 2p \right| \leq 1$ , then the RG procedure would yield an LSD which is markedly different (within the “body”) from  $P_c(s)$ . This is illustrated in Fig. 4.5. Both procedures, using quasienergies instead of real energies, as in [KM97a], and linearization of the energy dependence of phases [as in Eq. (4.6)] are not rigorous. Linearization is dictated by the RG concept. The coincidence of the results of the two procedures indicates that the concept of quasienergies, namely, that they obey the same statistics as real energies, is equivalent to the RG.

### 4.3.2 Small- $s$ and large- $s$ behavior

Here, the focus is on two further characteristic properties of  $P_c(s)$ , the small- $s$  and the large- $s$  behavior, which have received considerable attention previously [BS97, BSZK96, Eva94, Eva95, HS94a, KOSO96, KLAA94, Met98, SSS<sup>+</sup>93, ZK97].



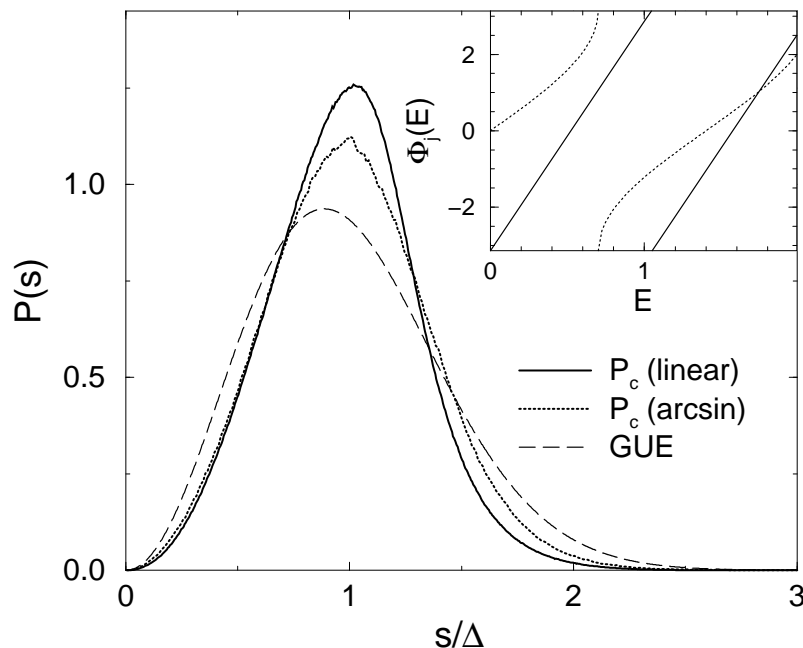


Figure 4.5: FP distributions  $P_c(s)$  for a linear and an arcsin energy dependence of the phases  $\Phi_j$ . The form of  $P_c(s)$  is clearly influenced by the actual choice of  $\Phi_j(E)$ . Thus universal behavior is not expected in the bulk shape. The inset illustrates examples of the two different functions  $\Phi_j(E)$  as in Eqs. (4.6) and (4.7).

As it was mentioned above, the general shape of the critical LSD is not universal. However, the small- $s$  behavior of  $P_c(s)$  must be the same as for the unitary random matrix ensemble, namely  $P_c(s) \propto s^2$ . This is because delocalization at the QH transition implies the level repulsion [FM97,SSS<sup>+</sup>93]. Earlier large-scale simulations of the critical LSD [BS97,BSK98,BSZK96,FAB95,KOSO96,KM97a,Met98,Met99,MV98,OO95,OOK96] satisfy this general requirement. The same holds also for the result of this work, as can be seen in Fig. 4.6. The given error bars of the numerical data are standard deviations computed from a statistical average of 100 FP distributions each obtained for different random sets of  $t_i$ 's and  $\Phi_j$ 's within the RG unit. In general, within the RG approach, the  $s^2$ -asymptotics of  $P(s)$  is most natural. This is because the levels are found from diagonalization of the  $4 \times 4$  unitary matrix (4.5) with absolute values of elements widely distributed between 0 and 1.

The right form of the large- $s$  tail of  $P(s)$  is Poissonian,  $P_c(s) \propto \exp(-bs)$  [SSS<sup>+</sup>93]. For the Anderson model in three dimensions, unambiguous confirmation of this prediction in numerical simulations became possible only when very high numerical accuracy had been achieved [BSZK96,ZK97]. This is because  $P_c(s)$  assumes the Poissonian asymptotics only at large enough  $s \gtrsim 3\Delta$ . For the QH transition, a linear behavior of  $\ln P_c(s)$  with a slope corresponding to the value  $b \approx 4.1$  has been found in [BS97] from the analysis of the interval  $2 < s/\Delta < 4$ . The data of this work, as shown in Fig. 4.7, has a high accuracy only for  $s/\Delta \lesssim 2.5$ . For such  $s$ , the distribution  $P_c(s)$  does not yet reach its large- $s$  tail. Thus, the value of parameter  $b$  extracted from this limited interval is somewhat ambiguous. Namely, one obtains

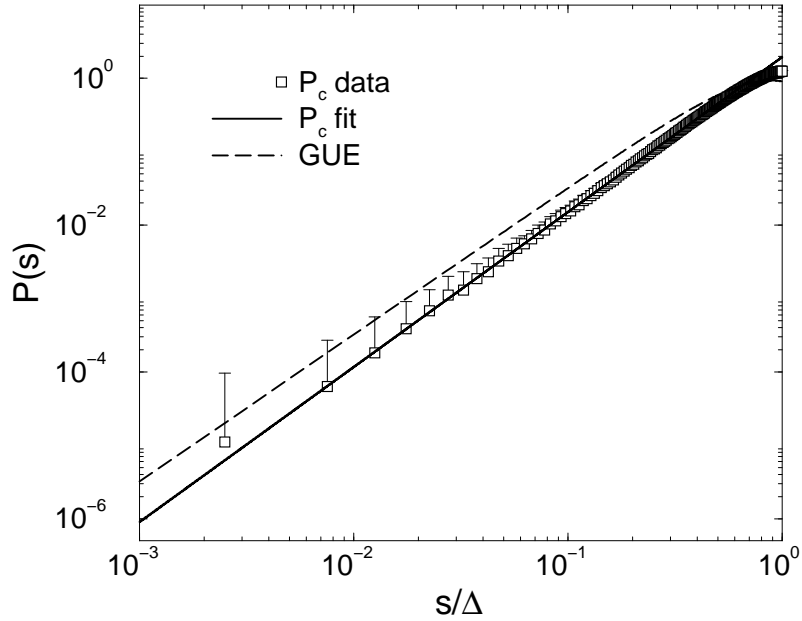


Figure 4.6:  $P_c(s)$  for small  $s$  in agreement with the predicted  $s^2$  behavior. Due to the log-log plot errors are shown in the upper direction only.

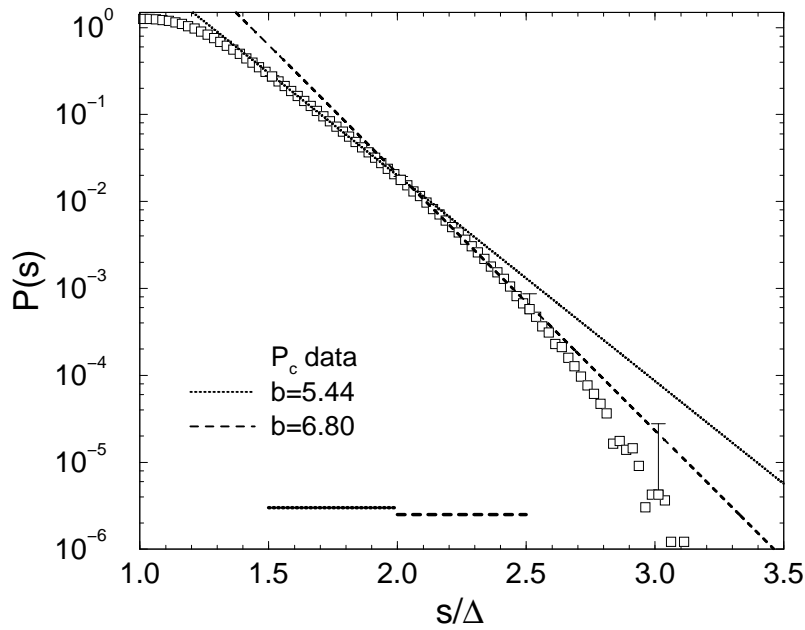


Figure 4.7: The large- $s$  tail of  $P_c(s)$  compared with fits according to the predictions of [SSS<sup>+</sup>93] (lines). The interval used for fitting is indicated by the bars close to the lower axis. For clarity errors are shown in upper direction and for  $s/\Delta \approx 1.5, 2.0, 2.5, 3.0$  only.

as decay coefficient  $b = 5.44$  for  $s/\Delta \in [1.5, 2.0]$  and  $b = 6.80$  for  $s/\Delta \in [2.0, 2.5]$ .

At this point it seems that only the  $s^2$ -behavior of  $P_c(s)$  for small  $s$  proves to be robust within the RG approach and obeys the expected universal level repulsion. The accuracy of the RG approach is insufficient to discern the non-trivial feature of the critical LSD, i.e., the Poissonian asymptotics. But as will be shown in the next Section universality can be found also in additional quantities derived from the critical LSD.

## 4.4 Scaling results for the LSD

### 4.4.1 Finite-size scaling at the QH transition

The critical exponent  $\nu$  of the QH transition governs the divergence of the correlation length  $\xi_\infty$  as a function of the control parameter  $z_0$ , i.e.,

$$\xi_\infty(z_0) \propto |z_c - z_0|^{-\nu}, \quad (4.8)$$

where  $z_c$  is the critical value. As presented in Chapter 3 the RG approach for the conductance distribution yields a rather accurate value  $\nu = 2.39 \pm 0.01$ . In Section 4.2 a complimentary RG approach to the distribution of the energy levels at the transition has been introduced. It can be expected on general grounds that the LSD obtained from the RG approach obeys scaling at small enough  $|z_c - z_0|$ . However, while it would be in accordance to universality, it is not known a priori, whether the values of  $\nu$  extracted from different variants of the RG approach are consistent.

The FSS analysis of the LSD is described by Eq. (4.2). In order to define a suitable control parameter  $z_0$  in the transition region, again the natural parametrization of the transmission coefficients  $t$ , i.e.,  $t = (e^z + 1)^{-1/2}$  [GR97], from Section 3.3 is used. One should recall that for such a parametrization,  $z$  can be identified with a dimensionless electron energy. The QH transition occurs at  $z = 0$ , which corresponds to the center of the Landau band. The universal conductance distribution at the transition,  $P_c(G)$ , corresponds to the distribution  $Q_c(z)$  which is symmetric with respect to  $z = 0$  and has a shape close to a Gaussian. The RG procedure for the conductance distribution converges and yields  $Q_c(z)$  only if the initial distribution is an even function of  $z$ . This suggests to choose as a control parameter in Eq. (4.2), the position  $z_0$  of the maximum of the function  $Q(z)$ , where  $z_0$  is an energy shift away from the center of the Landau band. Because the QH transition occurs exactly at  $z_0 = 0$  any initial distribution  $Q(z - z_0)$  with  $z_0 \neq 0$  will evolve during the RG procedure toward an insulator, either with complete transmission of the network nodes (for  $z_0 > 0$ ) or with complete reflection of the nodes (for  $z_0 < 0$ ).

### 4.4.2 Scaling for $\alpha_P$ and $\alpha_I$

In principle, one is free to choose for the FSS analysis any characteristic quantity  $\alpha(N; z_0)$  constructed from the LSD which has a systematic dependence on system size  $N$  for  $z_0 \neq 0$  while being constant at the transition  $z_0 = 0$ . Out of the large

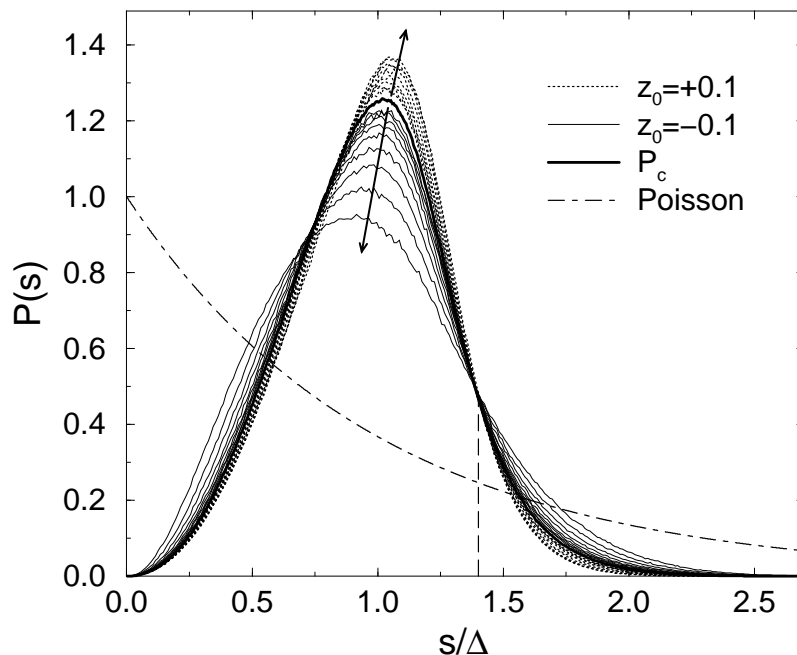


Figure 4.8: RG of the LSD used for the computation of  $\nu$ . The dotted lines corresponds to the first 9 RG iterations with an initial distribution  $P_0$  shifted to the metallic regime ( $z_0 = 0.1$ ) while the full thin lines represent results for a shift toward localization ( $z_0 = -0.1$ ). Within the RG procedure the LSD moves away from the FP as indicated by the arrows. At  $s/\Delta \approx 1.4$  the curves cross at the same point which is used when deriving a scaling quantity from the LSD.

number of possible choices [BS97, HS94b, SSS<sup>+</sup>93, ZK95b, ZK95a, ZK97] a restriction is made to quantities that are defined mainly by the small- $s$  behavior which is accurately described by the RG approach. The quantities are obtained by integration of the LSD and have already been successfully used in [HS93, HS94b], namely

$$\alpha_P = \int_0^{s_0} P(s) ds \quad (4.9)$$

and

$$\alpha_I = \frac{1}{s_0} \int_0^{s_0} I(s) ds, \quad (4.10)$$

with  $I(s) = \int_0^s P(s') ds'$ . The integration limit is chosen as  $s_0 = 1.4$  which approximates the common crossing point [HS94b] of all LSD curves as can be seen in Fig. 4.8. Thus  $P(s_0)$  is independent of the distance  $|z - z_c|$  to the critical point and the system size  $N$ . Note that  $N$  is directly related to the RG step  $n$  by  $N = 2^n$ . The double integration in  $\alpha_I$  is numerically advantageous since fluctuations in  $P(s)$  are smoothed. One can now apply the finite-size-scaling approach from Eq. (4.2)

$$\alpha_{I,P}(N, z_0) = f\left(\frac{N}{\xi_\infty(z_0)}\right). \quad (4.11)$$

Since  $\alpha_{\text{I,P}}(N, z_0)$  is analytical for finite  $N$ , one can expand the scaling function  $f$  at the critical point. The first-order approximation yields

$$\alpha(N, z_0) \sim \alpha(N, z_c) + a|z_0 - z_c|N^{1/\nu} \quad (4.12)$$

where  $a$  is a coefficient. Better results are obtained using a higher-order expansion proposed by Slevin and Ohtsuki [SO99]. In [SO99] they expand  $f$  twice, first, in terms of Chebyshev polynomials of order  $\mathcal{O}_\nu$  and, second, as Taylor expansion with terms  $|z_c - z_0|$  in the order  $\mathcal{O}_z$ . With this procedure one can describe deviations from linearity in  $|z_c - z_0|$  at the transition. Contributions from an irrelevant scaling variable can be neglected since the transition point  $z_0 = 0$  is known, as demonstrated by the data shown in the upper plots of Figs. 4.9 and 4.10.

In order to obtain the functional form of  $f$  the fitting parameters, including  $\nu$ , are evaluated by a nonlinear least-square ( $\chi^2$ ) optimization. In Figs. 4.9 and 4.10 the resulting fits for  $\alpha_{\text{P}}$  and  $\alpha_{\text{I}}$  at the transition are shown. The fits are chosen in a way such that the total number of parameters is kept at a minimal value and the fit agrees well with the numerical data. The corresponding scaling curves are displayed in the lower part of Figs. 4.9 and 4.10. In the plots the two branches for complete reflection ( $z_0 < 0$ ) and complete transmission ( $z_0 > 0$ ) can be distinguished clearly. In order to estimate the error of the fitting procedure the results for  $\nu$  obtained by different orders  $\mathcal{O}_\nu$  and  $\mathcal{O}_z$  of the expansion, system sizes  $N$ , and  $z$  ranges around the transition are compared. A part of the over 100 fit results that have been obtained is given in Table 4.1.

The value of  $\nu$  is calculated as average over all 120 individual fits for which the resulting error of  $\nu$  was smaller than 0.02. The error is then determined as the standard deviation of the contributing values. By this method one can assure that the result is not influenced by local minima of the nonlinear fit. So  $\nu = 2.37 \pm 0.02$  can be considered as a reliable value for the exponent of the localization length at the QH transition obtained from the LSD which is also in excellent agreement with  $2.39 \pm 0.01$  calculated in the previous Chapter.

Besides  $\alpha_{\text{P}}$  and  $\alpha_{\text{I}}$  also a parameter-free scaling quantity  $\alpha_{\text{S}} = \int_0^\infty s^2 P(s) ds$  [ZK95b] was tested, where the whole distribution  $P(s)$  is taken into account. The obtained data are presented in Fig. 4.11. Due to the influence of the large- $s$  tail only a less reliable value  $\nu = 2.33 \pm 0.05$  was obtained.

### 4.4.3 Test of different initial distributions

Finally the influence of the initial conditions on the result of the LSD and the one-parameter scaling is studied. So far the starting distributions  $P_0(G)$  and  $P_0(s)$  of the RG iteration were constructed from the critical distributions  $P_c(G)$  and  $P_c(s)$ . The function  $P_c(G)$  is shown in Fig. 4.12 (inset) with a full line. In order to understand the importance of the fact that  $P_c(G)$  is almost flat, the calculations have been repeated choosing instead of  $P_c(G)$  a relatively narrow Gaussian distribution  $P(G) \equiv P_{\text{Gau\ss}}(G)$ . This distribution is shown with a dashed line in Fig. 4.12 (inset). The corresponding LSD as presented in Fig. 4.12 is obtained similar to the calculation of  $P_c(s)$ , where now  $P_n(G) = P_{\text{Gau\ss}}(G)$  is used in all iterations. Obviously, it agrees

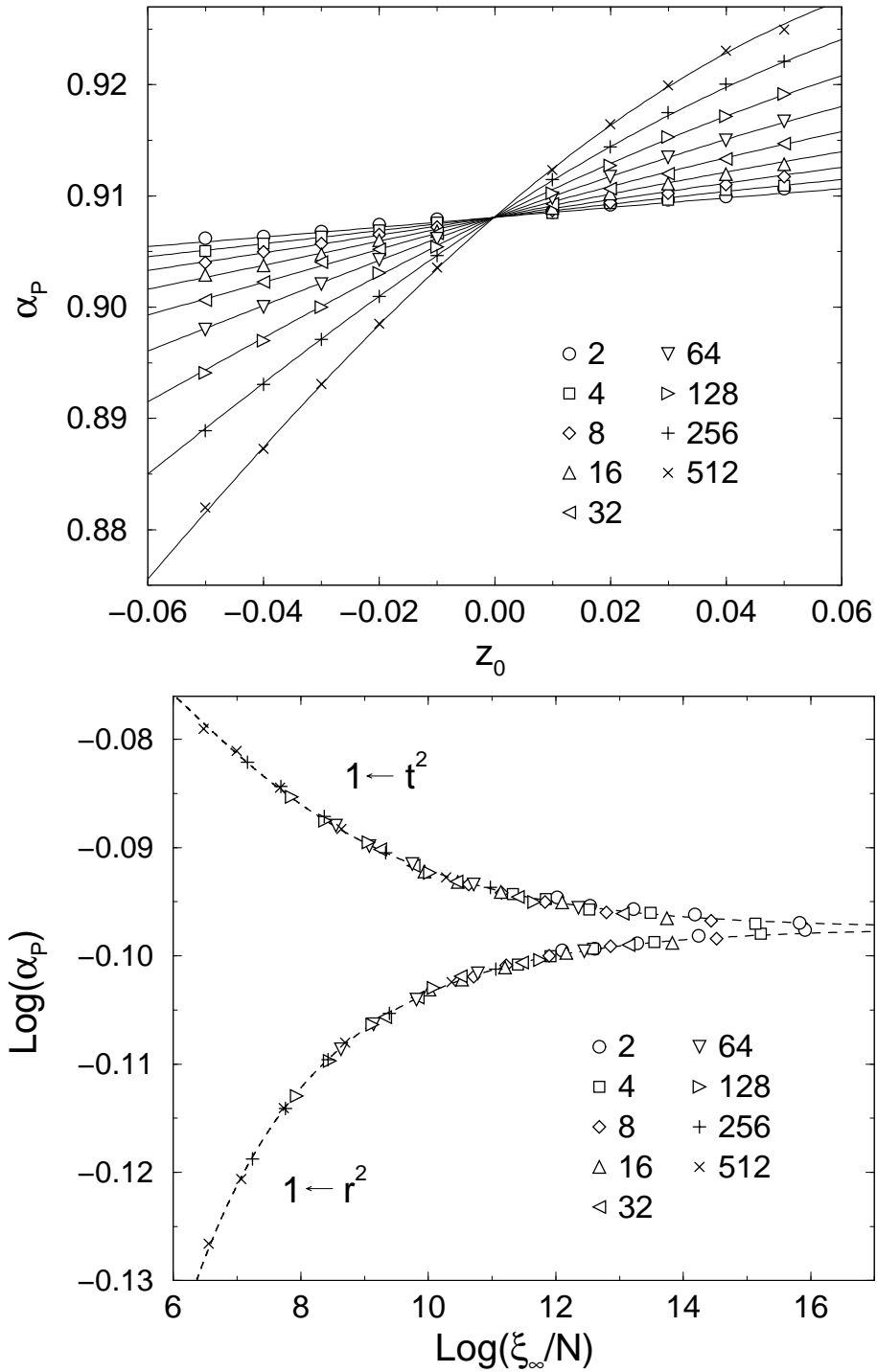


Figure 4.9: Upper plot: Behavior of  $\alpha_P$  at the QH transition as results of the RG of the LSD. Data are shown for RG iterations  $n = 1, \dots, 9$  corresponding to effective system sizes  $N = 2^n = 2, \dots, 512$ . Full lines indicate the functional dependence according to FSS using the  $\chi^2$  minimization with  $\mathcal{O}_\nu = 2$  and  $\mathcal{O}_z = 3$ . Lower plot: FSS curves resulting from the  $\chi^2$  fit of the upper data. Different symbols correspond to different effective system sizes  $N = 2^n$ . The data points collapse onto a single curve indicating the validity of the scaling approach.

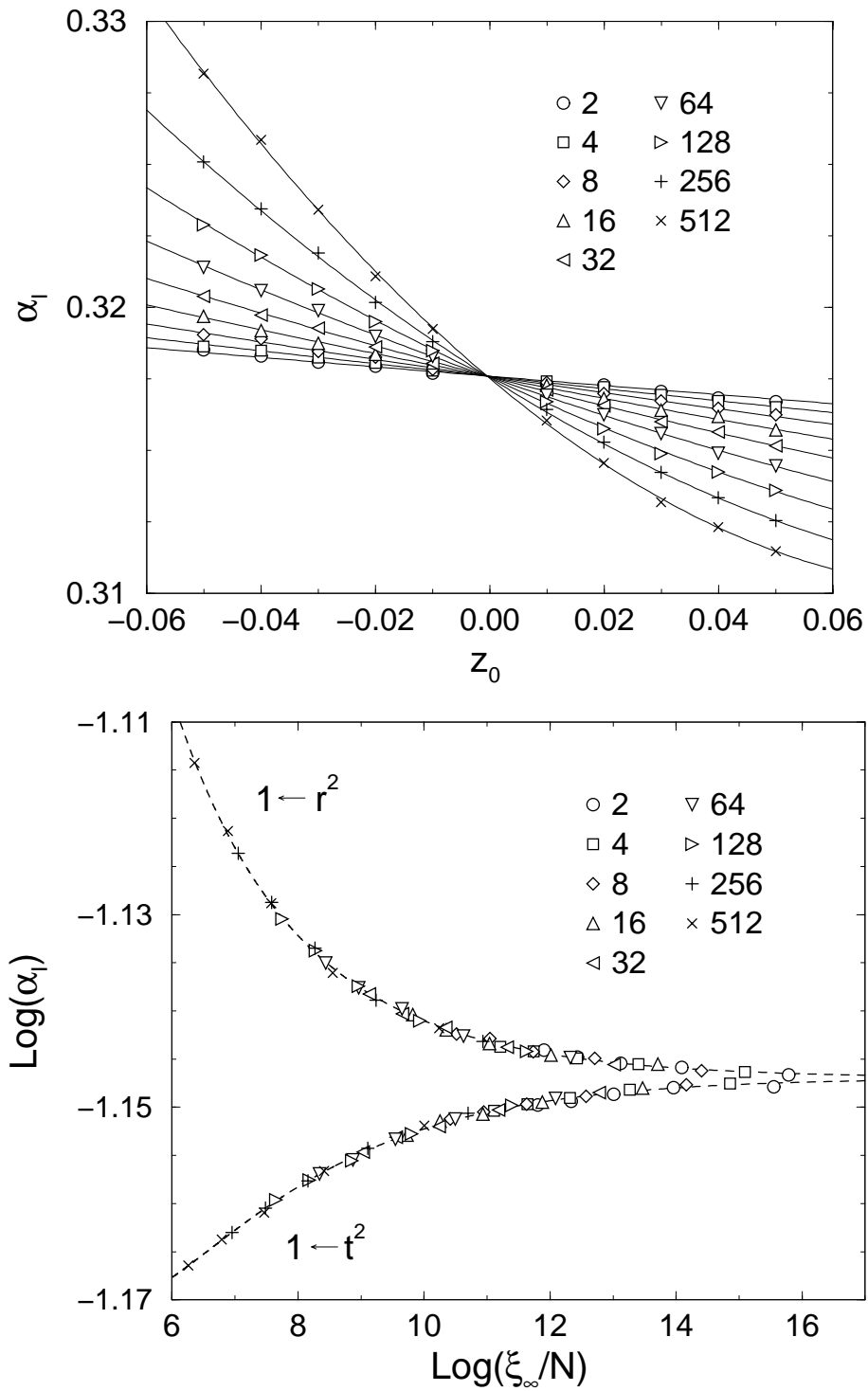


Figure 4.10: Behavior of  $\alpha_1$  at the QH transition and resulting FSS curves analogously to Fig. 4.9.

#### 4.4. SCALING RESULTS FOR THE LSD

$N$	$[z_{0\min}, z_{0\max}]$	$\mathcal{O}_\nu$	$\mathcal{O}_z$	$\nu$
$\alpha_P$				
2 – 64	$[-0.07, 0.07]$	2	1	$2.383 \pm 0.019$
2 – 64	$[-0.07, 0.07]$	2	3	$2.384 \pm 0.019$
2 – 128	$[-0.07, 0.07]$	1	3	$2.384 \pm 0.019$
2 – 128	$[-0.07, 0.07]$	3	2	$2.352 \pm 0.018$
2 – 128	$[-0.07, 0.07]$	1	2	$2.384 \pm 0.019$
2 – 128	$[-0.07, 0.07]$	2	3	$2.398 \pm 0.015$
2 – 256	$[-0.05, 0.05]$	2	1	$2.361 \pm 0.016$
<b>2 – 512</b>	<b><math>[-0.05, 0.05]</math></b>	<b>2</b>	<b>3</b>	<b><math>2.397 \pm 0.015</math></b>
4 – 512	$[-0.05, 0.05]$	2	2	$2.379 \pm 0.014$
8 – 512	$[-0.05, 0.05]$	2	2	$2.373 \pm 0.015$
16 – 512	$[-0.07, 0.07]$	3	1	$2.318 \pm 0.011$
$\vdots$				
$\alpha_I$				
2 – 256	$[-0.07, 0.07]$	2	1	$2.380 \pm 0.011$
2 – 512	$[-0.05, 0.05]$	2	2	$2.368 \pm 0.013$
<b>2 – 512</b>	<b><math>[-0.05, 0.05]</math></b>	<b>2</b>	<b>3</b>	<b><math>2.368 \pm 0.014</math></b>
2 – 512	$[-0.07, 0.07]$	3	2	$2.353 \pm 0.012$
2 – 128	$[-0.07, 0.07]$	2	2	$2.375 \pm 0.016$
2 – 512	$[-0.05, 0.05]$	3	2	$2.374 \pm 0.017$
4 – 512	$[-0.05, 0.05]$	3	1	$2.352 \pm 0.017$
8 – 512	$[-0.07, 0.07]$	2	3	$2.376 \pm 0.012$
8 – 512	$[-0.07, 0.07]$	3	3	$2.335 \pm 0.015$
16 – 512	$[-0.07, 0.07]$	2	3	$2.379 \pm 0.014$
16 – 512	$[-0.07, 0.07]$	2	1	$2.407 \pm 0.016$
$\vdots$				
$2.37 \pm 0.02$				

Table 4.1: Fit results for  $\nu$  obtained from  $\alpha_I$  and  $\alpha_P$  for different system sizes  $N$ , intervals around the transition, and orders  $\mathcal{O}_\nu$  and  $\mathcal{O}_z$  of the fitting procedure. The error of  $\nu$  is the standard deviation obtained as result of the nonlinear  $\chi^2$  fit. The two lines in bold face correspond to the plots in Figs. 4.9 and 4.10, respectively.

much worse with GUE than the LSD computed using the true  $P_c(G)$ , which can be considered as a reference point.

For the determination of the critical exponent, the distribution is again disturbed by an energy shift  $z_0$  and the change of the LSD in the course of the RG iterations is studied by means of  $\alpha_I$  and  $\alpha_P$ . The data for  $\alpha_P$  and  $\alpha_I$  calculated for  $P(G) = P_{\text{Gau\ss}}(G)$  are plotted in Fig. 4.13.

The curves for small system sizes  $N$  exhibit strong deviations, i.e., there is initially no common crossing point, while for large  $N$  a behavior similar to Figs. 4.9 and 4.10 is observed. On first sight this behavior might indicate the influence of an irrelevant scaling variable. A deeper look at Fig. 4.13 shows that the required



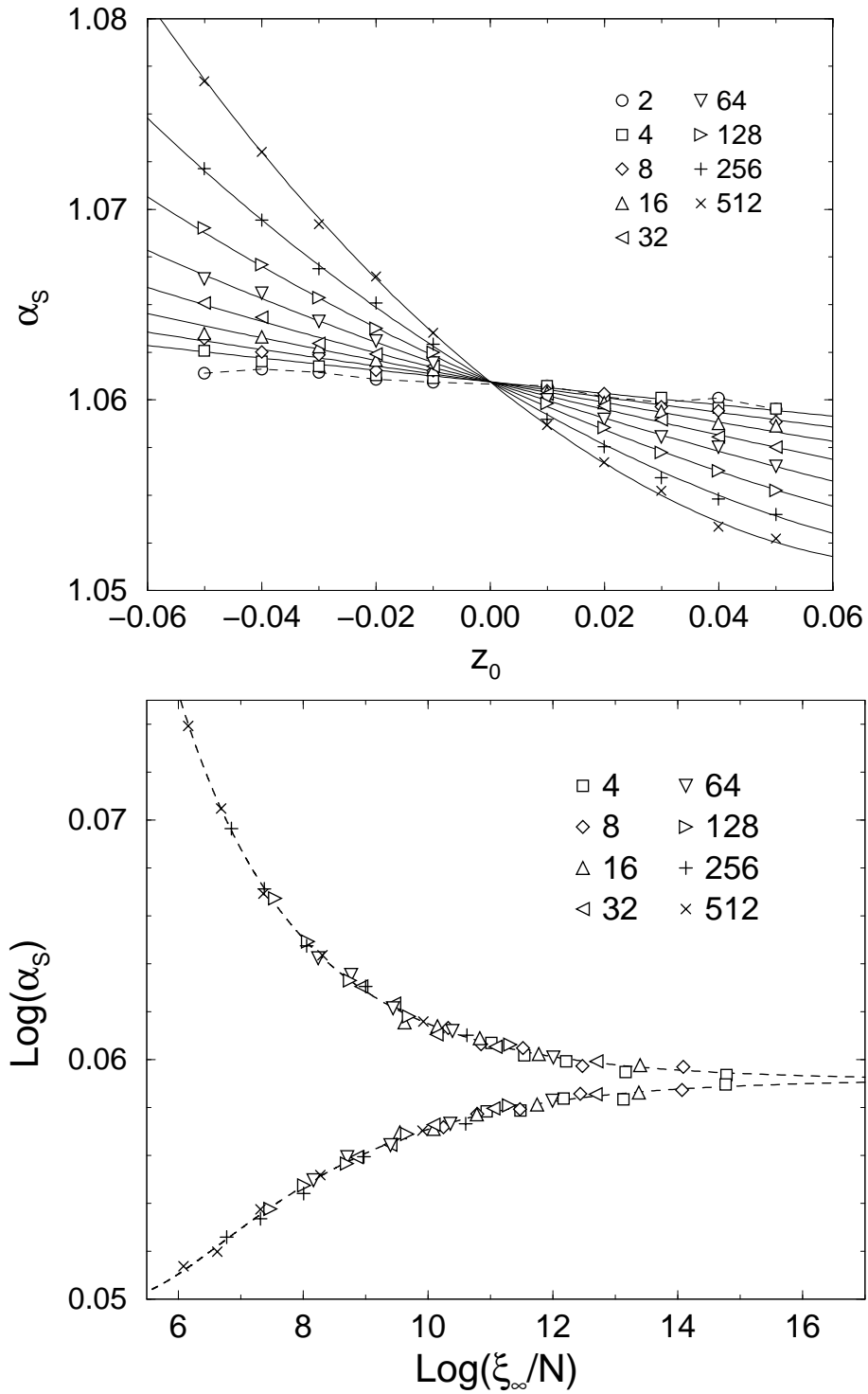


Figure 4.11: Behavior of  $\alpha_S$  at the QH transition and resulting FSS curves analogously to Fig. 4.9. Because of large deviations data for  $N = 2$  were excluded from the fitting.

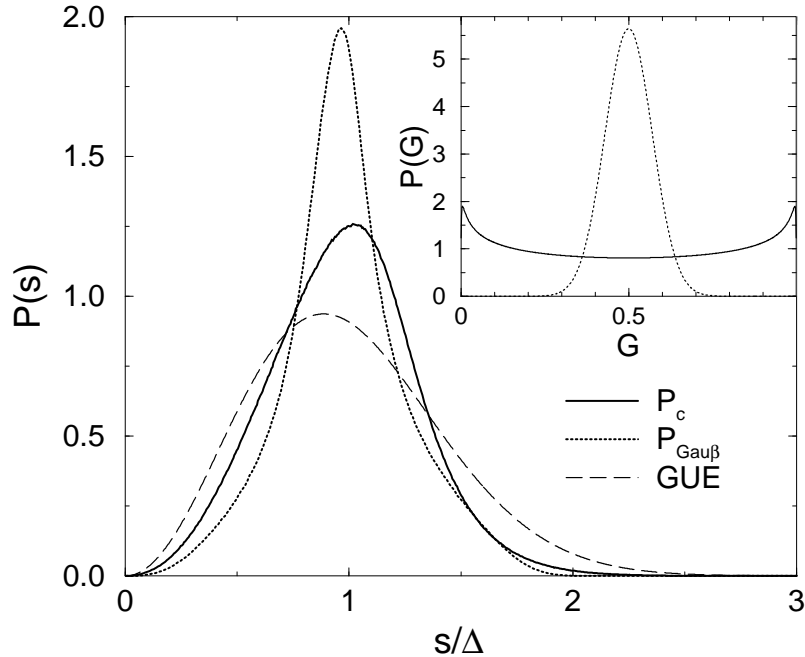


Figure 4.12: Comparison of the LSD  $P_c(s)$  and  $P_{\text{Gauß}}(s)$  obtained from the corresponding conductance distributions shown in the inset.

condition, a systematic system-size dependence of the crossing points, is not found for small  $N$ . Within the range of the data small- $N$  curves do not cross each other at all and for  $\alpha_I$  crossings with larger  $N$  even occur on both sides of the transition. On the other hand the crossing point between larger  $N$  curves stays the same. Therefore small- $N$  data are better neglected in the scaling analysis. The  $\chi^2$  fits for  $\alpha_I$  and  $\alpha_P$  are carried out using  $z_0 \in [-0.05, 0.05]$  and  $N = 16 - 512$ . They yield slightly less accurate values  $\nu_I = 2.43 \pm 0.02$  and  $\nu_P = 2.46 \pm 0.03$  which are still reasonably close to  $\nu = 2.37 \pm 0.02$  obtained for the correct initial distributions. Obviously the initial failure is reduced and smeared out already after a few RG iterations.

Overall, Figs. 4.12 and 4.13 illustrate the consistency of the RG approach for the conduction distribution and for the level statistics, in the sense, that a better FP distribution of the level spacings is obtained from the FP of the conductance distribution rather than from a strongly non-uniform distribution.

## 4.5 Conclusion

The usual way to study the LSD in lattice or network models is to examine the spectra of systems as large as possible. This allows one to obtain the huge number of energy levels required for a reliable statistics which is a prerequisite in order to compare to the predictions following from universality. In this study the energy spectrum is obtained by an alternative method. Instead of a large CC network only a 5SP RG unit is used to extract the eigenenergies. This RG approach is based on a specific assumption of the energy dependence (4.6) of the phases in the RG

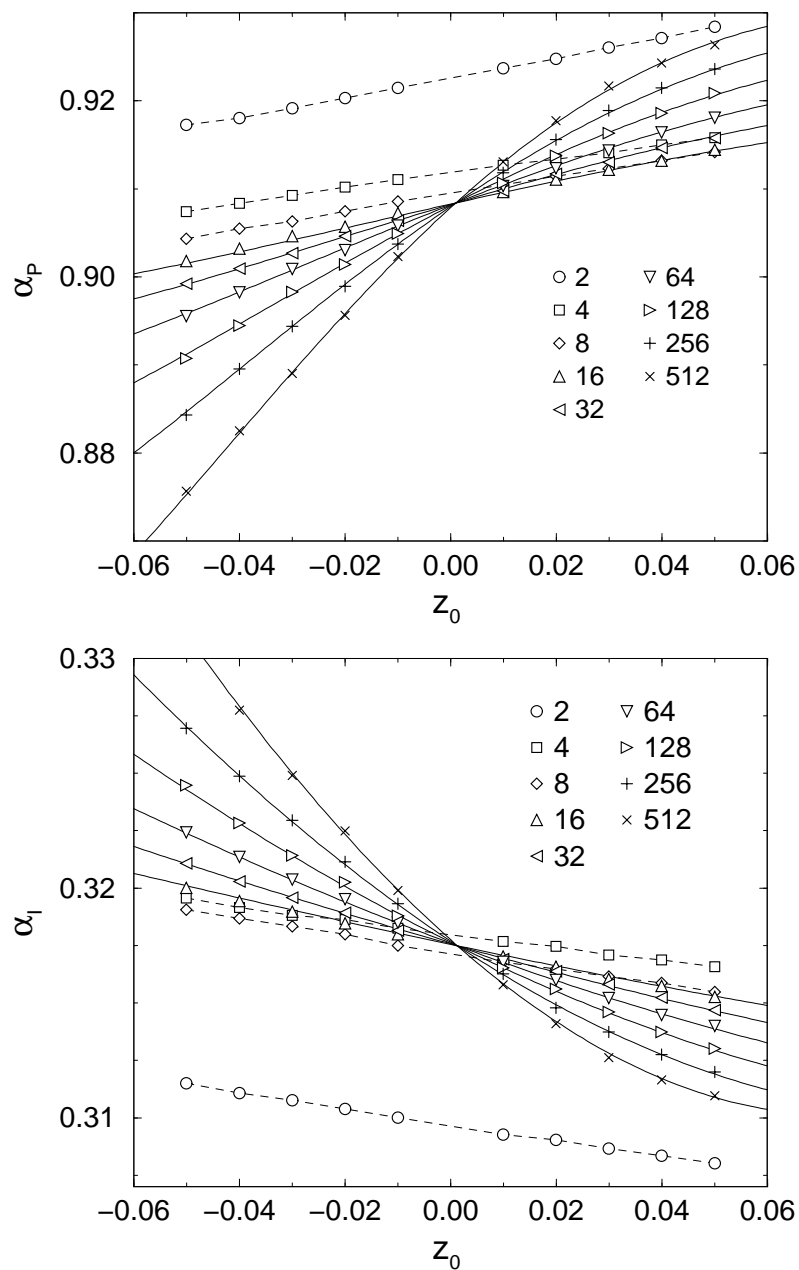


Figure 4.13: Behavior of  $\alpha_P$  and  $\alpha_I$  computed for initial distributions  $P_{\text{GauB}}$ , as shown in Fig. 4.12. Data are plotted for RG iterations  $n = 1, \dots, 9$  corresponding to effective system sizes  $N = 2^n = 2, \dots, 512$ . Curves for small  $n$  do not cross at the common point  $z_0 = 0$ . Full lines indicate the functional dependence according to FSS using the  $\chi^2$  minimization with  $\mathcal{O}_\nu = 2$  and  $\mathcal{O}_z = 3$  (for  $\alpha_P$ ) and  $\mathcal{O}_\nu = 2$  and  $\mathcal{O}_z = 2$  (for  $\alpha_I$ ).

unit which has an influence also on the shape of the LSD. The overall form of the computed critical LSD  $P_c$  is not universal but still shows a quadratic level repulsion for small  $s$ , which is one of the predicted characteristic properties.

The robustness of universal properties is moreover demonstrated by a FSS analysis of the LSD around the QH transition. The exponent  $\nu = 2.37 \pm 0.02$  of the localization length obtained by a nonlinear  $\chi^2$  minimization is in excellent agreement with the value calculated in previous works.

This result is surprisingly good when keeping in mind that it was derived just from the four loops of the RG unit. Nevertheless this RG unit seems to capture the essential physics of the QH transition. The success of the RG approach can be attributed to the description of the transmission amplitudes  $t$  of the SPs by a correct distribution function  $P(t)$  while for network models usually a fixed value  $t(E)$  is assigned to all SPs for simplicity. The phases are associated with full loops in the network and not with single SP-SP links, and the design of the RG unit describes the underlying symmetry of the QH transition, which is not accessible, e.g., with the 4SP RG unit considered in [ZS01]. Due to these reasons the RG iteration is always governed by the quantum critical point of the QH transition. Even when starting the iteration with a distribution  $P_0(G)$  totally different from  $P_c(G)$ , but still symmetric with respect to  $G = 0.5$ , one approaches the same results after a few iterations.

# Chapter 5

## Macroscopic inhomogeneities

### 5.1 Introduction

The investigation of the influence of macroscopic inhomogeneities is motivated by contradicting experimental results which are described in the following in more detail. The experimental study of the critical behavior of the resistivity in the transition region at strong magnetic field  $B$  has a long history which can be divided into three periods.

The first experimental works [HWE<sup>+</sup>93, KHKP91a, KHKP91b, KHKP92, WTP85, WLTP92, WTPP88] reported a narrowing of the transition peak of  $\rho_{xx}$  with temperature  $T$ , e.g. as in Fig. 5.1, according to a power law  $T^\kappa$  with  $\kappa \sim 0.4$ . The spread in the actual value of  $\kappa \propto 1/\nu$  measured in different experiments was attributed to the difference in the type of disorder in the samples of [WTP85, WTPP88] and [KHKP91a]. In another experimental method to explore the critical behavior [KHKP91b, KHKP92],  $\kappa$  was deduced from the sample size dependence of the width,  $\Delta B$ , of the transition region. The value of  $\kappa$  obtained by this technique appeared to be consistent with temperature measurements [KHKP91a], in the sense that  $\kappa$  was found to be sample dependent. On the other hand, it was argued [WLTP92] that the lack of universality in [KHKP91a, KHKP91b, KHKP92] has its origin in the long-ranged character of the disorder in GaAs-based heterostructures studied in these works. This is because for a smooth disorder the energy interval within which the electron transport is dominated by localization effects is relatively narrow [WLTP92]. The measurements [WTP85, WTPP88] suggesting the universality of  $\kappa$  were carried out on  $\text{In}_x\text{Ga}_{1-x}\text{As}/\text{InP}$  heterostructures in which disorder is believed to be short-ranged [Col99]. Despite the disagreement about the universality of the exponent  $\kappa$ , the fact that the narrowing of the plateau transition occurs as  $T^\kappa$  was not questioned [HWE<sup>+</sup>93, KHKP91a, KHKP91b, KHKP92, WLTP92, WTP85, WTPP88].

Absence of scaling was reported first for the QH plateau-insulator transition [SHL<sup>+</sup>98] and then for the plateau-plateau transition [BMB98]. In the latter paper the conclusion about the absence of scaling was drawn from the analysis of the frequency dependence of  $\Delta B$  in GaAs/ $\text{Al}_y\text{Ga}_{1-y}\text{As}$  heterostructures as shown in Fig. 5.2 (in contrast to the similar analysis in [ESKT93]). That is, the authors of [SHL<sup>+</sup>98] and [BMB98] concluded, that the width of the transition region *saturates* as  $T \rightarrow 0$ . A possible explanation of this behavior [Shi99, SAK98] is based

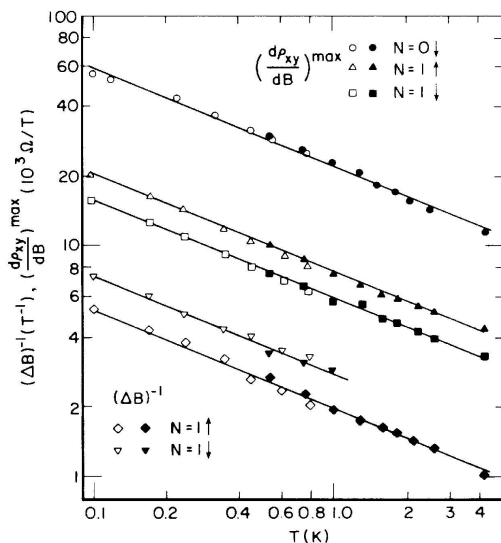


Figure 5.1: Experimentally observed temperature dependence of the width  $\Delta B$  of the  $\rho_{xx}$  peak from [WTPP88]. In the log-log scale the data (symbols) agree very well with linear fits (solid lines) indicating a power-law behavior. Different symbols correspond to different QH transitions and different refrigerators (filled –  $^3\text{He}$ , open – dilution). Note that a power law is also observed when studying the temperature dependence of the maximum slope of  $\rho_{xy}$  as shown by the upper three curves.

on the scenario of tunneling between electron puddles with a size larger than the dephasing length. The microscopic origin of these puddles was attributed to sample inhomogeneities [CHHR97, RCH96, SH94].

Very recent experimental results [SVO<sup>+</sup>00] on scaling of plateau-insulator as well as plateau-plateau QH transitions carried out on the same  $\text{In}_x\text{Ga}_{1-x}\text{As}/\text{InP}$  sample as in [HWE<sup>+</sup>93] suggested that the narrowing of the transition width with temperature follows a power-law dependence  $\Delta B \propto T^\kappa$  with  $\kappa \approx 0.4$ . Even when the authors of [SVO<sup>+</sup>00] analyzed their data using the procedure of [SHL<sup>+</sup>98], i.e., by plotting the logarithm of the longitudinal resistance versus  $\Delta B$ , they obtained straight lines with slopes proportional to  $T^{\kappa'}$  with  $\kappa' \approx 0.55$ . They attributed the difference between  $\kappa$  and  $\kappa'$  to the marginal dependence of the critical resistance on  $T$ . It was also speculated [SVO<sup>+</sup>00] that this dependence most likely results from macroscopic inhomogeneities in the sample. In the latest papers [HZH01, HZHP01, KMDK00] the frequency dependence of the QH transition width was studied. The results did not support the saturation of the width [BMB98, SHL<sup>+</sup>98], but rather confirmed the scaling hypothesis.

Summarizing, it is now conclusively established that the insulator-plateau and the plateau-plateau transitions exhibit the same critical behavior. It is also recognized that macroscopic inhomogeneities can either mask the scaling or alter the value of  $\kappa$  [SVO<sup>+</sup>00].

On the theoretical side, in all previous considerations inhomogeneities were incorporated into the theory through a spatial variation of the *local* resistivity [CHHR97, RCH96, Shi99, SAK98, SH94]. In other words, all existing theories are ei-

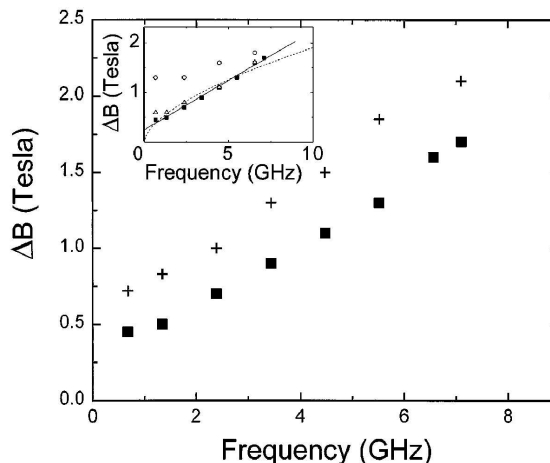


Figure 5.2: Saturation of the peak width  $\Delta B$  for microwave frequency  $f \rightarrow 0$  from [BMB98]. The results are obtained for the  $2 \rightarrow 1$  plateau-plateau transition. The width  $\Delta B$  is measured at half (■) and quarter (+) maximum. The inset shows half maximum data for temperatures 150 (■), 330 ( $\Delta$ ) and 700mK ( $\circ$ ). The linear fit for 150mK (solid line) leads to a finite intercept  $\Delta B(0)$  violating the scaling assumption.

ther "homogeneous quantum coherent" or "inhomogeneous *incoherent*". Note that sometimes the term "long-ranged disorder" is also used for a disorder that has a finite correlation radius which is larger than the magnetic length, see, e.g., [EMPW99]. This is different from the present situation. Meanwhile, there is another scenario which has never been explored. Close to the transition the localization length  $\xi$  becomes sufficiently large. Then the long-ranged disorder can affect the character of the divergence of  $\xi$ . In this Chapter the effects of quenched disorder on *quantum* percolation are investigated.

In order to study the role of the quenched disorder on the LD transition the CC model is treated again within the real-space RG approach. First, in Section 5.2 the classical case is briefly reviewed. After that, in Section 5.3, the quenched disorder is incorporated by an extension to the RG approach. The numerical results are the content of Section 5.4. The side effect of intrinsic short-range disorder is discussed in Section 5.5 before the concluding remarks are given in Section 5.6.

## 5.2 Macroscopic inhomogeneities in classical percolation

At the beginning one should recall the classical case where the motion of an electron in a strong magnetic field and a smooth potential reduces to the drift of the cyclotron orbit along the equipotential lines. Correspondingly, the description of the LD transition reduces to the classical percolation problem. In this limit [Wei84, WH83] the long-ranged disorder affects the value of the critical exponent in the percolation problem. Obviously, when the disorder is long-ranged but has a finite correlation radius, any changes in the critical behavior are not expected. The principle finding

of [WH83] and [Wei84] is that the critical exponent can change when the correlator of the disorder  $\langle V(\mathbf{r})V(\mathbf{r}') \rangle$  falls off with distance as a power law (quenched disorder)

$$\langle V(\mathbf{r})V(\mathbf{r}') \rangle \propto |\mathbf{r} - \mathbf{r}'|^{-\alpha}. \quad (5.1)$$

According to [Wei84,WH83] the critical exponent of the classical percolation  $\nu = 4/3$  crosses over to  $\nu = 2/\alpha$  for  $\alpha < 3/2$ , i.e., when the decay of the correlator is slow enough.

In order to understand how the critical behavior is affected by the quenched disorder, the following argument was put forward in [WH83]. In the absence of the quenched disorder, the correlation length,  $\xi_0$ , for a given energy  $\varepsilon$  in the vicinity of the transition is proportional to  $\varepsilon^{-\nu}$ . Now consider a sample with an area  $A = \xi_0^2$ . The variance of the quenched disorder within the sample is given by

$$\begin{aligned} \Delta_0^2 &= \frac{1}{A^2} \langle \int_A d^2r \varepsilon(\mathbf{r}) \int_A d^2r' \varepsilon(\mathbf{r}') \rangle \\ &= \frac{1}{A^2} \int_A d^2r \int_A d^2r' \langle \varepsilon(\mathbf{r})\varepsilon(\mathbf{r}') \rangle \\ &\propto \xi_0^{-2} \int_0^{\xi_0} dr r^{1-\alpha}, \end{aligned} \quad (5.2)$$

where the last relation follows from substituting Eq. (5.1), assuming an isotropic correlation and  $\xi \gg 1$ .

The critical behavior remains unaffected by the quenched disorder if the condition  $\Delta_0^2/\varepsilon^2 \rightarrow 0$  as  $\varepsilon \rightarrow 0$  is met. Using Eq. (5.2), the ratio  $\Delta_0^2/\varepsilon^2$  can be presented as

$$\frac{\Delta_0^2}{\varepsilon^2} \propto \begin{cases} \varepsilon^{2\nu-2}, & \alpha > 2 \\ \varepsilon^{2\nu-2} \ln(\varepsilon^{-\nu}), & \alpha = 2 \\ \varepsilon^{\alpha\nu-2}, & \alpha < 2 \end{cases} \quad (5.3)$$

Thus one can conclude that quenched disorder is irrelevant when

$$\begin{aligned} \nu > 1, & \quad \text{for } \alpha \geq 2, \\ \alpha\nu > 2, & \quad \text{for } \alpha < 2. \end{aligned} \quad (5.4)$$

The first condition corresponds to the original Harris criterion [Har74] for uncorrelated disorder, while the second condition is the extended Harris criterion [WH83]. It yields the critical value of the exponent  $\alpha$ , i.e.,  $\alpha_c = 2/\nu$ .

As follows from the above consideration, for classical percolation the quenched disorder is expected to cause a crossover in the exponent  $\nu_c$ , describing the size of a critical equipotential from  $\nu_c = 4/3$  to  $\nu_c = 2/\alpha$  for  $\alpha < 3/2$ . This prediction [Wei84] was made on the basis of Eq. (5.2). It was later tested by numerical simulations [PHSS92] which utilized the Fourier filtering method to generate a long-range-correlated random potential. The exponent  $\nu_c(\alpha)$  was studied using the same classical real-space RG method [RKS77] that was utilized above. The values of  $\nu_c$  inferred for  $\alpha < 1$  were consistently lower than  $2/\alpha$ . For example, from  $\alpha = 0.4$  follows  $\nu_c = 5$  [Wei84], whereas  $\nu_c = 3.4 \pm 0.3$  was observed.

The classical version of the LD transition is instructive, since it allows one to trace how the critical equipotentials grow in size upon approaching the percolation



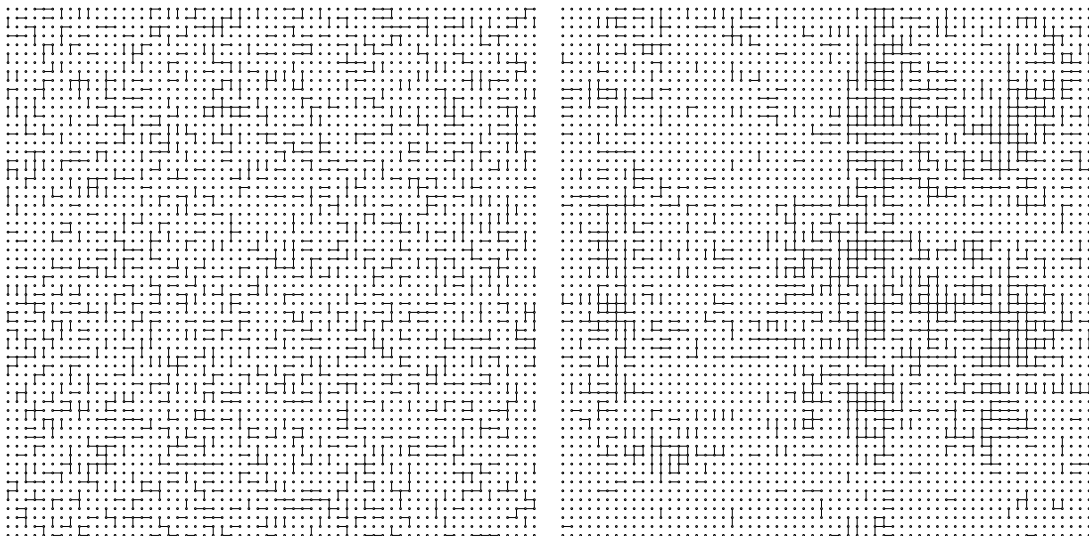


Figure 5.3: Illustration of the influence of quenched disorder by means of classical bond percolation on a  $60 \times 60$  square lattice with bond probability  $p = 0.2$ . In the uncorrelated case (left) bonds are distributed homogeneously. Adding correlation leads to a clustering of bonds (right).

threshold, and how the quenched disorder affects this growth. For an illustration of this behavior see Fig. 5.3. Roughly speaking, in the absence of long-ranged correlations, the growth of the equipotential size is due to the attachment of smaller equipotentials to the critical ones. As a result, the shape of a critical equipotential is dendritelike. As the threshold is approached, different critical equipotentials become connected through the narrow “arms” of the dendrite. Long-ranged correlations change this scenario drastically. As could be expected intuitively, and as follows from the simulations [MHSS96], critical equipotentials become more compact due to correlations. In fact, for  $\alpha < 0.25$ , the “arms” play no role [PHSS92], i.e., the morphology of a critical equipotential becomes identical to its “backbone”. As a result, the formation of the infinite equipotential at the threshold occurs through a sequence of “broad” merges of compact critical equipotentials. The correlation-induced enhancement of  $\nu_c$  indicates that due to these merges the size of the critical equipotential in the close vicinity of the threshold grows faster than in the uncorrelated case.

### 5.3 Macroscopic inhomogeneities in the RG approach

A natural way to incorporate a quenched disorder into the CC model is to ascribe a certain random shift,  $z_Q$ , to each SP height, and to assume that the shifts at different SP positions,  $\mathbf{r}$  and  $\mathbf{r}'$ , are correlated as

$$\langle z_Q(\mathbf{r})z_Q(\mathbf{r}') \rangle \propto |\mathbf{r} - \mathbf{r}'|^{-\alpha}, \quad (5.5)$$

with  $\alpha > 0$ . After this, the conventional transfer-matrix methods of [FL81, MK81] could be employed for numerically precise determination of  $\langle G \rangle$ , the distribution  $P_c(G)$ , its moments, and most importantly, the critical exponent,  $\nu$ . However, the transfer-matrix approach for a 2D sample is usually limited to fairly small sizes (e.g., up to 128 in [JW98]) due to the numerical complexity of the calculation. Therefore, the spatial decay of the power-law correlation by, say, more than an order in magnitude is hard to investigate for small  $\alpha$ . In principle the quasi-1D transfer-matrix method [CC88, MK81] can easily handle such decays at least in the longitudinal direction, where typically a few million lattice sites are considered iteratively. A major drawback, however, is the numerical generation of power-law correlated randomness since no iterative algorithm is known [PHSS92, MHSS96]. This necessitates the complete storage of different samples of correlated SP height landscapes [RKB<sup>+</sup>99], and the advantage of the iterative transfer-matrix approach is lost. Furthermore, in order to deduce the critical exponent [LWK93], one needs to perform finite-size scaling [MK81] with transverse sizes that should also be large enough to capture the main effect of the power-law disorder in the transverse direction. Consequently, even for a single transfer-matrix sample, the memory requirements add up to gigabytes.

On the other hand, the RG approach is perfectly suited to study the role of the quenched disorder. First, after each step of the RG procedure, the effective system size doubles. At the same time, the magnitude of the smooth potential, corresponding to the spatial scale  $r$ , falls off with  $r$  as  $r^{-\alpha/2}$ . As a result, the modification of the RG procedure due to the presence of the quenched disorder reduces to a scaling of the disorder magnitude by a *constant* factor  $2^{-\alpha/2}$  at each RG step. Second, the RG approach operates with the conductance distribution,  $P_n(G)$ , which carries information about *all* the realizations of the quenched disorder within a sample of size  $2^n$ . This is in contrast to the transfer-matrix approach [FL81, MK81], within which a small increase of the system size requires the averaging over the quenched disorder realizations to be conducted again.

The above consideration suggests the following algorithm. For the homogeneous case all SPs constituting the new super-SP are assumed to be identical, which means that the distribution of heights,  $Q_n(z)$ , for all of them is the same. For the correlated case these SPs are no longer identical, but rather their heights are randomly shifted by the long-ranged potential. In order to incorporate this potential into the RG scheme,  $Q_n(z_i)$  should be replaced by  $Q_n(z_i - \Delta_i^{(n)})$  for each SP,  $i$ , where  $\Delta_i^{(n)}$  is the random shift. Then the power-law correlation of the quenched disorder enters into the RG procedure through the distribution of  $\Delta_i^{(n)}$ . That is, for each  $n$  the distribution is Gaussian with the width  $\beta(2^n)^{-\alpha/2}$ . For large enough  $n$  the critical behavior should not depend on the magnitude of the correlation strength  $\beta$ , but on the power,  $\alpha$ , only.

## 5.4 Numerical results

Here the results of the application of the algorithm outlined in the previous Section are presented. First, for all values of  $\alpha > 0$  in correlator (5.5) the FP distribution

is identical to the uncorrelated case as found within the accuracy of the calculation. In particular,  $\langle G \rangle = 0.498$  is unchanged. However, the convergence to the FP is numerically less stable than for uncorrelated disorder due to the correlation-induced broadening of  $Q_n(z)$  during each iteration step. In order to compute the critical exponent  $\nu(\alpha)$  the RG procedure is started from  $Q_0(z - z_0)$ , as in the uncorrelated case, but in addition the random shifts are incorporated. As already explained these shifts are a result of the quenched disorder in generating the distribution of  $z$  at each RG step. The outcome is shown in Figs. 5.4–5.7. It illustrates that for increasing long-ranged character of the correlation (decreasing  $\alpha$ ) the convergence to a limiting value of  $\nu$  slows down drastically. Even after eight RG steps (i.e., a magnification of the system size by a factor of 256), the value of  $\nu$  with long-ranged correlations still differs appreciably from  $\nu = 2.39$  obtained for the uncorrelated case. The RG procedure becomes unstable after eight iterations, i.e.,  $z_{\max,9}$  can no longer be obtained reliably from  $Q_9(z)$ . Unfortunately, for small  $\alpha$  the convergence is too slow to yield the limiting value of  $\nu$  after eight steps only. For this reason, the above method is, strictly speaking, unable to unambiguously answer the question whether sufficiently long-ranged correlations result in an  $\alpha$ -dependent critical exponent  $\nu(\alpha)$ , or whether the value of  $\nu$  eventually approaches the uncorrelated value of 2.39. Nevertheless, the results in Figs. 5.4–5.7 indicate that the effective critical exponent exhibits a sensitivity to the long-ranged correlations even after a large magnification by  $256 \times 256$ . Since this factor coincides with the change in scale from the microscopic magnetic length to the realistic samples with finite sizes of several  $\mu\text{m}$ , macroscopic inhomogeneities are able to affect the results of scaling studies. Note further that as shown in the inset of Figs. 5.4–5.7 one can observe scaling of  $\nu$  values when plotted as function of a renormalized system size  $2^{\alpha n/2}$  only for large correlation strength  $\beta$ . In this case the disorder broadening during the first RG steps becomes comparable to the FP distribution. Therefore in the QH-RG the correlated disorder dominates over the initial FP distribution. One should emphasize that  $\nu(\alpha)$  obtained after eight RG steps always *exceeds* the uncorrelated value.

Figure 5.8 shows the values of  $\nu$  obtained after the eighth RG step as a function of the correlation exponent  $\alpha$  for different dimensionless strengths  $\beta$  of the quenched disorder. It is seen that in the domain of  $\alpha$ , where the values of  $\nu$  differ noticeably from  $\nu = 2.39$ , their dependence on  $\beta$  is strong. According to the extended Harris criterion,  $\nu(\alpha)$  is expected to exhibit a cusp at the  $\beta$ -independent value  $\alpha_c = 2/2.39 \approx 0.84$ . From the results in Fig. 5.8, two basic observations can be made. For a small enough magnitude of the long-range disorder, one observes a smooth enhancement of  $\nu(\alpha)$  with decreasing  $\alpha$  without a cusp. Although such a behavior might be caused by the relatively small number of RG steps, the data can be relevant for realistic samples which have a finite size and a finite phase-breaking length governed by temperature. At the largest  $\beta = 4$ , there is still no clear cusp but the  $\alpha$ -dependence for  $\alpha < \alpha_c$  is closer to the  $\nu = 2/\alpha$  predicted by the extended Harris criterion. Unfortunately, the numerics becomes progressively unstable, forbidding to go to even larger  $\beta$ . The origin for this strong  $\beta$  dependence of the results is a profound difference between the classical and quantum percolation problems as discussed in the next Section.

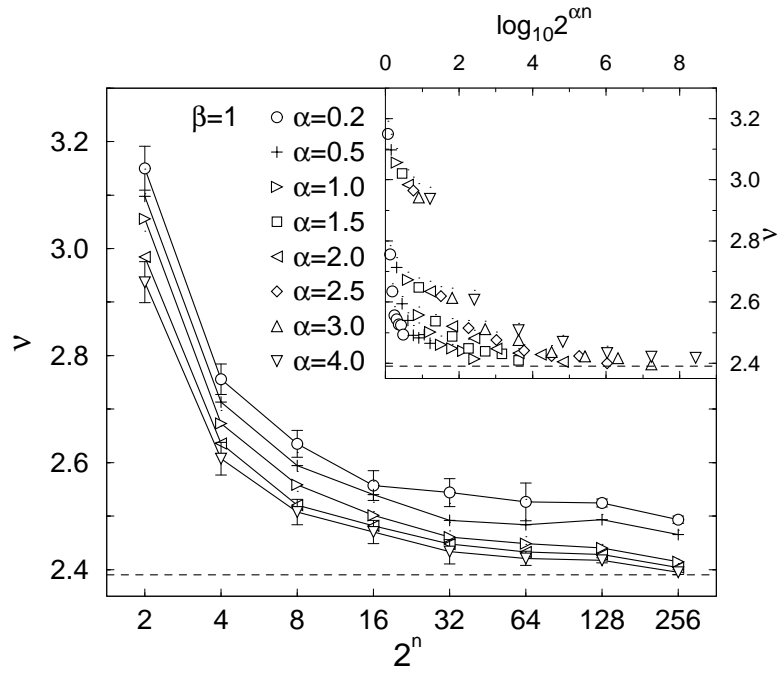


Figure 5.4: Critical exponent  $\nu$  obtained by the QH-RG approach as a function of RG scale  $2^n$  for  $\beta = 1$  and different correlation exponents  $\alpha$ . The dashed line indicates  $\nu = 2.39$ , which is the value obtained for uncorrelated disorder. For clarity, the errors are shown only for  $\alpha = 0.2$  and 4. Inset:  $\nu$  vs  $2^{\alpha n/2}$  does not scale.

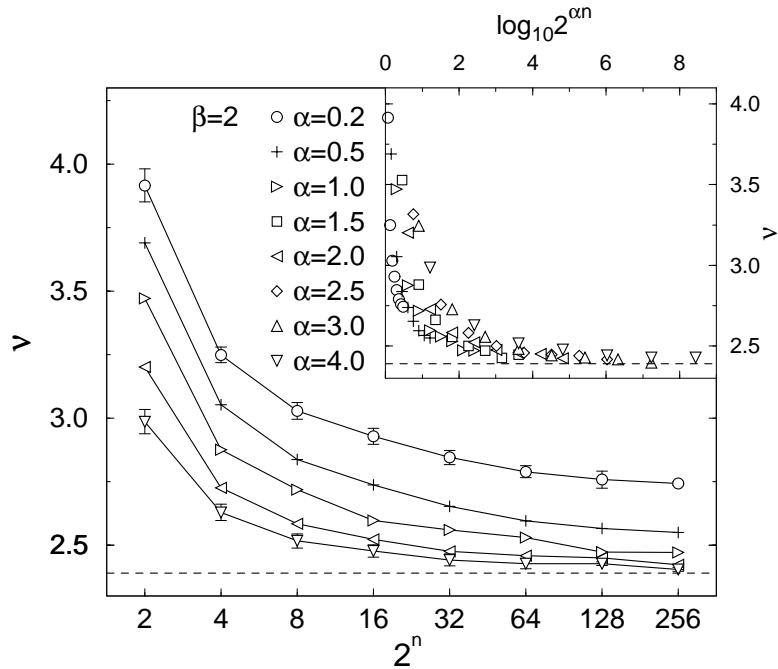


Figure 5.5: Critical exponent  $\nu$  obtained by the QH-RG for  $\beta = 2$  plotted analogously to Fig. 5.4. The increase of  $\beta$  leads to rising values  $\nu$ . Inset: Scaling is not observed.

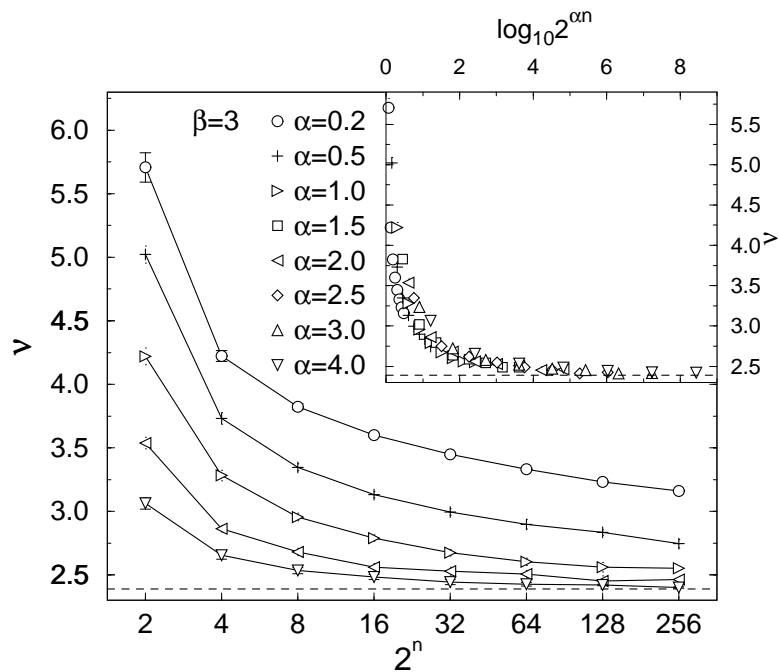


Figure 5.6: Critical exponent  $\nu$  obtained by the QH-RG for  $\beta = 3$  plotted analogously to Fig. 5.4.  $\nu$  is shifted again to higher values. Inset: Deviations from scaling decrease.

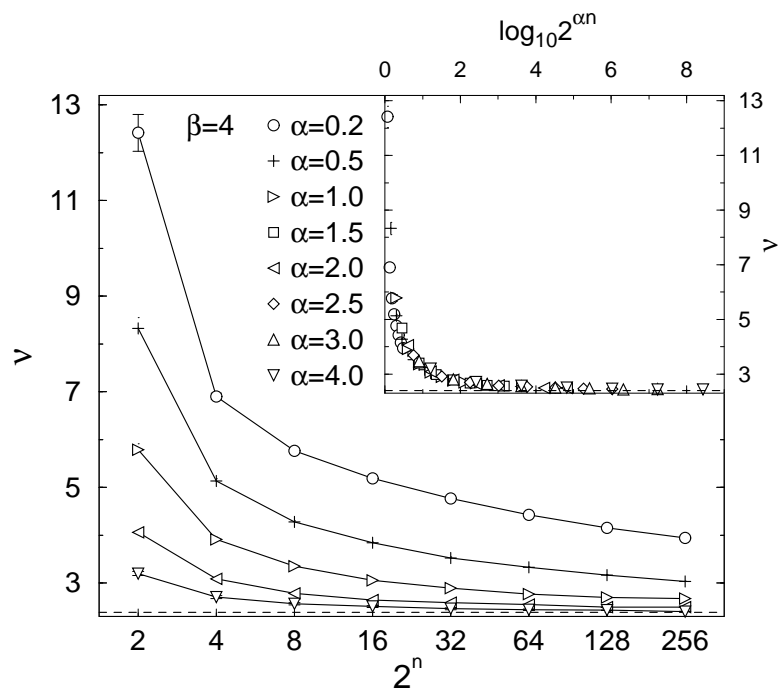


Figure 5.7: Critical exponent  $\nu$  obtained by the QH-RG for  $\beta = 4$  plotted analogously to Fig. 5.4. The values of  $\nu$  increased even further. Inset: Data show only small deviations from scaling indicating the dominating influence of correlated disorder due to the large  $\beta$ .

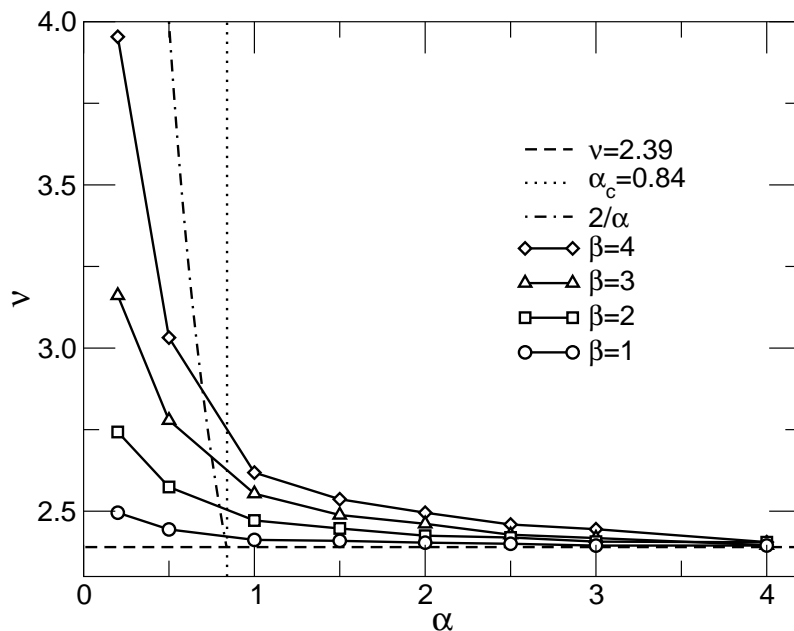


Figure 5.8: Dependence of the critical exponent  $\nu$  on correlation exponent  $\alpha$  for different  $\beta = 1, 2, 3$ , and  $4$  as obtained after eight QH-RG iterations. The dotted line indicates  $\alpha_c = 0.84$ . The dot-dashed line  $\nu = 2/\alpha$  for  $\alpha < \alpha_c$  follows from the extended Harris criterion [WH83] for classical percolation.

## 5.5 Intrinsic short-range disorder in quantum percolation

Here one should note that there is a crucial distinction between the classical case and the quantum regime of the electron motion considered in the present work. In this study, the correlation of the *heights* of the SPs has been incorporated into the RG scheme. At the same time it was assumed that the *Aharonov-Bohm phases* acquired by an electron upon traversing the neighboring loops are *uncorrelated*. This assumption implies that, in addition to the long-ranged potential, a certain short-ranged disorder causing a spread in the perimeters of neighboring loops of the order of the magnetic length is present in the sample. The consequence of this short-range disorder is the sensitivity of the results to the value of  $\beta$  which parametrizes the magnitude of the correlated potential. The presence of this short-range disorder affecting exclusively the Aharonov-Bohm phases significantly complicates the observation of the cusp in the  $\nu(\alpha)$  dependence at  $\alpha \approx 0.84$ , as is expected from the extended Harris criterion.

In order to understand the origin of these complications, one can consider a general form of the correlator for long-range disorder

$$\langle V(\mathbf{r})V(\mathbf{r}') \rangle = V_0^2 F\left(\frac{|\mathbf{r} - \mathbf{r}'|}{l}\right) \quad (5.6)$$

where  $l$  is the microscopic length and  $F(0) = 1$ ,  $F(x) \propto x^{-\alpha}$  for  $x \gg 1$ . Now suppose that the correlator contains an additional short-range term  $W_0^2 G(|\mathbf{r} - \mathbf{r}'|/l)$ , with

$G(0) = 1$  and  $G(x)$  falling off much more rapidly than  $F(x)$  for  $x \gg 1$ . The extended Harris criterion implies that this term will not change  $\nu(\alpha)$  in an *infinite sample*. It is obvious, however, that in order to “erase the memory” of the short-range disorder, many more RG iterations have to be performed or, equivalently, much larger system sizes should be analyzed. Moreover, the larger the ratio  $W_0/V_0$ , the more challenging the numerics becomes. At this point, one should take into account that in quantum percolation the short-range term emulated by the randomness in the phases has a huge magnitude. Indeed, if in the first RG step all five SPs were chosen to be identical with transmission amplitudes  $t_i^2 = 0.5$ , then due to the phases, the width of the  $Q(z)$  distribution after the first step is already  $\pm 2.5$  [GR97]. This translates into an enormously wide spread in the transmission coefficients of effective SPs ranging from 0.075 to 0.92. In order to suppress this intrinsic “quantum white noise”, one either has to perform more RG steps or to increase the magnitude of  $V_0$  ( $\sim \beta$  in the notation of Section 5.3). Both strategies are limited by numerical instabilities. In particular, a larger  $\beta$  leads to more weight in the tails of the  $Q(z)$  distribution in which the uncertainty is maximal. In other words, at large  $\beta$  the role of rare realizations is drastically emphasized.

The obtained numerical results demonstrate that when the critical exponent depends weakly on the sample size (large  $n$  in Figs. 5.4-5.7), it still depends on the “strength”  $\beta$  of the quenched disorder. Thus it is important to relate this strength to the observable quantities. One can roughly estimate  $\beta$  assuming that the microscopic spatial scale (lattice constant) is the magnetic length,  $l_B$ , while the microscopic energy scale (the SP height) is the width of the Landau level. Denoting by  $\gamma$  a typical fluctuation of the filling factor within a region with size  $L$ , then the estimate for  $\beta$  is  $\beta \sim \gamma (L/l_B)^{\alpha/2}$ . Naturally, for a given  $\gamma$ , the larger values of  $\alpha$  correspond to the “stronger” quenched disorder parameter  $\beta$ .

In fact, if one had to draw a quantitative conclusion on the basis of the accuracy achieved, it should be based on the curve in Fig. 5.8 corresponding to the maximal value  $\beta = 4$ . Actually, for this  $\beta$ , the agreement with the extended Harris criterion is fairly good. In particular, for  $\alpha = 0.5$ ,  $\nu \approx 3$  is found, whereas  $2/\alpha = 4$ . Note that only very recently the authors of [SMK03] could demonstrate by a different method a better agreement with the extended Harris criterion.

## 5.6 Conclusion

It was argued for a long time that the enhanced value of the critical exponent  $\nu$  extracted from the narrowing of the transition region with temperature has its origin in the long-ranged disorder present in GaAs-based samples. To my knowledge, the present work is the first attempt to quantify this argument. As a result the random potential with a power-law correlator leads to values of  $\nu$  exceeding  $\nu \approx 2.35$ , which is firmly established for short-ranged disorder. Since an enhancement of the critical exponent due to the correlations is observed also for classical case, the main result can be formulated as follows: quenched disorder affects classical and quantum percolation in a similar fashion.

The result indicates that macroscopic inhomogeneities must lead to smaller values of  $\kappa \propto 1/\nu$ . Experimentally, the value of  $\kappa$  smaller than 0.42 was reported in a number of early (see, e.g., [KHKP92] and references therein) as well as recent [Lan] works. This fact was accounted for by different reasons (such as temperature dependence of the phase breaking time, incomplete spin resolution, valley degeneracy in Si-based MOSFETs, and inhomogeneity of the carrier concentration in GaAs-based structures with a wide spacer). Briefly, the spread of the  $\kappa$  values was attributed to the fact that the temperatures were not low enough to assess the truly critical regime. The possibility of having  $\kappa < 0.4$  due to the correlation-induced dependence of the effective  $\nu$  on the phase-breaking length or, ultimately, on the sample size, as in Figs. 5.4–5.7, was never considered.

It should be pointed out that the limited number (eight) of RG steps permitted by the numerics nevertheless allows one to trace the evolution of the wave functions from *microscopic* scales (of the order of the magnetic length) to *macroscopic* scales (of the order of  $5\mu\text{m}$ ) which are comparable to the sizes of the samples used in the experimental studies of scaling (see e.g., [KHKP91b, KHKP92]) and much larger than the samples [CBF99, CK96] used for the studies of mesoscopic fluctuations.

Another *qualitative* conclusion of this study is that the spatial scale at which the exponent  $\nu$  assumes its “infinite-sample” value is much larger in the presence of the quenched disorder than in the uncorrelated case. In fact this scale can be of the order of microns. This conclusion can also have serious experimental implications. That is, even if the sample size is much larger than this characteristic scale, this scale can still exceed the phase-breaking length, which would mask the true critical behavior at the QH transition.

Note also, that throughout this study localization of a single electron has been considered. The role of electron-electron interactions in the scaling of the integer QH effect was recently addressed in [HB99] and [WFGC00].



# Chapter 6

## RG approach to the Hall resistivity

### 6.1 Introduction

In the previous Chapters the RG approach to the CC model has been applied successfully for the determination of the conductance distribution and the LSD. Now an RG approach is derived also for the computation of the Hall resistance  $R_H$  which allows a third independent characterization of the QH transition.

On the experimental side one usually considers the resistance rather than the conductance, because the components of the resistance tensor can be determined directly, e.g., by a four-terminal measurement using a Hall bar geometry [KDP80, Yos02]. Once knowing  $R_H$  and  $R_L$  the components of the conductance tensor are then calculated using Eqs. (2.3). In Chapter 3 it was demonstrated that the distribution  $P_c(G)$  of the conductance at the QH transition exhibits strong fluctuations, which should manifest also in  $P_c(R_H)$ . The shape of  $P_c(R_H)$  is therefore another possibility to study the characteristic of the fluctuations.

A second interesting question concerns the behavior of  $R_H$  in the insulating regime. For increasing  $B$  the sequence of QH transitions between adjacent Landau levels is finalized by a transition from a Landau plateau to an insulator, which is characterized by a diverging  $R_L$ . Note that recent experimental [HSS<sup>+</sup>00] and theoretical [SW00] works suggest the existence of a plateau-insulator transition also for higher Landau plateaus which are not considered in the context of this work. Since at the transition  $\sigma_{xx} \rightarrow 0$  and  $\sigma_{xy} \rightarrow 0$  the determination of  $R_H$  according to Eqs. (2.3) is difficult and depends on the relation between  $\sigma_{xx}$  and  $\sigma_{xy}$ . Especially, if the ratio  $\sigma_{xy}/\sigma_{xx}^2$  stays finite one obtains also a finite value for  $R_H$  which corresponds to a new insulating regime called *Hall insulator* [KLZ92]. In agreement with experimental results [GST88, GWSS93] (see Fig. 6.1a) a Drude-like behavior  $R_H \propto B/enc$  was predicted [KLZ92, ZKL92]. In contrast, more recent experimental studies [HSS<sup>+</sup>98, LPV<sup>+</sup>02, PSC<sup>+</sup>03, STS<sup>+</sup>97a, STS<sup>+</sup>96] of the insulating regime found a quantized  $R_H$  unchanged from the plateau value as demonstrated in Fig. 6.1b. The extension of the quantization of  $R_H$  into the insulator, dubbed *quantized Hall insulator*, was proven to be consistent with transport models based on the local-conductivity approach [DM94] and more generally with incoherent network models

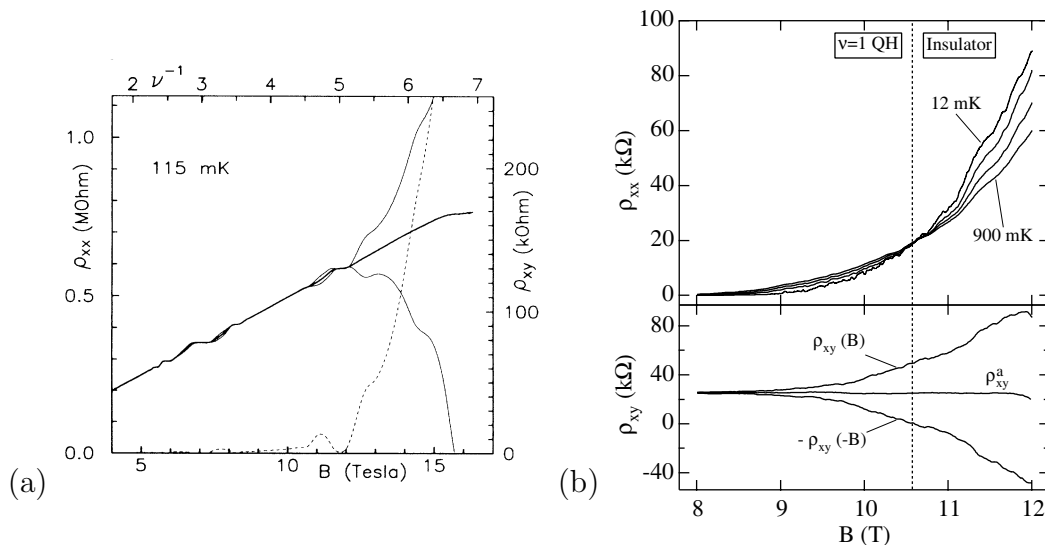


Figure 6.1: Different behavior of the Hall resistivity  $\rho_{xy}$  at the QH plateau to insulator transition observed in [GWSS93] (a) and [PSC<sup>+</sup>03] (b). The dotted line corresponds to  $\rho_{xx}$  (a) or the transition point (b), respectively.  $\rho_{xy}$  is obtained as average over two measurements with opposite directions of the magnetic field  $B$  (thin lines).

of weakly coupled QH puddles [SA97]. For strong localization where the localization length is much smaller than the dephasing length an incoherent model fails. Quantum interference becomes more and more important. As shown by coherent methods in recent theoretical works [PA99, SW99, ZS01] the quantized Hall insulator is not sustained but rather a diverging  $R_H$  is found. In particular, deep in the insulating regime  $R_H$  follows a power-law  $R_H \sim R_L^\mu$  [PA99, ZS01]. An exponent  $\mu \approx 0.32 - 0.35$  was obtained numerically in [PA99] while  $\mu = 1/2$  [ZS01] was derived by an analytical approximation based on a RG approach to the CC model using a 4SP RG unit. It was demonstrated in the previous Chapters that this 4SP unit yields less accurate results at the QH transition than the 5SP unit. Whether this situation is preserved also in the insulating regime is uncertain and should be verified.

## 6.2 RG equation for $R_H$

First, the value of  $R_H$  has to be related to the RG unit. For this purpose one calculates the resistance  $R = U/J$  defined by the potential difference  $U$  across the RG unit and the current  $J$  flowing through the unit. In Fig. 6.2 this ansatz is illustrated for the 5SP RG unit used previously.

Assuming that the current enters the RG unit via one incoming link ( $I'$ ) only and the other incoming link is inactive ( $I'^* = 0$ ) the resulting power transmission coefficient  $t'^2 = O^2/I'^2$  of the RG unit can be associated with  $J$ . In order to determine  $U$  one considers the quantities  $a_u = O_1^2/I'^2$  and  $a_v = O_5^{*2}/I'^2$  as chemical potentials measured by weakly coupled voltage probes at these opposite links of the RG unit. Thus the voltage drop is given by  $U = a_u - a_v$ . Because of the four-terminal geometry the obtained  $R$  contains beside the Hall resistance  $R_H$  also

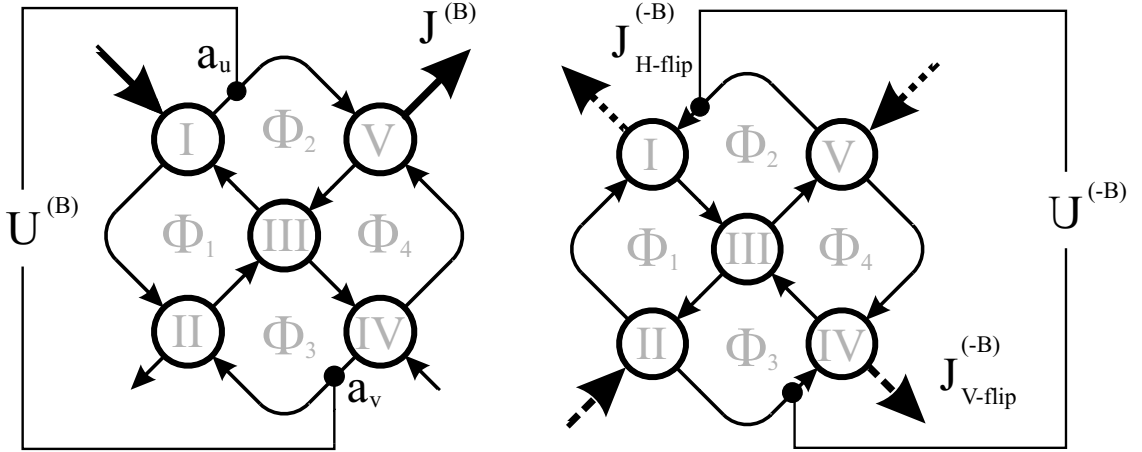


Figure 6.2: To determine the Hall resistance  $R_H$  of the RG unit as illustrated here for the 5SP case the voltage  $U$  and the current  $J$  are calculated for positive magnetic field  $B$  (left) and the opposite direction  $-B$  (right). For  $-B$  the value of  $R_H$  can be obtained by measuring  $J$  either between the upper (H-flip) or lower (V-flip) two links, respectively.

a contribution from the longitudinal resistance  $R_L$ . The separation of the unwanted part  $R_L$  is accomplished by employing the antisymmetry of the Hall voltage  $U_H$  under the reversal of the direction of the magnetic field  $B$

$$U_H = \frac{1}{2} (U^{(B)} - U^{(-B)}). \quad (6.1)$$

Considering the 5SP RG unit again one therefore obtains

$$R_H = \frac{1}{2} \frac{(a_u^{(B)} - a_v^{(B)}) - (a_u^{(-B)} - a_v^{(-B)})}{t'^2}. \quad (6.2)$$

The quantities  $a_u^{(B)}$  and  $a_v^{(B)}$  are calculated by solving the system of equations (3.4) analogously to the determination of  $t'$  in Section 3.2. One finds

$$a_u^{(B)} = \left| \frac{t_1(1 - r_2 r_3 r_4 e^{i\Phi_3} - t_3 t_4 t_5 e^{i\Phi_4}) - t_2 e^{i\Phi_1} (t_3 - t_4 t_5 e^{i\Phi_4})}{(r_3 - r_2 r_4 e^{i\Phi_3})(r_3 - r_1 r_5 e^{i\Phi_2}) + (t_3 - t_4 t_5 e^{i\Phi_4})(t_3 - t_1 t_2 e^{i\Phi_1})} \right|^2 \quad (6.3)$$

and

$$a_v^{(B)} = \left| \frac{r_4(r_1 r_3 t_2 e^{i\Phi_1} - r_5 t_2 e^{i(\Phi_1 + \Phi_2)} + r_5 t_1 t_3 e^{i\Phi_2})}{(r_3 - r_2 r_4 e^{i\Phi_3})(r_3 - r_1 r_5 e^{i\Phi_2}) + (t_3 - t_4 t_5 e^{i\Phi_4})(t_3 - t_1 t_2 e^{i\Phi_1})} \right|^2. \quad (6.4)$$

Under the reversed field  $-B$  the electrons travel along the same equipotentials but in the opposite direction. In the corresponding RG unit the links therefore only change their direction, as shown in Fig. 6.2. The value of  $U^{(-B)}$  can then be computed in two different ways. First, the same direction of the current is used for both  $B$  fields. Therefore one measures the currents  $J^{(B)}$  and  $J_{V\text{-flip}}^{(-B)}$  on different channels of the RG unit [ZS01]. Second, when measuring on the same channels the currents  $J^{(B)}$

and  $J_{H\text{-flip}}^{(-B)}$  have opposite directions. As a consequence the sign of  $U^{(-B)}$  changes too, which has to be incorporated in Eq. 6.2.

Technically, a full rederivation of the RG equation for  $-B$  can be omitted if the structure of the RG unit is taken into account. The result with identical directions of the current is obtained by flipping the unit vertically (V-flip) while the other case corresponds to a horizontal flip (H-flip). The comparison to the original RG unit then shows how to map the indices of the SPs and the phases in order to adopt the RG equation to  $-B$ , which is demonstrated here for the V-flip result where  $(r_1, t_1) \leftrightarrow (r_2, t_2)$ ,  $(r_4, t_4) \leftrightarrow (r_5, t_5)$ , and  $\Phi_2 \leftrightarrow \Phi_3$ :

$$a_u^{(-B)} = \left| \frac{r_5(r_2 r_3 t_1 e^{i\Phi_1} - r_4 t_1 e^{i(\Phi_1 + \Phi_3)} + r_4 t_2 t_3 e^{i\Phi_3})}{(r_3 - r_1 r_5 e^{i\Phi_2})(r_3 - r_2 r_4 e^{i\Phi_3}) + (t_3 - t_4 t_5 e^{i\Phi_4})(t_3 - t_1 t_2 e^{i\Phi_1})} \right|^2 \quad (6.5)$$

and

$$a_v^{(-B)} = \left| \frac{t_2(1 - r_1 r_3 r_5 e^{i\Phi_2} - t_3 t_4 t_5 e^{i\Phi_4}) - t_1 e^{i\Phi_1}(t_3 - t_4 t_5 e^{i\Phi_4})}{(r_3 - r_1 r_5 e^{i\Phi_2})(r_3 - r_2 r_4 e^{i\Phi_3}) + (t_3 - t_4 t_5 e^{i\Phi_4})(t_3 - t_1 t_2 e^{i\Phi_1})} \right|^2. \quad (6.6)$$

Using Eq. (6.2) one is now able to determine the distributions of  $P(R_H)$  at the QH transition iteratively in course of the RG iterations.

In the original work [ZS01] introducing the RG approach to  $R_H$ , the 4SP RG unit from Section 3.6 was used. As demonstrated in Section 3.6 this RG unit yields less accurate results. Nevertheless it might be useful to compare the numerical result with the analytically predicted behavior [ZS01]. The derivation of  $R_{H,4SP}$  resembles the construction of  $t'_{4SP}$  out of the 5SP result  $t'$ . Consequently, it yields

$$R_{H,4SP} = \frac{1}{2} \frac{\left( a_{u,4SP}^{(B)} - a_{v,4SP}^{(B)} \right) - \left( a_{u,4SP}^{(-B)} - a_{v,4SP}^{(-B)} \right)}{(t'_{4SP})^2} \quad (6.7)$$

with

$$a_{u,4SP}^{(B)} = \left| \frac{t_1(1 - r_2 r_3 e^{i\Phi_3}) + t_2 t_3 t_4 e^{i\Phi_2}}{(1 - r_2 r_3 e^{i\Phi_3})(1 - r_1 r_4 e^{i\Phi_1}) + t_1 t_2 t_3 t_4 e^{i\Phi_2}} \right|^2 \quad (6.8)$$

and

$$a_{v,4SP}^{(B)} = \left| \frac{r_3 t_2 (r_1 - r_4 e^{i\Phi_1})}{(1 - r_2 r_3 e^{i\Phi_3})(1 - r_1 r_4 e^{i\Phi_1}) + t_1 t_2 t_3 t_4 e^{i\Phi_2}} \right|^2. \quad (6.9)$$

Also for the 4SP unit one can derive  $U^{(-B)}$  in the two different ways, e.g. the V-flip result:

$$a_{u,4SP}^{(-B)} = \left| \frac{r_4 t_1 (r_2 - r_3 e^{i\Phi_3})}{(1 - r_1 r_4 e^{i\Phi_1})(1 - r_2 r_3 e^{i\Phi_3}) + t_1 t_2 t_3 t_4 e^{i\Phi_2}} \right|^2 \quad (6.10)$$

and

$$a_{v,4SP}^{(-B)} = \left| \frac{t_2(1 - r_1 r_4 e^{i\Phi_1}) + t_1 t_3 t_4 e^{i\Phi_2}}{(1 - r_1 r_4 e^{i\Phi_1})(1 - r_2 r_3 e^{i\Phi_3}) + t_1 t_2 t_3 t_4 e^{i\Phi_2}} \right|^2. \quad (6.11)$$

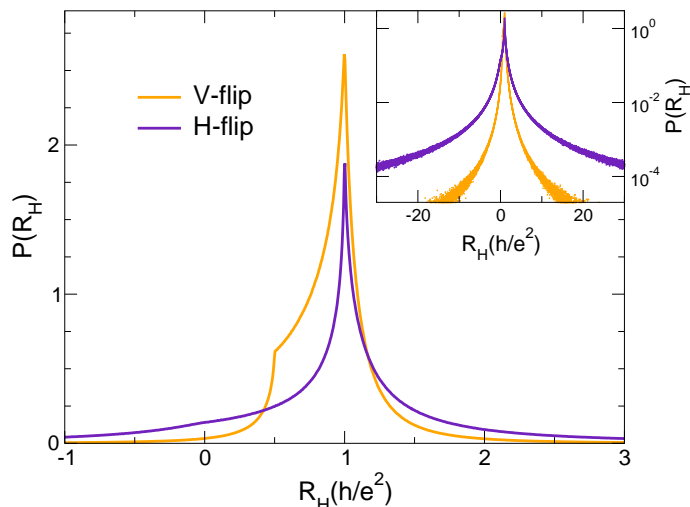


Figure 6.3: Critical distribution  $P_c(R_H)$  at the QH transition for the V-flip and the H-flip method obtained with the 5SP RG unit. Inset: The long tails of  $P_c(R_H)$  plotted logarithmically. Data points are the average over 10 consecutive bins.

## 6.3 Numerical results

### 6.3.1 Behavior at the QH transition

As explained above the RG approach can be used to determine the conductance distribution  $P(G)$  and the resistance distribution  $P(R_H)$  simultaneously. The numerical strategy therefore corresponds to the method used in Section 3.4. Namely, the RG is started from a certain initial  $P_0(t)$  and the  $P_i(t)$  are discretized in 1000 bins within  $t \in [0, 1]$ . Using Eq. (6.2) or (6.7), respectively, one obtains besides  $P_{i+1}(t)$  now also the distribution  $P_{i+1}(R_H)$ . Unlike  $t$  the value of  $R_H$  is not bound to a fixed interval. To perform a discretization requires to set lower and upper bounds appropriately. In this work the resulting histogram is limited to  $[-100, 100]$  containing 40000 bins. For the  $10^8$  samples used to construct each  $P_{i+1}(R_H)$ , the part of values exceeding these bounds is found to be less than  $< 1\%$  for calculations around the QH transition. Thus these values are neglected for the shape of the histogram. Nevertheless the resulting distribution  $P_{i+1}(R_H)$  can be normalized correctly because the total number of exceeding values is stored. By this RG approach, the FP distribution  $P_c(R_H)$  is now calculated. Since  $P_c(t)$  is already known from Section 3.4 one can speed up the determination by using  $P_c(t)$  as initial  $P_0(t)$  and therefore obtain  $P_c(R_H)$  already after the first iteration. In Figures 6.3 and 6.4 the resulting  $P_c(R_H)$  is plotted for the 5SP and the 4SP RG unit. Both graphs show a significant difference in the shape of  $P_c(R_H)$  between the results of H-flip and V-flip. The H-flip distributions are characterized by a very sharp nearly symmetric peak at  $R_H = 1$  which coincides with the value of  $R_H$  at the first Landau level. In addition there appears a small kink at  $R_H = 0$  which is more pronounced for the 4SP unit and hardly visible in case of the 5SP unit. For V-flip an asymmetric distribution is found with a strong peak at  $R_H = 1$ . Surprisingly, there exists also a kink at

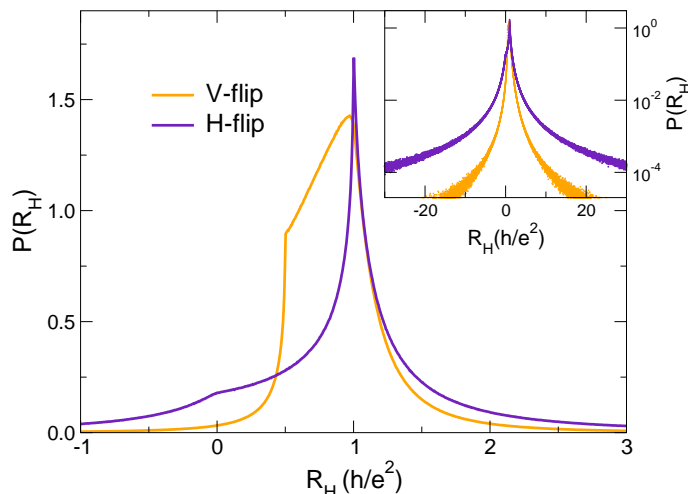


Figure 6.4: Critical distribution  $P_c(R_H)$  at the QH transition for V-flip and H-flip method calculated with the 4SP RG unit. Inset: The long tails of  $P_c(R_H)$  plotted as in Fig. 6.3.

$R_H = 0.5$  that would correspond to the second Landau level, which is not described by the CC model. The origin of the “wrong” kink must stem from a difference between the calculation of  $R_H$  according to H-flip and V-flip method, respectively. Both methods differ only in the  $(-B)$  part of  $R_H$ . As illustrated in Fig. 6.2, the H-flip method measures  $J$  between the same SPs  $I$  and  $V$  as for  $(+B)$ . In contrast, the  $J$  for V-flip is obtained between SPs  $II$  and  $IV$ . While one can expect the same result for H-flip and V-flip when considering only the  $(-B)$  contribution separately, the final V-flip result for  $R_H$  according to Eq. (6.2) obviously contains an additional correlation reflected by the kink at  $R_H = 0.5$ . A common attribute to all  $P_c(R_H)$  is demonstrated in the insets of Figs. 6.3 and 6.4. All FP distributions have very long tails indicating strong fluctuations of  $R_H$ .

The behavior of  $P(R_H)$  is now studied also around the QH transition. For this purpose the RG iteration is started using a disturbed FP distribution with an initial shift  $z_0$ , analogously to the calculation of the critical exponent in Section 3.3. The resulting distributions  $P_n(R_H)$  for  $z_0 = \pm 0.1$  are shown in Figures 6.5 and 6.6. For  $z_0 = 0.1$  the initial distribution  $P_0(t)$  is disturbed toward complete transmission ( $t = 1$ ). In course of the RG iterations the shift in this direction increases (see left insets in Figs. 6.5 and 6.6). Considering  $P_n(R_H)$  also a systematic behavior is observed. Originating from  $P_c(R_H)$  the width of the distribution starts to shrink while at the same time the peak at  $R_H = 1$  grows. This observation holds for both V-flip and H-flip results and is less pronounced for the 4SP unit. For  $z_0 = -0.1$  the distribution  $P_n(t)$  moves to the opposite direction toward complete reflection ( $t = 0$ ). Here the results of the V-flip and H-flip method behave differently. For the V-flip method the kink at  $R_H = 0.5$  transforms to an increasing peak while the peak at  $R_H = 1$  is shrinking. Thereby the width of the distribution is nearly unchanged compared with  $P_c(R_H)$ . This signature of a quantized  $R_H$  in the insulating regime is questioned by the origin of the structure at  $R_H = 0.5$  which has been discussed already above. On the other hand, for the H-flip  $P_n(R_H)$  the peak at  $R_H = 1$

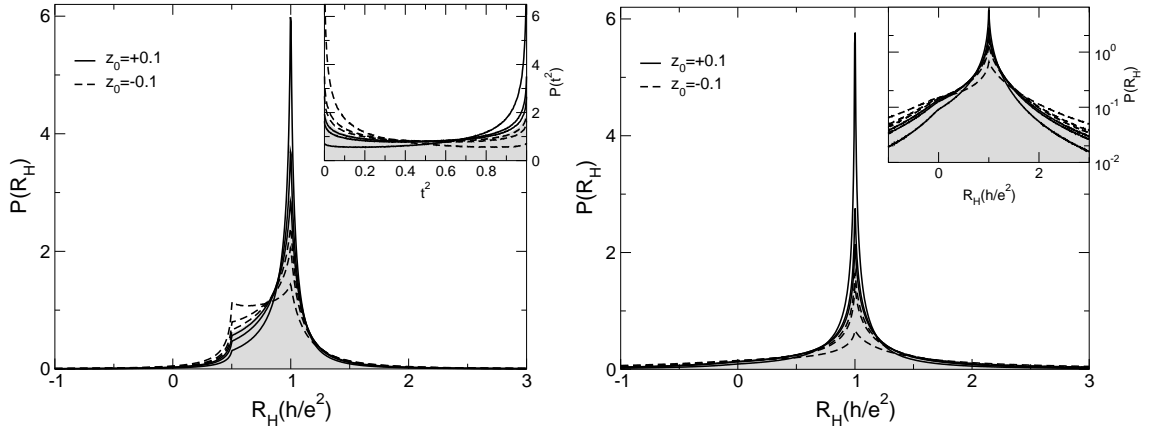


Figure 6.5: Change of  $P(R_H)$  in the course of the QH RG iterations when starting with initial shifts  $z_0 = \pm 0.1$  away from the FP using the 5SP RG unit. Only iteration steps 1, 4, and 8 are shown. The shaded area corresponds to the FP distribution. Left: Results for the V-flip unit. The inset contains the corresponding  $P(t^2)$ . Right: Same for the H-flip unit. In the inset the same data are plotted logarithmically.

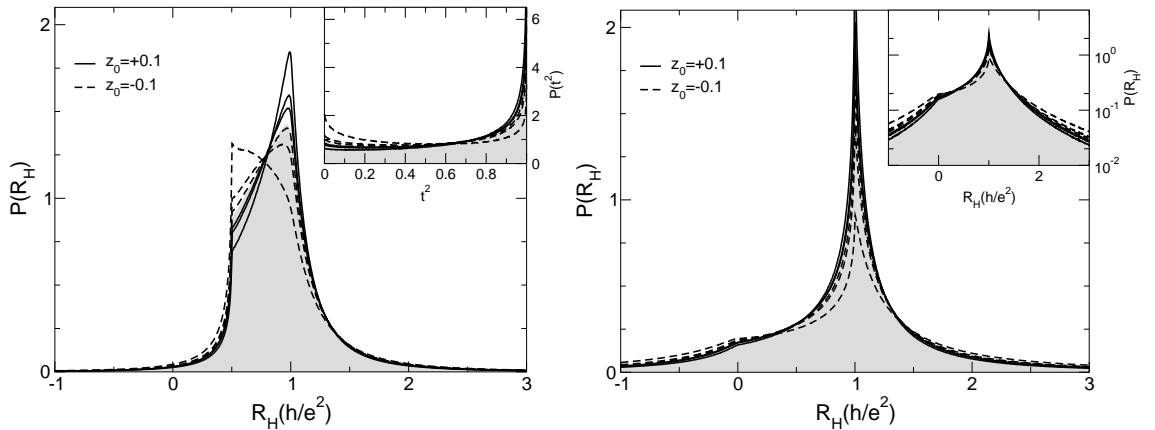


Figure 6.6: Change of  $P(R_H)$  in course of the QH RG iterations, analogously to Fig. 6.5 now using the 4SP RG unit.

stays at its position but broadens rapidly moving all weight into the tails. The H-flip result is dominated by strong fluctuations of  $R_H$ . For the characterization of  $P(R_H)$  the arithmetic mean is therefore ineligible, because it is highly influenced by rare  $R_H$  values from the tails. As another possible mean, the geometric mean is more suitable for long tails but cannot deal with the negative  $R_H$ . Instead a more robust averaging procedure was suggested by defining a typical value of  $R_H$  [ZS01]. Based on scattering through a one-dimensional chain, it is argued that this more appropriate mean is obtained by averaging not  $R_H$  itself but each of the constituting quantities separately [ZS01]

$$R_{H,\text{typ}} = \frac{1}{2} \frac{\left( \langle a_u^{(B)} \rangle_{\text{typ}} - \langle a_v^{(B)} \rangle_{\text{typ}} \right) - \left( \langle a_u^{(-B)} \rangle_{\text{typ}} - \langle a_v^{(-B)} \rangle_{\text{typ}} \right)}{\langle t^2 \rangle_{\text{typ}}}, \quad (6.12)$$

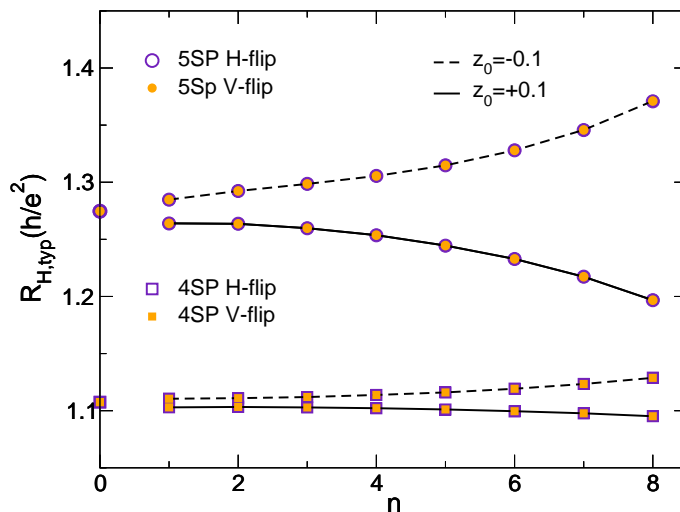


Figure 6.7: The typical value  $R_{H,\text{typ}}$  as function of the RG iteration  $n$  close to the QH transition. Data are shown for the 5SP unit (circles) and the 4SP unit (squares). With the initial disturbance  $z_0$  from the FP distribution one can drive the RG either toward complete transmission (solid line) or complete reflection (dashed line). The single symbols at  $n = 0$  correspond to the FP result.

where  $\langle x \rangle_{\text{typ}} \equiv \prod_{i=1}^N x_i^{1/N}$  is the geometric mean for  $N$  samples. Obviously, the calculation of  $R_{H,\text{typ}}$  is not limited to the chosen discretization interval and therefore all results can be taken into account. Furthermore this method of averaging should also resolve the discrepancy between the V-flip and H-flip results. Since in Eq. 6.12 all quantities, i.e. the amplitudes determining the value of  $U$ , are averaged separately, correlations between the ( $B$ ) and ( $-B$ ) representation of a single RG unit are not preserved. One can therefore expect the same  $R_{H,\text{typ}}$  for V-flip and H-flip.

In Figure 6.7 the evolution of  $R_{H,\text{typ}}$  is shown as function of the iteration step for  $z_0 = \pm 0.1$  and the 4SP and 5SP RG unit. As expected the typical means for the V-flip and the H-flip method yield identical results. All curves show a monotonic behavior. For  $z_0 = 0.1$  the value of  $R_{H,\text{typ}}$  decreases in course of the RG iterations which agrees with the more and more dominating influence of the peak at  $R_H = 1$  observed in Figs. 6.5 and 6.6. On the other hand, starting the iterations with a negative shift  $z_0 = -0.1$  leads to a steadily increasing  $R_{H,\text{typ}}$ . While for  $P(R_H)$  obtained by the H-flip method this behavior could be extracted from the very long tails of the distribution using the typical average (6.12), Figs. 6.5 and 6.6 suggest a different dependence for the V-flip results. The  $P(R_H)$  for the V-flip method shows an increasing peak at  $R_H = 0.5$  for  $t \rightarrow 0$ . Therefore one might expect rather a decrease of  $R_{H,\text{typ}}$  from a higher value  $\approx 1$  toward  $R_{H,\text{typ}} \approx 0.5$ . This contradiction is another indication that the shape of  $P(R_H)$  as obtained by the H-flip method seems to be more reasonable. Furthermore the FP value associated with  $P_c(R_H)$  is larger than 1 in contrast to the shape of  $P_c(R_H)$  in Figs. 6.3 and 6.4. The reason for this discrepancy lies in the very long tails of  $P(R_H)$  in connection with the definitions (6.2) and (6.12) of  $R_H$  and  $R_{H,\text{typ}}$ , respectively. Very large absolute values of  $R_H$



are obviously the consequence of a very small denominator  $t^2$  in Eq. (6.2) meaning that the current is almost totally reflected by the RG unit. As can be seen in the insets of Figs. 6.5 and 6.6 this scenario is possible since  $P_n(t^2)$  also exhibits strong fluctuations and spreads over the whole range between 0 and 1. In the definition of  $R_{H,\text{typ}}$  in Eq. (6.12) the independent averaging over each term does not preserve all correlations possible for  $R_H$  in Eq. (6.2) and suppresses the influence of rare realizations of the RG unit.

### 6.3.2 Behavior away from the QH transition

Throughout this study the strength of the RG approach close to the QH transition has been demonstrated. Now, at last, it will be applied to the two extreme cases where  $t \rightarrow 0$  and  $t \rightarrow 1$ . Recalling the results of Chapter 3, depending on the initial conditions one or the other limit is approached by default provided that the number of RG iterations was large enough. Unfortunately, this method has a numerical drawback. During the RG steps the distribution  $P_n(t)$  becomes sharply peaked at either  $t = 0$  or  $t = 1$ , which can already be seen in the left insets of Figs. 6.5 and 6.6. Thus the algorithm used for obtaining random  $t_i$  according to a  $P(t)$  is less and less efficient and finally breaks down. To circumvent this problem the  $t_i$  are chosen according to artificially constructed distributions

$$P(t^2) = \frac{1}{m}(t^2)^{\frac{1-m}{m}} \quad \text{and} \quad P(t^2) = \frac{1}{m}(1-t^2)^{\frac{1-m}{m}} \quad (6.13)$$

within the interval  $[0, 1]$  and an integer  $m > 0$ . Note that Eq. (6.13) is simply a result of taking uniformly distributed random numbers within  $[0, 1]$  to the power of  $m/2$ . By this method only one RG iteration can be calculated, because the resulting distributions are even sharper peaked and cannot be used as initial distributions for the next RG step as explained above. The accuracy of the method therefore depends crucially on how fast the RG transforms the artificial input distribution to the quantum regime. From the findings of the previous Chapters one can assume that a few iterations are sufficient and a single RG step allows only a crude approximation. The results for  $P(t^2)$  and  $P(R_H)$  of the 5SP unit are shown in Figs. 6.8 and 6.9. For  $t \rightarrow 0$  a similar behavior as for  $z_0 = -0.1$  is observed. In the V-flip result the peak at  $R_H = 0.5$  grows to a maximum of 50.0 for  $m = 15$  while the peak at  $R_H = 1$  is still preserved and only shrinks in width. In addition a small peak occurs at  $R_H = 0$ . Contrary, the H-flip method shows a strong broadening of the peak at  $R_H = 1$ . For  $m = 15$  the maximum of the distribution is below 0.01 and 82% of the  $R_H$  results lie outside the discretization interval  $[-100, 100]$ . The distributions exhibit long tails following from the very small values of  $t$  as described above and also demonstrated in Fig. 6.10. Seemingly, the shape of  $P(R_H)$  cannot be directly related to the expected insulating behavior for  $t \rightarrow 0$ . On the other side, for  $t \rightarrow 1$ , the situation is clearer. Only one sharp peak at  $R_H = 1$  is found which is steadily growing, e.g., for  $m = 15$  it is exceeding 100 for both V-flip and H-flip method. This observation indicates the regime of the Landau plateau  $R_H = 1$  where  $R_H$  takes a constant value without fluctuations.

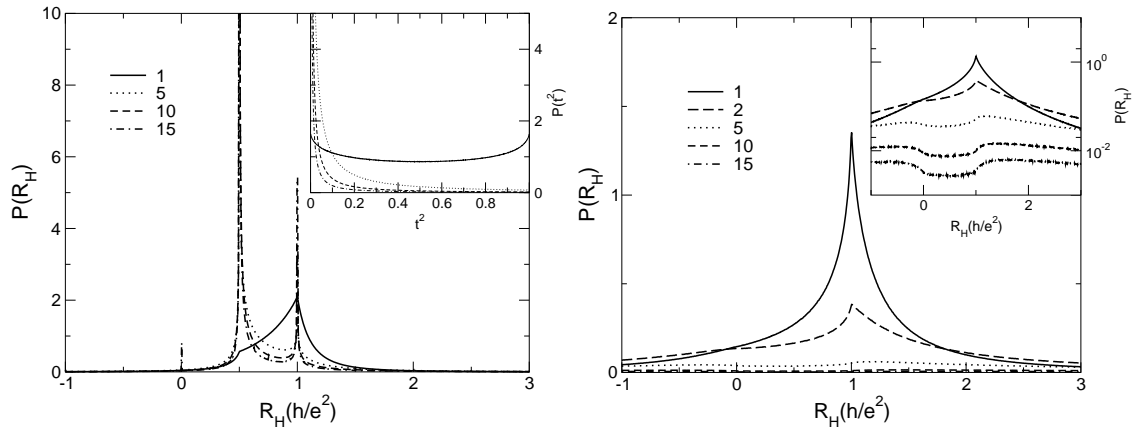


Figure 6.8: Behavior of  $P(R_H)$  calculated by the V-flip (left) and the H-flip (right) method for  $t \rightarrow 0$  as a result of a single RG iteration using the 5SP unit. The  $t_i$  were chosen according to the distribution functions (6.13) with  $m = 1, 5, 10, 15$ . For better visibility the peaks of the distributions are cut, e.g. in the left plot at  $m = 15$  the peak has a maximum of 50.0. The left inset displays the corresponding  $P(t^2)$ . The right inset shows  $P(R_H)$  on a logarithmic scale.

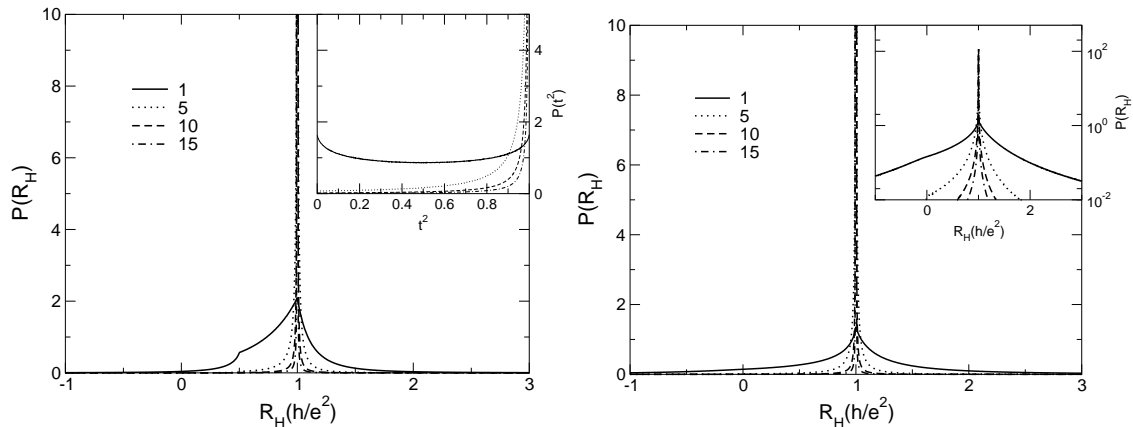


Figure 6.9: Behavior of  $P(R_H)$  calculated by the V-flip (left) and the H-flip (right) method for  $t \rightarrow 1$  analogously to Fig. 6.8.

In order to clarify the behavior of  $R_H$  on the insulating side again  $R_{H,\text{typ}}$  is evaluated. Similar to Fig. 6.7  $R_{H,\text{typ}}$  is shown in Fig. 6.11 using  $m = 1, \dots, 15$  for  $t \rightarrow 0$  and  $t \rightarrow 1$ . When  $t \rightarrow 1$  the value of  $R_{H,\text{typ}}$  converges to 1 which resembles the result obtained from  $P(R_H)$ . Not so in case of  $t \rightarrow 0$ . Now one finds agreement with an insulator characterized by a diverging  $R_{H,\text{typ}}$  for  $t \rightarrow 0$ . Therefore the result does not support the existence of a quantized behavior in the insulating regime [DM94, STS<sup>+</sup>97a, SA97].

For the comparison with other works it is useful to plot  $R_{H,\text{typ}}$  independent of the parameter  $m$  as function of the typical longitudinal resistance  $R_{L,\text{typ}}$ . The value of  $R_{L,\text{typ}}$  can be calculated simultaneously to  $R_{H,\text{typ}}$  within the RG step according

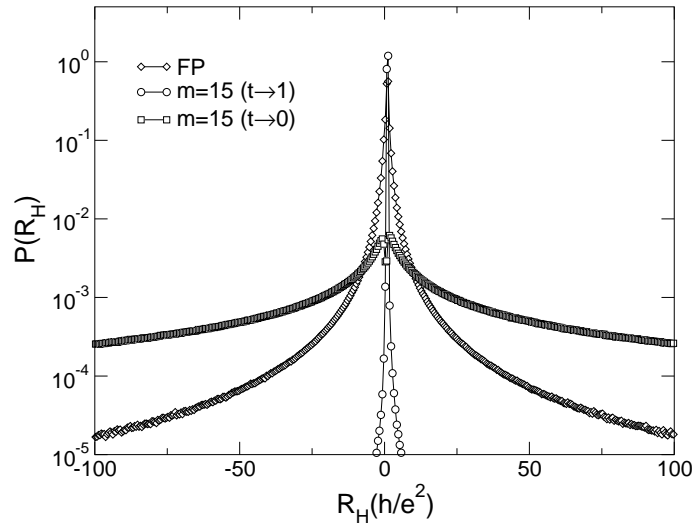


Figure 6.10: Comparison of the tails of  $P(R_H)$  for  $t \rightarrow 1$  ( $\circ$ ),  $t \rightarrow 0$  ( $\square$ ), and  $P_c(R_H)$  ( $\diamond$ ) calculated by the H-flip method for the 5SP unit. The range of the tails increases when the transmission  $t'$  through the RG unit becomes smaller. Symbols correspond to an average over 100 consecutive bins of the original distribution.

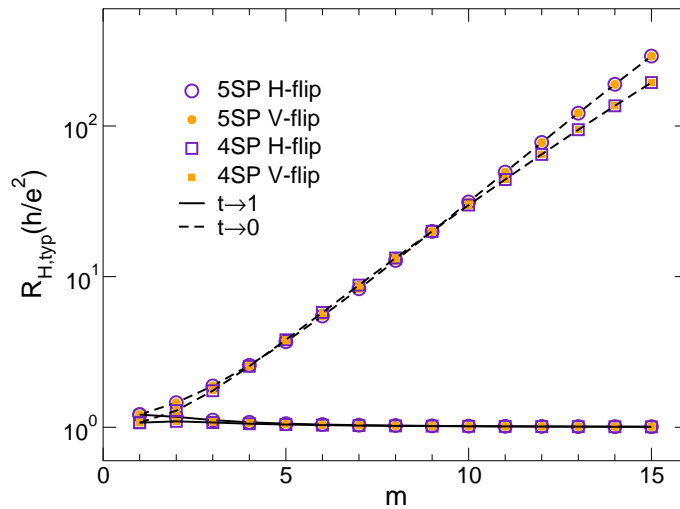


Figure 6.11:  $R_{H,\text{typ}}$  for  $t \rightarrow 0$  and  $t \rightarrow 1$  as a result of a single RG iteration using the 4SP and the 5SP unit. The  $t_i$  were chosen according to the distribution functions (6.13) with  $m = 1, \dots, 15$ . Considering the typical mean the V-flip and the H-flip method yield identical values.

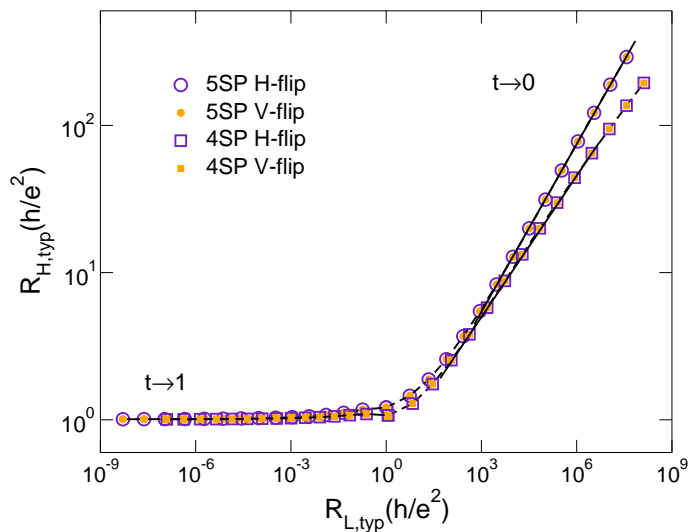


Figure 6.12:  $R_{H,\text{typ}}$  as function of  $R_{L,\text{typ}}$  for the 4SP and the 5SP RG unit. The results are obtained using the distribution functions (6.13) with  $m = 1, \dots, 15$ . The straight lines indicate power-law fits.

to

$$R_{L,\text{typ}} = \frac{\langle r'^2 \rangle_{\text{typ}}}{\langle t'^2 \rangle_{\text{typ}}}. \quad (6.14)$$

The resulting dependence is presented in Fig. 6.12. For  $R_{L,\text{typ}} \rightarrow 0$  the Landau plateau at  $R_{H,\text{typ}} = 1$  is approached. In the other limit  $R_{L,\text{typ}} \rightarrow \infty$  the data suggest a power-law divergence of  $R_{H,\text{typ}}$ . As already shown in Fig. 6.11, the typical means for H-flip and V-flip method coincide. Nonlinear fits in the range of  $R_{L,\text{typ}}$  within  $[10^3, 10^8]$  yield the exponent  $\mu = 0.38$  for the 5SP unit within  $[10^2, 10^7]$  the exponent  $\mu = 0.32$  for the 4SP unit which is in agreement with the result  $\mu \approx 0.32 - 0.35$  from [PA99]. Surprisingly, the values of  $\mu$  for the 4SP and the 5SP unit are rather close and deviate clearly from the analytically obtained  $\mu \approx 1/2$  [ZS01] using the 4SP unit.

## 6.4 Conclusion

The RG approach was extended to the calculation of the Hall resistance  $R_H$ . Analogously to the RG approaches to the transmission coefficient in Chapter 3 and to the level spacings in Chapter 4 an analytical form of the RG transformation (6.2) was derived. With this prerequisite for a fast numerical computation the FP distribution  $P_c(R_H)$  at the QH transition could be calculated with high accuracy. The value of  $R_H$  was computed for two different assumptions about the current when the magnetic field is reversed. In the first case the shape of  $P_c(R_H)$  is characterized by two structures, a kink and a peak, exactly at the position of the first and the second Landau plateau with  $R_H = 1$  and  $R_H = 0.5$ , respectively. In the study of  $P(R_H)$  around the transition the weight of  $P(R_H)$  shifts from the peak at  $R_H = 1$  to  $R_H = 0.5$  when approaching the insulating regime. The occurrence of the structure

at  $R_H = 0.5$  is rather surprising since the CC model used as basis of this RG approach can describe a single QH transition only. In order to relate the distribution to a single quantity comparable to experiments the typical value  $R_{H,\text{typ}}$ , which is the same for both cases, was introduced. Since the shape of  $P(R_H)$  also contradicts the behavior of  $R_{H,\text{typ}}$  this method appears to be unsuitable for the calculation of  $P(R_H)$ . More reasonable results are obtained in the second case, where  $P_c(R_H)$  has a single peak at  $R_H = 1$ . The distribution is characterized by very long tails, which can be attributed to the strong fluctuations already observed in  $P_c(G)$ . Toward the insulating regime the peak at  $R_H = 1$  broadens until  $P(R_H)$  is nearly flat. On the other side  $R_{H,\text{typ}}$  steadily increases. The reason of this behavior is again the strong fluctuations in  $P(R_H)$  that become even stronger toward the insulator but are averaged out in the typical value  $R_{H,\text{typ}}$ .

Furthermore the existence of a quantized Hall insulator was tested by computing  $P(R_H)$  and  $R_{H,\text{typ}}$  away from transition in the strong insulating regime. In contrast to previous studies [DM94,SA97] the CC model allows a coherent description of a QH system. Instead of a quantization of  $R_{H,\text{typ}}$  a divergence was observed in agreement with other works [PA99,SW99,ZS01] using coherent methods. Considering  $P(R_H)$  as function of  $P(R_L)$  the divergence follows a power law with an exponent  $\mu = 0.38$ , very close to  $\mu \approx 0.32 - 0.35$  found in [PA99].

The comparison between the 5SP and the 4SP unit shows qualitatively equivalent behavior. Because of the lack of predictions a quantitative analysis is difficult. An exception is the insulating regime where a power-law divergence with  $\mu = 0.32$  is obtained for the 4SP RG unit which agrees within the expected accuracy to the 5SP result. This might indicate that away from the transition the difference in accuracy between both RG units decreases. Both values deviate clearly from the analytical result for the 4SP unit  $\mu \approx 0.5$  of [ZS01].

# Chapter 7

## Summary

In this work the integer quantum Hall (QH) effect was studied by the application of a real-space renormalization group (RG) approach to the Chalker-Coddington (CC) model. The focus was laid on the determination of universal properties of the QH transition. Here, the first part including the calculation of the critical exponent  $\nu$  of the localization length concerned mainly the comparison with other methods in order to show the stability and accuracy of the RG approach. On this ground the second part was dedicated to a deeper understanding of the influence of macroscopic inhomogeneities and the distribution of the Hall resistance at the QH transition.

Before a more detailed discussion is given the essential idea behind the RG approach is briefly recalled. The underlying CC model describes the motion of non-interacting electrons in a smoothly varying two-dimensional disorder potential under a strong perpendicular magnetic field in terms of a semi-classical quantum percolation. The percolation network consists of saddle points (SPs) which are connected by equipotentials. This basic CC model characterizes a single Landau band and therefore contains only one integer QH transition at the band center. Within the RG approach the SP network is represented by a fragment, the RG unit, which itself can be mapped by a transformation on a single super-SP. Iterating this procedure, large effective system sizes are easily attained exceeding the dimension of CC networks used in numerical simulations.

To prove the accuracy of the RG approach it was demonstrated that the conductance distribution at the QH transition,  $P_c(G)$ , can be reproduced very precisely. The shape of  $P_c(G)$  was shown to be symmetric with respect to  $G = 0.5$ . The distribution is governed by a broad flat minimum around  $G = 0.5$  surrounded by sharp peaks close to  $G = 0$  and  $G = 1$ . Therefore the moments of  $P_c(G)$  are close to the moments of a uniform distribution and agree with the distribution observed experimentally [CK96]. Because of the instability of the fixed point (FP) distribution  $P_c(G)$  the drift of  $P(G)$  away from the FP provides a method to calculate the critical exponent  $\nu$ . The obtained value  $\nu = 2.39 \pm 0.01$  is in accordance with the results of large scale numerical simulations [CC88, Huc92, LWK93].

The RG approach was then extended to the study of energy level spacings. While the conductance distribution depends on the absolute value of the transmission amplitude of the SPs, the energy levels of the RG unit are defined by the phases. The RG unit contains only four independent phases from which four energy levels

and consequently only three level spacings are derived. The determination of the level spacing distribution (LSD) therefore relies on the averaging over a very large number of different random realizations of the RG unit in contrast to the study of large SP networks, where the statistics of energy levels can be calculated from a single sample. Unfortunately, this alternative method requires an initial assumption on the energy dependence of the phases which affects also the shape of the resulting LSD. Hence a universal shape of the LSD was not found. Nevertheless prominent universal features are preserved. First, the quadratic level repulsion for small spacings could be observed. Second, from a finite-size-scaling analysis of the LSD around the QH transition the exponent  $\nu = 2.37 \pm 0.02$  was computed. This value agrees very well with the result of other numerical approaches and also with the  $\nu$  from the conductance distribution obtained previously. Taking into account that the RG approach is based on a rather crude approximation the accuracy of the results is surprisingly good. Therefore the RG approach appears to be a suitable method for the study of universal properties at the QH transition.

Encouraged by these results it seems to be justified to apply the RG approach to the new scenario where the QH transition is influenced by macroscopic inhomogeneities in the sample. The modeling of the macroscopic inhomogeneities using a long-range power-law correlation allows one to introduce the inhomogeneities in the RG approach easily, because each RG step is naturally connected with an effective length scale. The outcome of the computations indicates an increase of the critical exponent  $\nu$  for growing strength and range of the correlations exceeding the value for the usual short-range disorder studied before. This behavior resembles the classical case where the extended Harris criterion [Wei84, WH83] predicts the dependence of  $\nu$  on the power-law exponent  $\alpha$  of the correlation. Comparing this relation to the results of the RG approach one observes only qualitative agreement. Instead of a sharp crossover at the critical  $\alpha_c$ , when the correlation starts to increase the value of  $\nu$ , a rather smooth transition is found. The reason of the discrepancy seems to be attributed to the additional intrinsic short-range disorder contained in the phases of the RG unit. Note that only a very recent work [SMK03] using a different approach shows better agreement with the extended Harris criterion.

Since the numerics limit the calculation to eight iteration steps one cannot unambiguously exclude that  $\nu$  approaches finally the value of the uncorrelated case. Nevertheless already within these iterations the effective system size increases by a factor of 256 corresponding to a magnification from microscopic scales, like the magnetic length, to macroscopic scales of several microns. Therefore one should expect that the results are relevant also for experiments where the system is much larger but the true critical behavior is hidden because the phase breaking length does not exceed the characteristic length covered by the RG approach.

In the last part of this work the RG approach was employed for the calculation of the Hall resistance  $R_H$ . From two possible ways to compute  $R_H$  only one method could obtain a reasonable distribution  $P(R_H)$ . The FP distribution  $P_c(R_H)$  is characterized by a sharp nearly symmetric peak at  $R_H = 1$ , which corresponds to the center of the first Landau band, and very long tails. Away from the transition toward the plateau regime ( $G \rightarrow 1$ ) the width of the peak shrinks while the

---

peak broadens to an almost flat distribution toward the insulator ( $G \rightarrow 0$ ). In the latter case  $P(R_H)$  is dominated by strong fluctuations. In order to extract a typical value  $R_{H,\text{typ}}$  the averaging procedure from [ZS01] was applied which is less sensitive to the rare events from the tails. In the plateau regime  $R_{H,\text{typ}} \rightarrow 1$ . For the strong insulating regime  $R_{H,\text{typ}}$  diverges as shown in [PA99, SW99, ZS01]. A power-law dependence  $R_{H,\text{typ}} \sim R_L^\mu$  with  $\mu = 0.38$  is found which agrees very well to  $\mu \approx 0.32 - 0.35$  observed in [PA99]. The results therefore contradict a quantized Hall insulator.

Throughout this study also the influence of the chosen RG unit on the results was investigated. Beside the five SPs RG unit a RG unit consisting of four SPs was tested. Because of the smaller size this structure can contain less information from the underlying CC network and is therefore expected to provide less accurate results. This assumption is confirmed in the majority of the calculations, e.g. the obtained asymmetric FP distribution  $P_c(G)$  and the value of  $\nu = 2.74 \pm 0.02$  differing about 15% from the five SPs result. These findings illustrate that the construction of the RG unit is the prominent part for the successful application of the RG approach. The chosen five SPs RG unit seems to be the smallest part of the CC network suitable to describe the QH transition.

One can argue that the presented findings indicate a large robustness of universal properties of the QH transition. Using a simple non-interacting semiclassical picture of electron propagation and the rather crude RG approach one is able to reveal universal behavior. On the other hand experimental results [ESKT93, PST<sup>+</sup>97] clearly show the influence of electron interaction at the QH transition. A fundamental theory of the QH transition is still far from complete.



# Chapter 8

## Outlook

Finally, the results of this work form the basis of a number of possible continued studies, which can be grouped in i) improvements of the algorithm and the computation and ii) application of the RG approach to a broader class of physical problems. This is explained in the following in more detail.

To the first group belongs the construction of the RG unit out of the CC network. In this work it was shown that a 5SP RG unit describes the QH transition quite accurately in contrast to the results of a smaller 4SP unit. On the other hand a larger RG unit should produce even more accurate results. In [JMMW98, JMW98, WJ98] several of these RG units have already been tested but with rather pure statistics because an analytical formulation of the RG equation was not obtained. To preserve the statistical quality of this work, a larger RG unit has to be found, which still allows the derivation of the RG equation analytically. Another improvement of the calculations concerns the numerics limiting the number of RG steps especially in the study of the macroscopic inhomogeneities and of the Hall resistivity  $R_H$  away from the transition. So far all computations are based on the distribution  $P(t)$  of the transmission coefficient  $t$ , which is bound to the interval  $[0, 1]$  and discretized in bins with equal width. When starting the RG iteration with an initial distribution disturbed from the FP distribution the weight of  $P(t)$  moves either toward  $t = 0$  or  $t = 1$ , respectively. The resulting large peaks then lead, first, to a slowing down of the computation because the algorithm to draw random  $t$ 's is less efficient and, second, to a pure representation of the peak by only a few bins. These problems can be circumvented when instead the distribution  $Q(z)$  of the SP heights  $z$  is used. Then the number of RG steps should be limited by the size of the discretization interval of  $Q(z)$  only. This will also permit to study the transition of  $P(R_H)$  from the FP toward the insulator within a real RG iteration instead of using artificially chosen distributions. Connected to this problem is the choice of a suitable averaging procedure for  $P(R_H)$  because of the influence of strong fluctuations. Beside the typical value [ZS01] used here also other characteristic quantities such as median, mode, and harmonic mean should be investigated.

The second part concerns the application of the RG approach to other problems. A broad and obvious area of research is the application to extended variants of the standard CC model, e.g. a network with two channels per link in order to describe the mixing of Landau levels [WLW94]. Since these problems were already studied

---

by other methods, e.g. large scale simulations, the application of the RG approach would be only another test of the reliability of the method but no new physical insight can be revealed. Nevertheless there are still some interesting questions. One example is the behavior of the critical properties at the QH transition when changing from strong to weak magnetic field. This case could be modeled by bi-directional links in the network, which would allow one to trace the transition from the universality class GUE to GOE. And there still exists the most striking controversy, that the integer QH effect can be very well described within a non-interacting electron picture, but experimental results clearly indicate the influence of interactions [ESKT93,PST<sup>+</sup>97]. Because a full treatment of many-body interactions is rather difficult one considers in an approximate view only a few interacting particles. In this approach the two-interacting particle problem is reduced to a single-particle problem by increasing the effective spatial dimension and including long-range correlations in the disorder potential [She94]. Concerning the CC model one has to construct an effective four-dimensional network. From this new CC network a suitable RG unit should be extracted. These tasks are by no means trivial and there is no guarantee for success.

# Bibliography

- [AA81] H. Aoki and T. Ando. Effect of localization on the Hall conductivity in the two-dimensional system in strong magnetic fields. *Solid State Commun.*, 38:1079–1082, 1981.
- [AALR79] E. Abrahams, P. W. Anderson, D. C. Licciardello, and T. V. Ramakrishnan. Scaling theory of localization: absence of quantum diffusion in two dimensions. *Phys. Rev. Lett.*, 42:673–676, 1979.
- [ABB99] Y. Avishai, Y. Band, and D. Brown. Conductance distribution between Hall plateaus. *Phys. Rev. B*, 60:8992–8998, 1999.
- [AJS97] D. P. Arovas, M. Janssen, and B. Shapiro. Real-space renormalization of the Chalker-Coddington model. *Phys. Rev. B*, 56:4751–4759, 1997. ArXiv: cond-mat/9702146.
- [AM76] N. W. Ashcroft and N. D. Mermin. *Solid State Physics*. Saunders College, New York, 1976.
- [And58] P. W. Anderson. Absence of diffusion in certain random lattices. *Phys. Rev.*, 109:1492–1505, 1958.
- [BDFN92] J. J. Binney, N. J. Dowrick, A. J. Fisher, and M. E. J. Newman. *The Theory of Critical Phenomena: An Introduction to the Renormalization Group*. Oxford University Press, Oxford, UK, 1992.
- [Ber78] J. Bernasconi. Real-space renormalization of bond-disordered conductance lattices. *Phys. Rev. B*, 18:2185–2191, 1978.
- [BILP85] M. Büttiker, Y. Imry, R. Landauer, and S. Pinhas. Generalized many-channel conductance formula with application to small rings. *Phys. Rev. B*, 31:6207–6215, 1985.
- [BMB98] N. Q. Balaban, U. Meirav, and I. Bar-Joseph. Absence of scaling in the integer quantum Hall effect. *Phys. Rev. Lett.*, 81:4967–4970, 1998.
- [BMP98] D. Braun, G. Montambaux, and M. Pascaud. Boundary conditions at the mobility edge. *Phys. Rev. Lett.*, 81:1062–1065, 1998. ArXiv: cond-mat/9712256.
- [BS97] M. Batsch and L. Schweitzer. Level statistics in the quantum Hall regime. In G. Landwehr and W. Ossau, editors, *High Magnetic Fields in Physics of Semiconductors II: Proceedings of the International Conference, Würzburg*

- 1996, pages 47–50, Singapore, 1997. World Scientific Publishers Co. ArXiv: cond-mat/9608148.
- [BSK98] M. Batsch, L. Schweitzer, and B. Kramer. Energy-level statistics and localization of 2d electrons in random magnetic fields. *Physica B*, 249:792–795, 1998. ArXiv: cond-mat/9710011.
- [BSZK96] M. Batsch, L. Schweitzer, I. K. Zharekeshev, and B. Kramer. Crossover from critical orthogonal to critical unitary statistics at the Anderson transition. *Phys. Rev. Lett.*, 77:1552–1555, 1996. ArXiv: cond-mat/9607070.
- [Car96] J. L. Cardy. *Scaling and Renormalization in Statistical Physics*. Cambridge University Press, Cambridge, 1996.
- [CBF99] D. H. Cobden, C. H. W. Barnes, and C. J. B. Ford. Fluctuations and evidence for charging in the quantum Hall effect. *Phys. Rev. Lett.*, 82:4695–4698, 1999.
- [CC88] J. T. Chalker and P. D Coddington. Percolation, quantum tunneling and the integer Hall effect. *J. Phys.: Condens. Matter*, 21:2665–2679, 1988.
- [CF97] S. Cho and M. P. A. Fisher. Conductance fluctuations at the integer quantum Hall plateau transition. *Phys. Rev. B*, 55:1637–1641, 1997.
- [CHHR97] N. R. Cooper, B. I. Halperin, C.-K. Hu, and I. M. Ruzin. Statistical properties of the low-temperature conductance peak heights for Corbino disks in the quantum Hall regime. *Phys. Rev. B*, 55:4551–4557, 1997.
- [CK96] D. H. Cobden and E. Kogan. Measurement of the conductance distribution function at a quantum Hall transition. *Phys. Rev. B*, 54:R17316–R17319, 1996.
- [Col99] P. T. Coleridge. Universality in an integer quantum Hall transition. *Phys. Rev. B*, 60:4493–4496, 1999.
- [CP95] T. Chakraborty and P. Pietiläinen. *The Quantum Hall Effects*. Springer, Berlin, 1995.
- [CRK<sup>+</sup>02] J. T. Chalker, N. Read, V. Kagalovsky, B. Horovitz, Y. Avishai, and A. W. W. Ludwig. Thermal metal network models of a disordered two-dimensional superconductor. *Phys. Rev. B*, 65:012506–4, 2002. ArXiv: cond-mat/0009463.
- [DM94] A. M. Dykhne and Ruzin I. M. Theory of the fractional quantum Hall effect: The two-phase model. *Phys. Rev. B*, 50:2369–2379, 1994.
- [EMPW99] F. Evers, A. D. Mirlin, D. G. Polyakov, and P. Wölfle. Semiclassical theory of transport in a random magnetic field. *Phys. Rev. B*, 60:8951–8969, 1999.
- [ESKT93] L. W. Engel, D. Shahar, C. Kurdak, and D. C. Tsui. Microwave frequency dependence of integer quantum Hall effect: Evidence of finite-size scaling. *Phys. Rev. Lett.*, 71:2638–2641, 1993.

- [Eva94] S. N. Evangelou. Level-spacing function  $p(s)$  at the mobility edge. *Phys. Rev. B*, 49:16805–16808, 1994.
- [Eva95] S. N. Evangelou. Anderson transition, scaling, and level statistics in the presence of spin orbit coupling. *Phys. Rev. Lett.*, 75:2550–2553, 1995.
- [FAB95] M. Feingold, Y. Avishai, and R. Berkovits. Spectral statistics in the lowest Landau band. *Phys. Rev. B*, 52:8400–8406, 1995. ArXiv: cond-mat/9503058.
- [Fer88] H. A. Fertig. Semiclassical description of a two-dimensional electron in a strong magnetic field and an external potential. *Phys. Rev. B*, 38:996–1015, 1988.
- [FJM98] P. Freche, M. Janssen, and R. Merkt. Two-dimensional disordered electron systems: A network model approach. In D. Neilson, editor, *Proceedings of the Ninth International Conference on Recent Progress in Many Body Theories*, Singapore, 1998. World Scientific. ArXiv: cond-mat/9710297.
- [FJM99] P. Freche, M. Janssen, and R. Merkt. Localization in nonchiral network models for two-dimensional disordered wave mechanical systems. *Phys. Rev. Lett.*, 82:149–152, 1999.
- [FL81] D. S. Fisher and P. A. Lee. Relation between conductivity and transmission matrix. *Phys. Rev. B*, 23:6851–6854, 1981.
- [FM97] Y. V. Fyodorov and A. D. Mirlin. Strong eigenfunction correlations near the Anderson-localization transition. *Phys. Rev. B*, 55:16001–16004, 1997.
- [GR97] A. G. Galstyan and M. E. Raikh. Localization and conductance fluctuations in the integer quantum Hall effect: Real-space renormalization group approach. *Phys. Rev. B*, 56:1422–1429, 1997.
- [Gri89] G. Grimmett. *Percolation*. Springer Verlag, Berlin, 1989.
- [GRS97] I. A. Gruzberg, N. Read, and S. Sachdev. Scaling and crossover functions for the conductance in the directed network model of edge states. *Phys. Rev. B*, 55:10593–10601, 1997.
- [GST88] V. J. Goldman, M. Shayegan, and D. C. Tsui. Evidence for the fractional quantum Hall state at  $\nu = \frac{1}{7}$ . *Phys. Rev. Lett.*, 61:881–884, 1988.
- [GWSS93] V. J. Goldman, J. K. Wang, Bo Su, and M. Shayegan. Universality of the Hall effect in a magnetic-field-localized two-dimensional electron system. *Phys. Rev. Lett.*, 70:647–650, 1993.
- [Haa92] F. Haake. *Quantum Signatures of Chaos*. Springer, Berlin, 2nd edition, 1992.
- [Hal79] E. H. Hall. On a new action of the magnet on electrical current. *Amer. Jour. Math.*, 2:287–292, 1879.
- [Har74] A. B. Harris. Effect of random defects on the critical behavior of Ising models. *J. Phys. C*, 7:1671–1689, 1974.

- [HB92] Y. Huo and R. N. Bhatt. Current carrying states in the lowest Landau level. *Phys. Rev. Lett.*, 68:1375–1378, 1992.
- [HB99] B. Huckestein and M. Backhaus. Integer quantum Hall effect of interacting electrons: Dynamical scaling and critical conductivity. *Phys. Rev. Lett.*, 82:5100–5103, 1999.
- [HC96] C.-M. Ho and J. T. Chalker. Models for the integer quantum Hall effect: the network model, the Dirac equation, and a tight-binding Hamiltonian. *Phys. Rev. B*, 54:8708–8713, 1996. ArXiv: cond-mat/9605073.
- [HK90] B. Huckestein and B. Kramer. One-parameter scaling in the lowest Landau band: precise determination of the critical behaviour of the localization length. *Phys. Rev. Lett.*, 64:1437–1440, 1990.
- [HNF<sup>+</sup>94] R. Hughes, J. Nicholls, J. Frost, E. Linfield, M. Pepper, C. Ford, D. Ritchie, G. Jones, E. Kogan, and M. Kaveh. Magnetic-field-induced insulator-quantum Hall-insulator transition in a disordered two-dimensional electron gas. *J. Phys.: Condens. Matter*, 6:4763–4770, 1994.
- [HS93] E. Hofstetter and M. Schreiber. Statistical properties of the eigenvalue spectrum of the three-dimensional Anderson Hamiltonian. *Phys. Rev. B*, 48:16979–16985, 1993.
- [HS94a] E. Hofstetter and M. Schreiber. Does broken time reversal symmetry modify the critical behavior at the metal-insulator transition in 3-dimensional disordered systems? *Phys. Rev. Lett.*, 73:3137–3140, 1994. ArXiv: cond-mat/9408040.
- [HS94b] E. Hofstetter and M. Schreiber. Relation between energy-level statistics and phase transition and its application to the Anderson model. *Phys. Rev. B*, 49:14726–14729, 1994. ArXiv: cond-mat/9402093.
- [HSS<sup>+</sup>98] M. Hilke, D. Shahar, P. H. Song, D. C. Tsui, Y. H. Xie, and D. Monroe. Experimental evidence for a two-dimensional quantized Hall insulator. *Nature*, 395:675–677, 1998.
- [HSS<sup>+</sup>00] M. Hilke, D. Shahar, P. H. Song, D. C. Tsui, and Y. H. Xie. Phase diagram of the integer quantum Hall effect in *p*-type germanium. *Phys. Rev. B*, 62:6940–6943, 2000.
- [Huc92] B. Huckestein. Scaling and universality in the integer quantum Hall effect. *Europhys. Lett.*, 20:451–456, 1992.
- [Huc95] B. Huckestein. Scaling theory of the integer quantum Hall effect. *Rev. Mod. Phys.*, 67:357–396, 1995.
- [HWE<sup>+</sup>93] S. W. Hwang, H. P. Wei, L. W. Engel, D. C. Tsui, and A. M. M. Pruisken. Scaling in spin-degenerate Landau levels in the integer quantum Hall effect. *Phys. Rev. B*, 48:11416–11419, 1993.

- [HZH01] F. Hohls, U. Zeitler, and R. J. Haug. High frequency conductivity in the quantum Hall regime. *Phys. Rev. Lett.*, 86:5124–5127, 2001. ArXiv: cond-mat/0011009.
- [HZHP01] F. Hohls, U. Zeitler, R. J. Haug, and K. Pierz. High frequency conductivity in the quantum Hall effect. *Physica B*, 298:88–92, 2001. ArXiv: cond-mat/0010417.
- [Ior82] S. V. Iordanskii. On the conductivity of two dimensional electrons in a strong magnetic field. *Solid State Commun.*, 43:1–3, 1982.
- [Jan98] Martin Janssen. Statistics and scaling in disordered mesoscopic electron systems. *Phys. Rep.*, 295:1–91, 1998.
- [JJI97] B. Jeckelmann, B. Jeanneret, and D. Inglis. High-precision measurements of the quantized Hall resistance: Experimental conditions for universality. *Phys. Rev. B*, 55:13124–13134, 1997.
- [JK88] J. K. Jain and S. A. Kivelson. Quantum Hall effect in quasi one-dimensional systems: Resistance fluctuations and breakdown. *Phys. Rev. Lett.*, 60:1542–1545, 1988.
- [JMMW98] M. Janssen, R. Merkt, J. Meyer, and A. Weymer. Hierarchical network models for the quantum Hall effect. *Physica*, 256–258:65–68, 1998.
- [JMW98] M. Janssen, R. Merkt, and A. Weymer. S-matrix network models for coherent waves in random media: construction and renormalization. *Ann. Phys. (Leipzig)*, 7:353–362, 1998.
- [JMZ99] M. Janssen, M. Metzler, and M. R. Zirnbauer. Point-contact conductances at the quantum Hall transition. *Phys. Rev. B*, 59:15836–15853, 1999.
- [JVFH94] M. Janssen, O. Viehweger, U. Fastenrath, and J. Hajdu. *Introduction to the Theory of the Integer Quantum Hall effect*. VCH, Weinheim, 1994.
- [JW98] B. Jovanovic and Z. Wang. Conductance correlations near integer quantum Hall transitions. *Phys. Rev. Lett.*, 81:2767–2770, 1998.
- [KDP80] K. v. Klitzing, G. Dorda, and M. Pepper. New method for high-accuracy determination of the fine-structure constant based on quantized Hall resistance. *Phys. Rev. Lett.*, 45:494–497, 1980.
- [KHA95] V. Kagalovsky, B. Horovitz, and Y. Avishai. Landau-level mixing and extended states in the quantum Hall effect. *Phys. Rev. B*, 52:R17044–R17047, 1995.
- [KHA97] V. Kagalovsky, B. Horovitz, and Y. Avishai. Landau-level mixing and spin degeneracy in the quantum Hall effect. *Phys. Rev. B*, 55:7761–7770, 1997.
- [KHAC99] V. Kagalovsky, B. Horovitz, Y. Avishai, and J. T. Chalker. Quantum Hall plateau transitions in disordered superconductors. *Phys. Rev. Lett.*, 82:3516–3519, 1999.

- [KHKP91a] S. Koch, R. J. Haug, K. v. Klitzing, and K. Ploog. Experiments on scaling in  $\text{Al}_x\text{Ga}_{1-x}\text{As}/\text{GaAs}$  heterostructures under quantum Hall conditions. *Phys. Rev. B*, 43:6828–6831, 1991.
- [KHKP91b] S. Koch, R. J. Haug, K. v. Klitzing, and K. Ploog. Size-dependent analysis of the metal-insulator transition in the integral quantum Hall effect. *Phys. Rev. Lett.*, 67:883–886, 1991.
- [KHKP92] S. Koch, R. J. Haug, K. v. Klitzing, and K. Ploog. Experimental studies of the localization transition in the quantum Hall regime. *Phys. Rev. B*, 46:1596–1602, 1992.
- [Kim96] Y. B. Kim. Edge states of integral quantum Hall states versus edge states of antiferromagnetic quantum spin chains. *Phys. Rev. B*, 53:16420–16424, 1996.
- [KLAA94] V. E. Kravtsov, I. V. Lerner, B. L. Altshuler, and A. G. Aronov. Universal spectral correlations at the mobility edge. *Phys. Rev. Lett.*, 72:888–891, 1994.
- [KLZ92] S. Kivelson, D.-H. Lee, and S.-C. Zhang. Global phase diagram in the quantum Hall effect. *Phys. Rev. B*, 46:2223–2238, 1992.
- [KM95] R. Klesse and M. Metzler. Universal multifractality in quantum Hall systems with long-range disorder potential. *Europhys. Lett.*, 32:229–234, 1995.
- [KM97a] R. Klesse and M. Metzler. Spectral compressibility at the metal-insulator transition of the quantum Hall effect. *Phys. Rev. Lett.*, 79:721–724, 1997.
- [KM97b] J. Kondev and J. B. Marston. Supersymmetry and localization in the quantum Hall effect. *Nucl. Phys. B*, 497:639, 1997. ArXiv: cond-mat/9612223.
- [KMDK00] F. Kuchar, R. Meisels, K. Dybko, and B. Kramer. DC- and AC-scaling of the integer quantum Hall effect in the presence of interactions. *Europhys. Lett.*, 49:480–486, 2000.
- [KOSO96] T. Kawarabayashi, T. Ohtsuki, K. Slevin, and Y. Ono. Anderson transition in three-dimensional disordered systems with symplectic symmetry. *Phys. Rev. Lett.*, 77:3593–3596, 1996. ArXiv: cond-mat/9609226.
- [KZ01] R. Klesse and M. R. Zirnbauer. Point-contact conductances from density correlations. *Phys. Rev. Lett.*, 86:2094–2097, 2001. ArXiv: cond-mat/0010005.
- [Lan] G. Landwehr. private communication.
- [Lan70] R. Landauer. Electrical resistance of disordered one-dimensional lattices. *Phil. Mag.*, 21:863–867, 1970.
- [Lau81] R. B. Laughlin. Quantized Hall conductivity in two dimensions. *Phys. Rev. B*, 23:5632–5633, 1981.



- [LC94] D. K. K. Lee and J. T. Chalker. Unified model for two localization problems: Electron states in spin-degenerate Landau levels and in a random magnetic field. *Phys. Rev. Lett.*, 72:1510–1513, 1994.
- [LCK94] D. K. K. Lee, J. T. Chalker, and D. Y. K. Ko. Localization in a random magnetic field: The semiclassical limit. *Phys. Rev. B*, 50:5272–5285, 1994.
- [Lee94] D.-H. Lee. Network models of quantum percolation and their field-theory representation. *Phys. Rev. B*, 50:10788–10791, 1994.
- [LFSG94] A. W. W. Ludwig, M. P. A. Fisher, R. Shankar, and G. Grinstein. Integer quantum Hall transition: An alternative approach and exact results. *Phys. Rev. B*, 50:7526, 1994.
- [LPV<sup>+</sup>02] D. de Lang, L. Ponomarenko, A. de Visser, C. Possanzini, S. Olsthoorn, and A. Pruisken. Evidence for a quantum Hall insulator in an InGaAs/InP heterostructure. *Physica E*, 12:666–669, 2002.
- [LWK93] D.-H. Lee, Z. Wang, and S. Kivelson. Quantum percolation and plateau transitions in the quantum Hall effect. *Phys. Rev. Lett.*, 70:4130–4133, 1993.
- [Meh91] M. L. Mehta. *Random Matrices and the Statistical Theory of Energy Levels*. Academic Press, New York, 1991.
- [Met98] M. Metzler. Spectral properties of three-dimensional layered quantum Hall systems. *J. Phys. Soc. Japan*, 67:4006–4009, 1998.
- [Met99] M. Metzler. The influence of percolation in the generalized Chalker-Coddington model. *J. Phys. Soc. Japan*, 68:144–145, 1999.
- [MHL<sup>+</sup>00] S. Q. Murphy, J. L. Hicks, W. K. Liu, S. J. Chung, K. J. Goldammer, and M. B. Santos. Studies of the quantum Hall to quantum Hall insulator transition in InSb-based 2DESs. *Physica E*, 6:293–296, 2000.
- [MHSS96] H. A. Makse, S. Havlin, M. Schwartz, and H. E. Stanley. Method for generating long-range correlations for large systems. *Phys. Rev. E*, 53:5445–5449, 1996.
- [MJH98] R. Merkt, M. Janssen, and B. Huckestein. Network model for a two-dimensional disordered electron system with spin-orbit scattering. *Phys. Rev. B*, 58:4394–4405, 1998.
- [MK81] A. MacKinnon and B. Kramer. One-parameter scaling of localization length and conductance in disordered systems. *Phys. Rev. Lett.*, 47:1546–1549, 1981.
- [MK83] A. MacKinnon and B. Kramer. The scaling theory of electrons in disordered solids: additional numerical results. *Z. Phys. B*, 53:1–13, 1983.
- [MT99] J. B. Marston and S. Tsai. Chalker-Coddington network model is quantum critical. *Phys. Rev. Lett.*, 82:4906–4909, 1999.

- [MV98] M. Metzler and I. Varga. Spectral properties of the Chalker-Coddington network. *J. Phys. Soc. Japan*, 67:1856–1859, 1998.
- [OO95] T. Ohtsuki and Y. Ono. Critical level statistics in two-dimensional disordered electron systems. *J. Phys. Soc. Japan*, 64:4088, 1995. ArXiv: cond-mat/9509146.
- [OOK96] Y. Ono, T. Ohtsuki, and B. Kramer. Scaling behavior of level statistics in quantum Hall regime. *J. Phys. Soc. Japan*, 65:1734–1743, 1996. ArXiv: cond-mat/9603099.
- [PA99] L. P. Pryadko and A. Auerbach. Hall resistivity and dephasing in the quantum Hall insulator. *Phys. Rev. Lett.*, 82:1253–1256, 1999.
- [PFTV92] W. H. Press, B. P. Flannery, S. A. Teukolsky, and W. T. Vetterling. *Numerical Recipes in FORTRAN*. Cambridge University Press, Cambridge, 2nd edition, 1992.
- [PHSS92] S. Prakash, S. Havlin, M. Schwartz, and H. E. Stanley. Structural and dynamical properties of long-range correlated percolation. *Phys. Rev. A*, 46:R1724–R1727, 1992.
- [Pra81] R. E. Prange. Quantized Hall resistance and the measurement of the fine-structure constant. *Phys. Rev. B*, 23:4802–4805, 1981.
- [Pru84] A. M. M. Pruisken. On localization in the theory of the quantized Hall effect: A two-dimensional realization of the  $\theta$ -vacuum. *Nucl. Phys. B*, 235:277–298, 1984.
- [PS81a] J.-L. Pichard and G. Sarma. Finite-size scaling approach to Anderson localisation. *J. Phys. C*, 14:L127–L132, 1981.
- [PS81b] J.-L. Pichard and G. Sarma. Finite-size scaling approach to Anderson localisation: II. quantitative analysis and new results. *J. Phys. C*, 14:L617–L625, 1981.
- [PS98] H. Potempa and L. Schweitzer. Dependence of critical level statistics on the sample shape. *J. Phys.: Condens. Matter*, 10:L431–L435, 1998. ArXiv: cond-mat/9804312.
- [PSC<sup>+</sup>03] E. Peled, D. Shahar, Y. Chen, D. L. Sivco, and A. Y. Cho. Observation of a quantized Hall resistivity in the presence of mesoscopic fluctuations. *Phys. Rev. Lett.*, 90:246802–4, 2003.
- [PST<sup>+</sup>97] W. Pan, D. Shahar, D. C. Tsui, H. P. Wei, and M. Razeghi. Quantum Hall liquid-to-insulator transition in  $\text{In}_{1-x}\text{Ga}_x\text{As}/\text{InP}$  heterostructures. *Phys. Rev. B*, 55:15431–15433, 1997.
- [RCH96] I. M. Ruzin, N. R. Cooper, and B. I. Halperin. Nonuniversal behavior of finite quantum Hall systems as a result of weak macroscopic inhomogeneities. *Phys. Rev. B*, 53:1558–1572, 1996.

- [RF95] I. Ruzin and S. Feng. Universal relation between longitudinal and transverse conductivities in quantum Hall effect. *Phys. Rev. Lett.*, 74:154–157, 1995.
- [RKB<sup>+</sup>99] S. Russ, J. W. Kantelhardt, A. Bunde, S. Havlin, and I. Webman. Anderson localization in a random correlated energy landscape. *Physica A*, 266:492–496, 1999.
- [RKS77] P. J. Reynolds, W. Klein, and H. E. Stanley. A real-space renormalization group for site and bond percolation. *J. Phys. C*, 10:L167–L172, 1977.
- [SA92] D. Stauffer and A. Aharony. *Introduction to Percolation Theory*. Taylor and Francis, London, 1992.
- [SA95] D. Stauffer and A. Aharony. *Perkolationsstheorie*. VCH, Weinheim, 1995.
- [SA97] E. Shimshoni and A. Auerbach. Quantized Hall insulator: Transverse and longitudinal transport. *Phys. Rev. B*, 55:9817–9823, 1997.
- [SAK98] E. Shimshoni, A. Auerbach, and A. Kapitulnik. Transport through quantum melts. *Phys. Rev. Lett.*, 80:3352–3355, 1998.
- [Sal99] M. Salmhofer. *Renormalization: an Introduction*. Springer, Berlin, 1999.
- [SH94] S. H. Simon and B. I. Halperin. Explanation for the resistivity law in quantum Hall systems. *Phys. Rev. Lett.*, 73:3278–3281, 1994.
- [Sha82] B. Shapiro. Renormalization-group transformation for the Anderson transition. *Phys. Rev. Lett.*, 48:823–825, 1982.
- [She94] D. L. Shepelyansky. Coherent propagation of two interacting particles in a random potential. *Phys. Rev. Lett.*, 73:2607–2610, 1994.
- [Shi99] E. Shimshoni. Classical versus quantum transport near quantum Hall transitions. *Phys. Rev. B*, 60:10691–10694, 1999.
- [SHL<sup>+</sup>98] D. Shahar, M. Hilke, C. C. Li, D. C. Tsui, S. L. Sondhi, and M. Razeghi. A new transport regime in the quantum Hall effect. *Solid State Commun.*, 107:19, 1998. ArXiv: cond-mat/9706045.
- [SMK03] N. Sandler, H. R. Maei, and J. Kondev. Quantum and classical localization in the lowest Landau level. *Phys. Rev. B*, 68:205315–4, 2003. ArXiv: cond-mat/0304616.
- [SO99] K. Slevin and T. Ohtsuki. Corrections to scaling at the Anderson transition. *Phys. Rev. Lett.*, 82:382–385, 1999. ArXiv: cond-mat/9812065.
- [SP98] L. Schweitzer and H. Potempa. Influence of boundary conditions on level statistics and eigenstates at the metal-insulator transition. *Physica A*, 266:486–491, 1998. ArXiv: cond-mat/9809248.
- [SSS<sup>+</sup>93] B. I. Shklovskii, B. Shapiro, B. R. Sears, P. Lambrianides, and H. B. Shore. Statistics of spectra of disordered systems near the metal-insulator transition. *Phys. Rev. B*, 47:11487–11490, 1993.

- [STS<sup>+</sup>95] D. Shahar, D. C. Tsui, M. Shayegan, R. N. Bhatt, and J. E. Cunningham. Universal conductivity at the quantum Hall liquid to insulator transition. *Phys. Rev. Lett.*, 74:4511–4514, 1995.
- [STS<sup>+</sup>96] D. Shahar, D. C. Tsui, M. Shayegan, E. Shimshoni, and S. L. Sondhi. Evidence for charge-flux duality near the quantum Hall liquid-to-insulator transition. *Science*, 274:589–592, 1996.
- [STS<sup>+</sup>97a] D. Shahar, D. C. Tsui, M. Shayegan, J. E. Cunningham, E. Shimshoni, and S. L. Sondhi. On the nature of the Hall insulator. *Solid State Commun.*, 102:817–821, 1997.
- [STS<sup>+</sup>97b] D. Shahar, D. C. Tsui, M. Shayegan, E. Shimshoni, and S. L. Sondhi. A different view of the quantum Hall plateau-to-plateau transitions. *Phys. Rev. Lett.*, 79:479–482, 1997.
- [SVO<sup>+</sup>00] R. T. F. van Schaijk, A. de Visser, S. M. Olsthoorn, H. P. Wei, and A. M. M. Pruisken. Probing the plateau-insulator quantum phase in the quantum Hall regime. *Phys. Rev. Lett.*, 84:1567–1570, 2000.
- [SW99] D. N. Sheng and Z. Y. Weng. Reflection symmetry and quantized Hall resistivity near the quantum Hall transition. *Phys. Rev. B*, 59:R7821–R7824, 1999.
- [SW00] D. N. Sheng and Z. Y. Weng. Phase diagram of the integer quantum Hall effect. *Phys. Rev. B*, 62:15363–15366, 2000.
- [SZ95] L. Schweitzer and I. Kh. Zharekeshev. Critical level spacing distribution of two-dimensional disordered systems with spin-orbit coupling. *J. Phys.: Condens. Matter*, 7:L377–L381, 1995. ArXiv: cond-mat/9506072.
- [TKNN82] D. J. Thouless, M. Kohmoto, M. P. Nightingale, and M. den Nijs. Quantized Hall conductance in a two-dimensional periodic potential. *Phys. Rev. Lett.*, 49:405–408, 1982.
- [TSG82] D. C. Tsui, H. L. Störmer, and A. C. Gossard. Two-dimensional magnetotransport in the extreme quantum limit. *Phys. Rev. Lett.*, 48:1559–1562, 1982.
- [VHSP95] I. Varga, E. Hofstetter, M. Schreiber, and J. Pipek. Shape analysis of the level-spacing distribution around the metal-insulator transition in the three-dimensional Anderson model. *Phys. Rev. B*, 52:7783–7786, 1995. ArXiv: cond-mat/9407058.
- [Wei84] A. Weinrib. Long-range correlated percolation. *Phys. Rev. B*, 29:387–395, 1984.
- [WES<sup>+</sup>87] R. Willett, J. P. Eisenstein, H. L. Störmer, D. C. Tsui, A. C. Gossard, and J. H. English. Observation of an even-denominator quantum number in the fractional quantum Hall effect. *Phys. Rev. Lett.*, 59:1776–1779, 1987.

- [WFGC00] Z. Wang, M. P. A. Fisher, M. Girvin, and J. T. Chalker. Short-range interactions and scaling near integer quantum Hall transitions. *Phys. Rev. B*, 61:8326–8333, 2000. ArXiv: cond-mat/9906454.
- [WH83] A. Weinrib and B. I. Halperin. Critical phenomena in systems with long-range-correlated quenched disorder. *Phys. Rev. B*, 27:413–427, 1983.
- [Wig51] E. P. Wigner. On the statistical distribution of the widths and spacings of nuclear resonance levels. *Proc. Camb. Phil. Soc.*, 47:790–798, 1951.
- [Wig55] E. P. Wigner. Characteristic vectors of bordered matrices with infinite dimensions. *Ann. Math.*, 62:548–564, 1955.
- [Wil83] K. G. Wilson. The renormalization group and critical phenomena. *Rev. Mod. Phys.*, 55:583–600, 1983.
- [WJ98] A. Weymer and M. Janssen. Localization length exponent, critical conductance distribution and multifractality in hierarchical network models for the quantum Hall effect. *Ann. Phys. (Leipzig)*, 7:159–173, 1998. ArXiv: cond-mat/9805063.
- [WJL96] Z. Wang, B. Jovanovic, and D.-H. Lee. Critical conductance and its fluctuations at the integer-Hall plateau transitions. *Phys. Rev. Lett.*, 77:4426–4429, 1996.
- [WLS98] X. Wang, Q. Li, and C. M. Soukoulis. Scaling properties of conductance at integer quantum Hall plateau transitions. *Phys. Rev. B*, 58:3576–3579, 1998.
- [WLTP92] H. P. Wei, S. Y. Lin, D. C. Tsui, and A. M. M. Pruisken. Effect of long-range potential fluctuations on scaling in the integer quantum Hall effect. *Phys. Rev. B*, 45:3926–3928, 1992.
- [WLW94] Z. Wang, D.-H. Lee, and X.-G. Wen. Transitions between Hall plateaus in the presence of strong Landau level mixing. *Phys. Rev. Lett.*, 72:2454–2457, 1994.
- [WTP85] H. P. Wei, D. C. Tsui, and A. M. M. Pruisken. Localization and scaling in the quantum Hall regime. *Phys. Rev. B*, 33:1488–1491, 1985.
- [WTPP88] H. P. Wei, D. C. Tsui, M. A. Paalanen, and A. M. M. Pruisken. Experiments on delocalization and universality in the integral quantum Hall effect. *Phys. Rev. Lett.*, 61:1294–1296, 1988.
- [Yos02] D. Yoshioka. *The Quantum Hall Effect*. Springer Series in Solid-State Sciences 133. Springer, Berlin, 2002.
- [Zir94] M. R. Zirnbauer. Towards a theory of the integer quantum Hall transition: From the nonlinear sigma model to superspin chains. *Ann. Phys. (Leipzig)*, 3:513–577, 1994.
- [Zir97] M. R. Zirnbauer. Toward a theory of the integer quantum Hall transition: Continuum limit of the Chalker-Coddington model. *J. Math. Phys.*, 38:2007–2036, 1997. ArXiv: cond-mat/9701024.

- [ZK95a] I. K. Zharekeshev and B. Kramer. Scaling of level statistics at the disorder-induced metal-insulator transition. *Phys. Rev. B*, 51:17239–17242, 1995.
- [ZK95b] I. K. Zharekeshev and B. Kramer. Universal fluctuations in spectra of disordered systems at the Anderson transition. *Jpn. J. Appl. Phys.*, 34:4361–4364, 1995. ArXiv: cond-mat/9506114.
- [ZK97] I. K. Zharekeshev and B. Kramer. Asymptotics of universal probability of neighboring level spacings at the Anderson transition. *Phys. Rev. Lett.*, 79:717–720, 1997. ArXiv: cond-mat/9706255.
- [ZKL92] S.-C. Zhang, S. Kivelson, and D.-H. Lee. Zero-temperature Hall coefficient of an insulator. *Phys. Rev. Lett.*, 69:1252–1255, 1992.
- [ZS01] U. Zülicke and E. Shimshoni. Quantum breakdown of the quantized Hall insulator. *Phys. Rev. B*, 63:241301–4, 2001. ArXiv: cond-mat/0101443.

# Publications

- [10] *Fluctuating Hall resistance defeats the quantized Hall insulator*, P. Cain and R. A. Römer, accepted for publication in *Europhys. Lett.*, ArXiv: cond-mat/0309669.
- [9] *Real-space renormalization and energy-level statistics at the quantum Hall transition*, R. A. Römer and P. Cain, *Adv. Solid State Phys.* **42**, 237–252 (2003), ArXiv: cond-mat/0304612.
- [8] *Renormalization group approach to energy level statistics at the integer quantum Hall transition*, P. Cain, R. A. Römer, and M. E. Raikh, *Phys. Rev. B* **67**, 075307-9 (2003), ArXiv: cond-mat/0209356.
- [7] *Real-space renormalization group approach to the quantum Hall transition*, P. Cain, M. E. Raikh, and R. A. Römer, *J. Phys. Soc. Jpn.* **72** Suppl. A, 135-136 (2003).
- [6] *Renormalization group approach to the energy level statistics at the integer quantum Hall transition*, P. Cain, M. E. Raikh, and R. A. Römer, *Physica E* **18**, 126–127 (2003).
- [5] *Applications of cluster computing for the Anderson model of localization*, P. Cain, F. Milde, R. A. Römer, and M. Schreiber, In S. G. Pandalai, editor, *Recent Research Developments in Physics Vol. 2-2001 Part II*, pages 171–184, Fort P.O. Trivandrum, 2002. Transworld Research Network.
- [4] *Use of cluster computing for the Anderson model of localization*, P. Cain, F. Milde, R. A. Römer, and M. Schreiber, *Comp. Phys. Comm.* **147**, 246–250 (2002).
- [3] *Integer quantum Hall transition in the presence of a long-ranged-correlated quenched disorder*, P. Cain, M. E. Raikh, R. A. Römer, and M. Schreiber, *Phys. Rev. B* **64**, 235326–9 (2001), ArXiv: cond-mat/0104045.
- [2] *Off-diagonal disorder in the Anderson model of localization*, P. Biswas, P. Cain, R. A. Römer, and M. Schreiber, *phys. stat. sol. (b)* **218**, 205–209 (2000), ArXiv: cond-mat/0001315.
- [1] *Phase diagram of the three-dimensional Anderson model of localization with random hopping*, P. Cain, R. A. Römer, and M. Schreiber, *Ann. Phys. (Leipzig)* **8**, SI-33–SI-36 (1999), ArXiv: cond-mat/9908255.

# Erklärung gemäß Promotionsordnung §6 (2) 4, 5

Hiermit erkläre ich, dass ich die vorliegende Arbeit selbständig angefertigt und nur die angegebenen Hilfsmittel verwendet habe. Die Stellen, die in Sinn und Wortlaut anderen Werken entnommen wurden, habe ich entsprechend gekennzeichnet. Ich habe weder früher noch derzeit an anderer Stelle ein Promotionsverfahren beantragt. Die aktuell gültige Promotionsordnung der Fakultät für Naturwissenschaften der Technischen Universität Chemnitz ist mir bekannt.

Chemnitz, den 5. März 2004

Philipp Cain



# Lebenslauf

## **Akademische Grade:**

15. Dez. 1998                      Diplomphysiker

## **Ausbildung:**

seit Jan. 1999                      Doktorand bei Prof. Dr. M. Schreiber an der Technischen Universität Chemnitz

Dez. 1997 – Nov. 1998              Diplomarbeit bei Prof. Dr. M. Schreiber an der Technischen Universität Chemnitz über das Anderson Modell der Lokalisierung in 3D mit nichtdiagonaler Unordnung, Note: 1,3

Okt. 1993 – Nov. 1998              Physikstudium an der Technischen Universität Chemnitz

Sep. 1990 – Jun. 1992              Abitur an der Spezialklasse der Technischen Universität Chemnitz

Sep. 1980 – Jul. 1990              Mittlere Reife an der polytechnischen Oberschule Johann-Gottfried-Herder in Chemnitz

## **Anstellungen:**

seit Jan. 1999                      wissenschaftlicher Mitarbeiter an der Technischen Universität Chemnitz

Jan. 1996 – Okt. 1997              Arbeit als wissenschaftliche Hilfskraft an der Technischen Universität Chemnitz, Problemstellung u.a. Simulation neuronaler Netze, Relaxation von Spingläsern

## **Persönliches:**

Okt. 1992 – Sep. 1993              Grundwehrdienst

19. Sep. 1973                      Geboren als Sohn von Hans-Dieter Cain, Dipl.-Ing., und Liselotte Cain, geb. Kretzschmar, Ökonom, in Karl-Marx-Stadt

## **Nationalität:**

Deutsch

# Acknowledgments

First, I would like to thank Prof. Michael Schreiber for his guidance and support during this work. He has built up a group providing the 'fruitful functional environment' which makes work easier.

Second, but not less important, I'm grateful to Dr. Rudolf A. Römer. He actually opened up the opportunity to study this interesting physical topic. He was also my first reference whenever I got stuck and help was required. His experience and constructive criticism have been very valuable not only with respect to this work.

During my visits at the University of Utah I could benefit also from the instructive explanations and the discussions with Prof. Michael E. Raikh, who is an excellent expert in the field.

Furthermore I want to thank all group members for making the administration of their accounts that simple. A special thank goes to Ville for the Bourbon and to Macleans for teaching the African slang.

Finally, I want to acknowledge the financial support from DFG-Sonderforschungsbereich 393, DFG-Schwerpunktprogramm "Quanten-Hall-Systeme", and DAAD.